5-2014

System Identification of a Small Low-Cost Unmanned Aerial Vehicle Using Flight Data from Low-Cost Sensors

Nathan V. Hoffer
Utah State University

SYSTEM IDENTIFICATION OF A SMALL LOW-COST UNMANNED AERIAL VEHICLE USING FLIGHT DATA FROM LOW-COST SENSORS

by

Nathan V. Hoffer

A thesis submitted in partial fulfillment
of the requirements for the degree

of

MASTER OF SCIENCE

in

Mechanical Engineering

Approved:

Dr. R. Rees Fullmer Major Professor	Dr. Aaron Katz Committee Member
Dr. YangQuan Chen Committee Member	Dr. Mark R. McLellan Vice President for Research and Dean of the School of Graduate Studies

UTAH STATE UNIVERSITY
Logan, Utah

2014

Abstract

System Identification of a Small Low-Cost Unmanned Aerial Vehicle Using Flight Data from Low-Cost Sensors

by

Nathan V. Hoffer, Master of Science

Utah State University, 2014

Major Professor: Dr. R. Rees Fullmer
Department: Mechanical and Aerospace Engineering

Remote sensing has traditionally been done with satellites and manned aircraft. While these methods can yield useful scientific data, satellites and manned aircraft have limitations in data frequency, process time, and real time re-tasking. Small low-cost unmanned aerial vehicles (UAVs) provide greater possibilities for personal scientific research than traditional remote sensing platforms. Precision aerial data requires an accurate vehicle dynamics model for controller development, robust flight characteristics, and fault tolerance. One method of developing a model is system identification (system ID). In this thesis system ID of a small low-cost fixed-wing T-tail UAV is conducted. The linerized longitudinal equations of motion are derived from first principles. Foundations of Recursive Least Squares (RLS) are presented along with RLS with an Error Filtering Online Learning scheme (EFOL). Sensors, data collection, data consistency checking, and data processing are described. Batch least squares (BLS) and BLS with EFOL are used to identify aerodynamic coefficients of the UAV. Results of these two methods with flight data are discussed.

(145 pages)

Public Abstract

System Identification of a Small Low-Cost Unmanned Aerial Vehicle Using Flight Data from Low-Cost Sensors

by

Nathan V. Hoffer, Master of Science

Utah State University, 2014

Major Professor: Dr. R. Rees Fullmer
Department: Mechanical and Aerospace Engineering

Remote sensing has usually been done with satellites and manned aircraft. While they can be useful, satellites and manned aircraft have issues in how quickly you can get data, process it, and go back to get more data. Small low-cost unmanned aerial vehicles (UAVs) overcome these issues. To collect precise data a precise model of the UAV is needed to develop the autopilot, make sure the aircraft flies well, and does not break. One method of making a model is system identification (system ID). In this thesis system ID of a small low-cost fixed-wing T-tail UAV is done. The equations used to show how the aircraft moves are developed. The algorithms used to do the system ID are developed. Sensors and how the data is corrected are described. Results of two methods of system ID with flight data are shown. The model found from system ID fits for some of the data.

To KaDee, Ella, and Ryker (Make it so Number One).

Acknowledgments

I would like to thank Dr. R. Rees Fullmer who has patiently helped me through my mistakes and lack of understanding. Without his guidance and keen understanding of the difficulties of using flight data I would not have been able to succeed. Thank you Dr. YangQuan Chen for bringing me in to CSOIS and giving me the opportunity not only to research what I wanted to, but also to put all of my learning to use and actually engineer real systems...and others want them! Thank you Dr. Aaron Katz for being part of my committee and helping me with edits. A special thanks to Dr. Mac McKee of the Utah Water Research Laboratory who has supported my research. This work is supported by Utah Water Research Laboratory MLF 2006-2014.

Cal Coopmans, thank you for teaching me what it means to really dig to the heart of a problem and then find the simplest solution to solve it. Austin Jensen, I am grateful for your example of outstanding engineering. Michal, thank you for listening to my endless problems and giving me many solutions. Also I could not have collected the flight data without your help and excellent programming skills. I would also like to thank the members of CSOIS and AggieAir , especially Dan, who kept the Enterprise in the air and Chris who kept the data flowing.

I would also like to thank Dr. Warren F. Phillips for writing the most comprehensive book on flight mechanics. It has been an invaluable wealth of knowledge. Thank you for taking the time to do it right.

And most of all I would like to thank my wife, children, family, and God who have helped me along this long and difficult journey.

Nathan V. Hoffer

Contents

List of Tables

List of Figures

Notation

u	x_{body}-component of airspeed
v	y_{body}-component of airspeed
w	z_{body}-component of airspeed
u_0	equilibrium x_{body}-component of airspeed
v_0	equilibrium y_{body}-component of airspeed
w_0	equilibrium z_{body}-component of airspeed
Δu	deviation from equilibrium x_{body}-component of airspeed
Δv	deviation from equilibrium y_{body}-component of airspeed
Δw	deviation from equilibrium z_{body}-component of airspeed
$\dot{u}$	x_{body}-component of acceleration
$\dot{v}$	y_{body}-component of acceleration
$\dot{w}$	z_{body}-component of acceleration
$\Delta\dot{u}$	deviation from equilibrium x_{body}-component of acceleration
$\Delta\dot{v}$	deviation from equilibrium y_{body}-component of acceleration
$\Delta\dot{w}$	deviation from equilibrium z_{body}-component of acceleration
ξ_x	x position relative to the surface of the earth
ξ_y	y position relative to the surface of the earth
ξ_z	z position relative to the surface of the earth or altitude

ϕ	Euler bank angle
θ	Euler elevation angle
ψ	Euler azimuth angle
ϕ_0	equilibrium Euler bank angle
θ_0	equilibrium Euler elevation angle
ψ_0	equilibrium Euler azimuth angle
$\Delta\phi$	deviation equilibrium Euler bank angle
$\Delta\theta$	deviation equilibrium Euler elevation angle
$\Delta\psi$	deviation equilibrium Euler azimuth angle
δ_a	aileron deflection
δ_e	elevator deflection
δ_r	rudder deflection
$\Delta\delta_a$	deviation from trim aileron deflection
$\Delta\delta_e$	deviation from trim elevator deflection
$\Delta\delta_r$	deviation from trim rudder deflection
ρ	air density
S_w	planform area of main wing
$\bar{c}_w$	mean chord length of main wing
W	weight of UAV
g	gravitational acceleration
V_0	initial airspeed magnitude
α_{T0}	thrust angle of attack at 0 fuselage angle of attack

I_{xx_b}	moment of inertia
I_{xz_b}	product of inertia
I_{yy_b}	moment of inertia
I_{zz_b}	moment of inertia
$T_{,V}$	change in thrust with respect to air speed
p	rolling rate (x_{body}-component of angular rate)
q	pitching rate (y_{body}-component of angular rate)
r	yaw rate (z_{body}-component of angular rate)
Δp	deviation equilibrium rolling rate (x_{body}-component of angular rate)
Δq	deviation equilibrium pitching rate (y_{body}-component of angular rate)
Δr	deviation equilibrium yaw rate (z_{body}-component of angular rate)
$\dot{p}$	rolling rate (x_{body}-component of angular acceleration)
$\dot{q}$	pitching rate (y_{body}-component of angular acceleration)
$\dot{r}$	yaw rate (z_{body}-component of angular acceleration)
$\Delta\dot{p}$	rolling rate (x_{body}-component of angular acceleration)
$\Delta\dot{q}$	pitching rate (y_{body}-component of angular acceleration)
$\Delta\dot{r}$	yaw rate (z_{body}-component of angular acceleration)

Acronyms

ADS	Air Data System
ARX	Auto-regressive Exogenous
ARXMAX	Auto-regressive Moving Average Exogenous
BJ	Box Jenkins
BS	Barometric Sensor
CSD	Control System Design
CMA-ES	Covariance Matrix Adaptation Evolution Strategy
DP	Differential Pressure
DOF	Degree of Freedom
EEM	Equation-error Method
EFOL	Error Filtering Online Learning Scheme
EKF	Extended Kalman Filter
EMID	Error Mapping Identification
FD	Frequency Domain
FTR	Fourier Transform Regression
GA	Genetic Algorithm
GP	Gaussian Process
GPS	Global Positioning System
HILS	Hardware In The Loop Simulations
IMU	Inertial Measurement Unit
INS	Inertial Navigation System
LA	Laser Altimeter
LM	Levenberg Marquardt
LR	Linear Regression
LS	Least Squares
MC	Magnetic Compass
MCS	Motion Capture System

MIMO	Multiple Input Multiple Output
MLP	Multi-layer Preceptron
MLM	Maximum Likelihood Method
NN	Neural Network
NARXM	Nonlinear Auto-regressive Exogenous Model
NNARXM	Neural Network Auto-regressive Exogenous Model
OEM	Output-error Method
OKID	Observe/Kalman Filter Identification
OLS	Orthogonal Least Squares
PE	Parameter Estimation
PEM	Prediction-Error Method
PS	Pressure Sensor
PT	Position Transducer
RFB	Radial Basis Function
RLS	Recursive Least Squares
RT	Real-Time
SOM	Self-organizing Map
SS	State Space
Sys. ID	System Identification
TD	Time-Domain
TF	Transfer Function
TLS	Total Least Squares
UAV	Unmanned Aerial Vehicle
UKF	Unscented Kalman Filter
US	Ultrasonic Sensor

Chapter 1

Introduction

1.1 Motivation

Small low-cost unmanned aerial vehicles (UAVs) are a newly emerging resource for personal remote sensing for scientific research and civilian application. These UAVs can provide researchers with the means to gather multi-spectral imagery with shorter set up and data return times which is crucial for dynamic, time sensitive data. UAVs are also well suited for agricultural research and optimization, characterized by small data collection areas and the necessity for high resolution imagery and rapid data availability [1]. Rango et. al. explores how UAVs can fill in the resolution gap for rangeland applications, providing needed data for rangeland management [2]. Jensen et. al. discussed UAV applications to riparian and wetland mapping and change detection. They specifically cite how UAVs can provide multispectral imagery at high resolutions with the flexibility of the user fully controlling when and where imagery is taken [3].

There are several obstacles that must be overcome before UAVs can be successfully integrated into civilian airspace. Of these obstacles the most pressing deal with safety such as obstacle avoidance, communication between manned and unmanned aircraft, and robust and fault tolerant systems [4–6]. Robust and fault tolerant UAV control systems are integral for successful and safe personal remote sensing. Development of such control systems requires dynamic system models that are well-characterized. Traditionally aircraft and rotorcraft dynamic system models have been analytically determined from first principles such as Newton's Second Law for rigid-body dynamics [7]. The parameters of these dynamic system are usually determined through costly and time consuming wind tunnel testing. These methods, while useful, have limitations when applied to small and micro UAVs due to several key differences which include:

- Low Reynolds numbers and airspeeds [8]
- Increased dynamic rates due to decreased mass moments of inertia
- Dominance of propulsion dynamics forces and moments versus aerodynamic body forces and moments
- Asymmetric or atypical designs [9]
- Cannot characterize all flight regimes (e.g. transition from pre- to post-stall, aerobatic maneuvers, and inverted helicopter flight)

As an alternative to analytical methods and wind tunnel testing, system identification (system ID) provides several well suited methods for developing dynamic system models and identifying their parameters. There are several methods of system ID that have been successfully applied to small low-cost UAVs, which will be discussed later. Through system ID, a UAV's dynamic model can be determined from flight data, after which the dynamic model can be used to develop and validate autopilot control systems. Thus system ID is an indispensable tool for modeling, simulating, and developing controllers for small UAVs. System ID provides a base for reliable and robust UAV control systems increasing the success and safety of personal remote sensing.

The main contribution of this thesis is the design and implementation of a method of system ID using recursive least squares with an error filtering online learning scheme. This method is implemented on a small fixed-wing UAV and utilizes low-cost sensors. The thesis will be developed as follows: Chapter 2 reviews the literature on UAV system ID. Chapter 3 list the thesis and research objectives. Chapter 4 derives the linear longitudinal equations of motion of the UAV from Newton's Second Law for rigid-body motion. Chapter 5 derives the recursive least squares algorithm with an error filtering online learning scheme. Chapter 6 reviews the UAV, sensors, and system ID maneuvers. Chapter 7 detail the processing of flight data. Chapter 8 gives the model found through the method of system ID and compares the model response to flight data and Chapter 9 gives concluding remarks and a suggested future research direction.

Chapter 2

System Identification

2.1 UAV System ID Process Overview

System ID is the process of determining a mathematical model of a dynamic system by analyzing the measured input signals and output states of the system. System ID uses much of the same theory that optimal estimation [10] and control [11] use. However rather than estimating the states of a system or observing the states to drive a controller, system ID uses the inputs and states to develop a model that describes the relationship between the input signals and the response of the system.

For the specific case of UAVs the process of system ID begins with designing the input signals. Then the pilot or auto pilot performs maneuvers designed to excite the UAV's dynamics. The signals given to the control surfaces and actuators are recorded. The actual deflection of the control surfaces can also be recorded. Then various sensors record the current state of the UAV: acceleration, velocities, angular velocities, positions, aerodynamic angles, and angles relative to the earth's surface. From this training data a model of the UAV dynamics can be identified. If the model structure is already known then its parameters can be identified. This is referred to as parameter estimation, which is a more specific type of system ID. The model's response is validated using test data. This validation uses inputs to a set of test data separate from the training used to generate the model. If the test data and identified model match then the model can be used. If the model does not sufficiently predict the flight characteristics of the UAV then the system ID method, and inputs must be re-examined. This process is summarized in Fig. 2.1. There are six main elements to system ID:

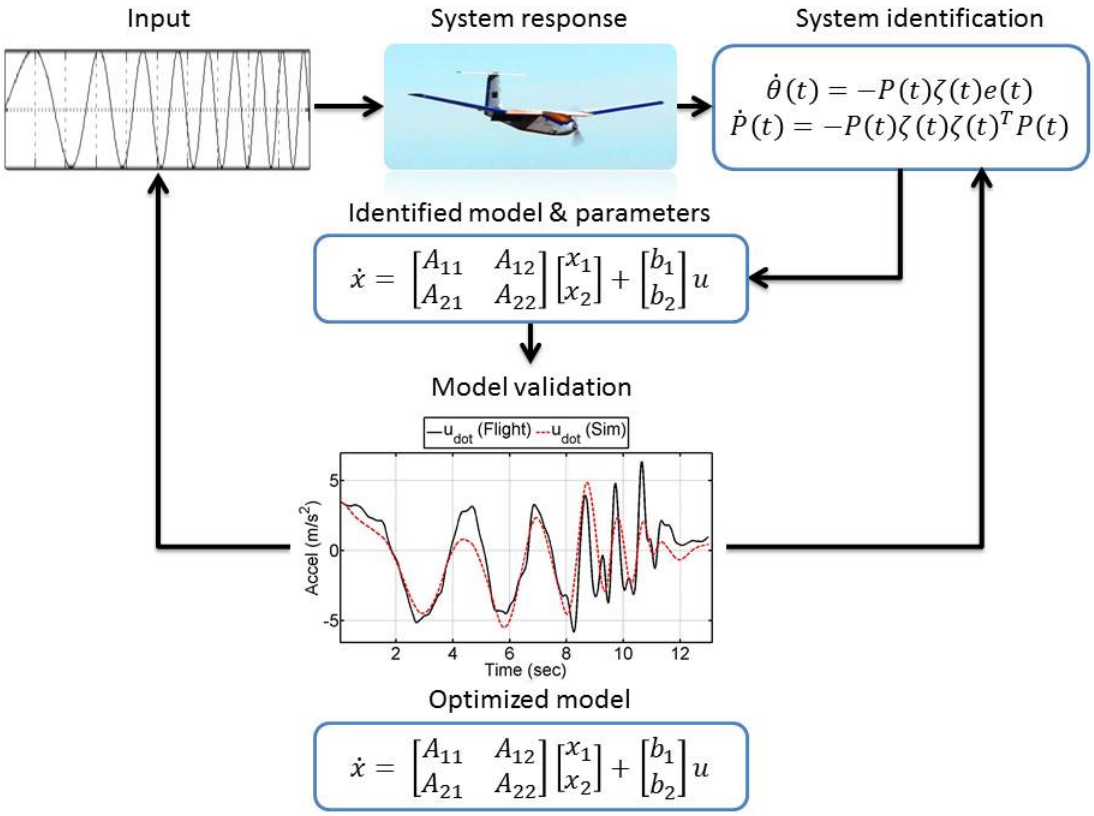

Fig. 2.1: Overview of the system identification process

1. Input signals
2. Data collection
3. Selection of the model structure
4. Selection of the system ID method
5. Optimization of the model using system ID method, model structure, and test data

These elements will be discussed more in-depth in the following sections. These sections are intend to provide a base of knowledge for real world implementation of system ID specifically geared toward UAV dynamics.

2.1.1 Input Signals

Input signals are perhaps the most important part of system ID since they affect all other aspects of the identification process. Inputs are used to excite the dynamic modes of a system. By analyzing the inputs and the response of the system, the model and model parameters of the system can be identified. If the dynamic modes of a system are not excited then the dynamic modes will not show up in the training data and cannot be identified in the model. Thus it is very important to have inputs specifically designed to excite the system dynamics. However simply exciting the dynamic modes of a system will not guarantee that the system ID method will resolve the full dynamics. Dynamic modes must also be well excited or persistently excited which means that all of the modes (of interest) are excited. Persistent excitation may also require that the modes be excited long enough so that the system ID method has time to identify the modes. This is the case for dynamic modes with long periods such as the phugoid mode for a fixed-wing UAV.

Inputs can be designed if there is sufficient information already given about the dynamics of the system. This is usually not the case when performing system ID for UAVs especially when prototyping. For general inputs Tischler and Remple [9] recommend frequency sweeps (Fig. 2.2) for system ID and doublets (Fig. 2.3) for model verification. Frequency sweeps can be constant or varying depending on the dynamics that need to be excited. Generally frequency sweeps start at a given low frequency and increase to the desired stopping frequency. These inputs can be performed manually by a pilot or automatically by the autopilot. Inputs for system ID are generally done by a pilot to keep the UAV under complete control. However there is recent work using an autopilot for optimal system ID maneuvers [12]. Having the autopilot perform system ID maneuvers requires in-depth understanding of the system and its response to inputs and disturbances.

In summary when developing inputs for system ID the following should be considered:

- Applicable frequency range
- Persistent excitation
- Duration of excitation

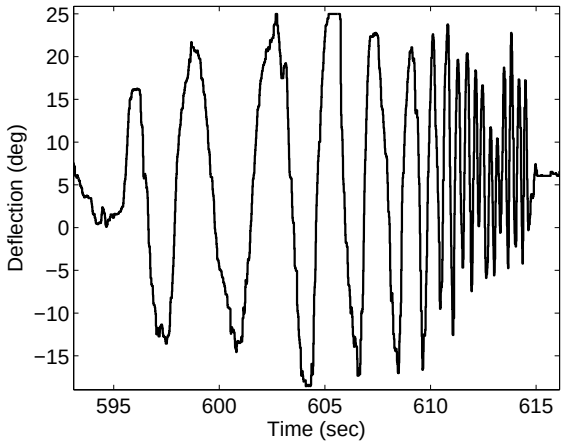

Fig. 2.2: Elevator frequency sweep for system ID from flight data

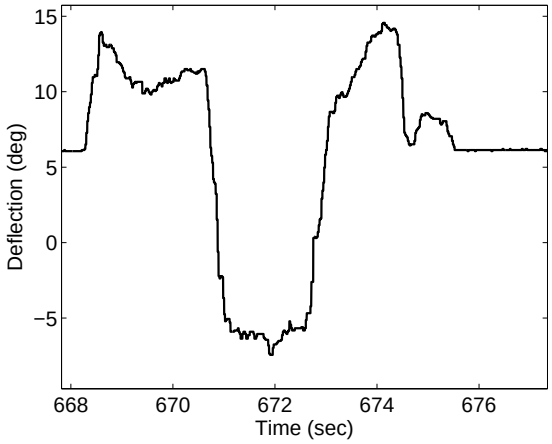

Fig. 2.3: Elevator doublet for system ID model validation from flight data

- Types of inputs
- Model verification set of inputs

2.1.2 Training and test data collection

There are several things to consider when defining instrumentation requirements for system ID. One of the challenges of system ID is using real flight data. Flight data can be extremely noisy. The amount of noise depends on the sensor as well as how it is integrated with avionics, the structure of the UAV, and the type of propulsion. For example an inertial measurement unit (IMU) will record accelerations due to changes in the aerodynamic forces and moments as well as structural vibrations caused by the propulsion system. This type of vibration can be seen in Fig. 2.4 - Fig. 2.7. Figure 2.4 and Fig. 2.6 show the general acceleration motion during a frequency sweep maneuver. The noise from the electric motor can be seen in Figure 2.5 and Fig. 2.7. For the z acceleration the signal to noise ratio is high and the motion is relatively slow compared to the noise. In this case a low pass filter can be used to filter out the noise from the motor. Tischler and Remple suggest using the same filter on all input and output signals to avoid biasing the system ID [9].

Sensor sample rates must be considered for collecting training and test data. If the sensor has a lower sample rate than the frequency of the dynamic modes of the system then system ID cannot resolve the model and parameters.

Sensor type requirements are driven by the model and by the input and output data needed for system ID. It is important to characterizes sensors before flight testing to ensure data fidelity. If a sensor is inherently noisy or dose not have sufficient resolution then other sensors or filtering should be considered. Sources of data collection for UAVs found in the literature can be grouped as the following:

- Inertial Measurement Unit (IMU), GPS and differential pressure sensor, laser altimeter, or ultrasonic altimeter
- GPS only

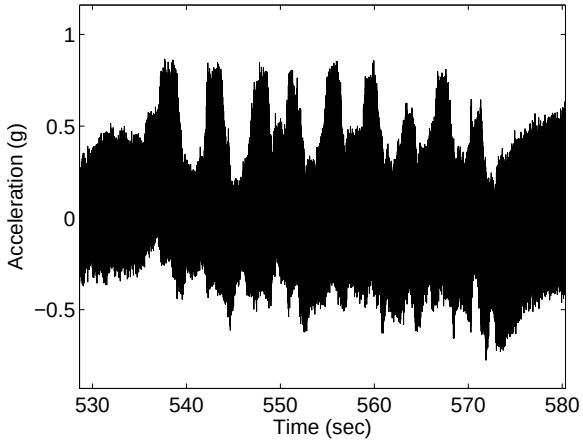

Fig. 2.4: X acceleration from flight data

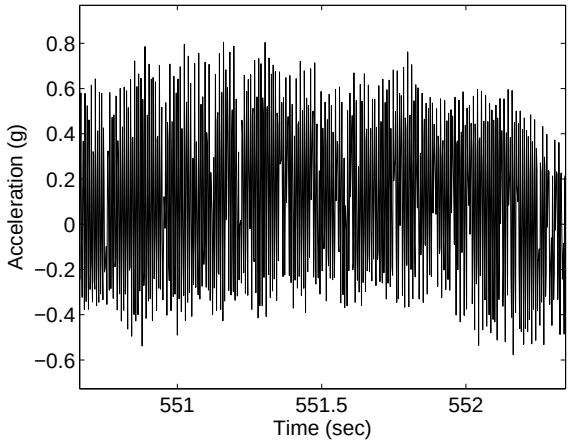

Fig. 2.5: X acceleration close up with high frequency noise

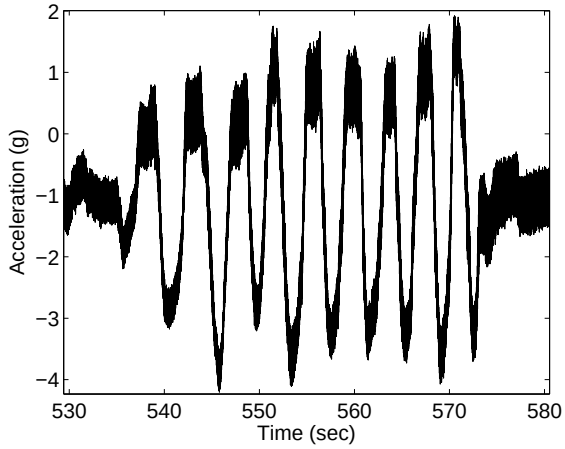

Fig. 2.6: Z acceleration from flight data

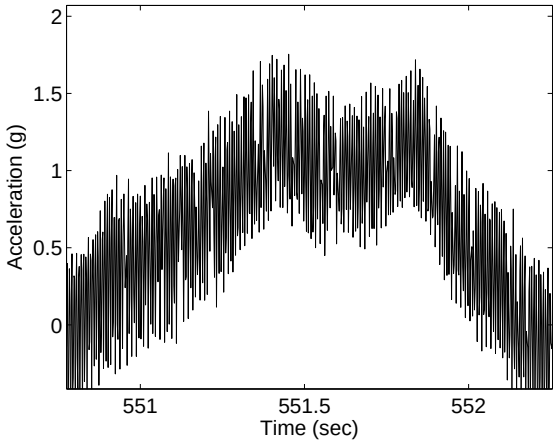

Fig. 2.7: Z acceleration close up with high frequency noise

- Motion capture systems
- Radar [13]
- Hardware in the loop simulations (for system ID methods comparison) [14]

Generally system ID uses data from an IMU and GPS, however the literature shows that other sensors have been successfully used in system ID [15] and [16].

In summary the following should be considered for training and test data collection:

- Noise
- Filters
- Sensor sample rates
- Sensors types

2.1.3 Selection of the model structure

Model structure selection is an important and difficult step in system ID. This step requires *a priori* knowledge of the system dynamics, understanding of model properties, and an understanding of the end application. Incorrect model selection can lead to a model that only partially describes the system dynamics. The application of system ID is perhaps

the strongest driver for model selection. If aerodynamics coefficients are desired then the model must have these parameters as part of its structure. On the other hand if the model is used for control systems design then an auto-regressive exogenous input model may be appropriate [9].

2.1.4 Selection of the system ID method

The selection of the system ID method depends heavily on the application as well as the dynamics of the system. System ID methods can be differentiated into two groups: parametric and nonparametric [9]. Nonparametric methods identify a system from impulse or frequency responses, and do not require any *a priori* knowledge about system dynamics or model structure. Parametric methods assume a structure for the dynamic model and the model parameters are then identified from training data. Parametric models can then be subdivided in to the following sub groups:

1. Time-varying and time-invariant systems [17]
2. Static and dynamic systems
3. Linear and nonlinear systems [17]
4. Continuous and discrete systems [17]

All of these categorizations are interrelated and each captures only one particular aspect of system ID. These categorizations are provided as reference for the methods of system ID. Fig 2.8 is a decision tree for system ID methods. The decision tree gives distinct questions about the dynamics of a system which when answered lead to a set of system ID methods. The tree is not currently filled in but should give the basic idea for choosing a system ID method. For further in-depth discussion on which methods are best suited for a particular system or application see [9], [17], [18], and [19].

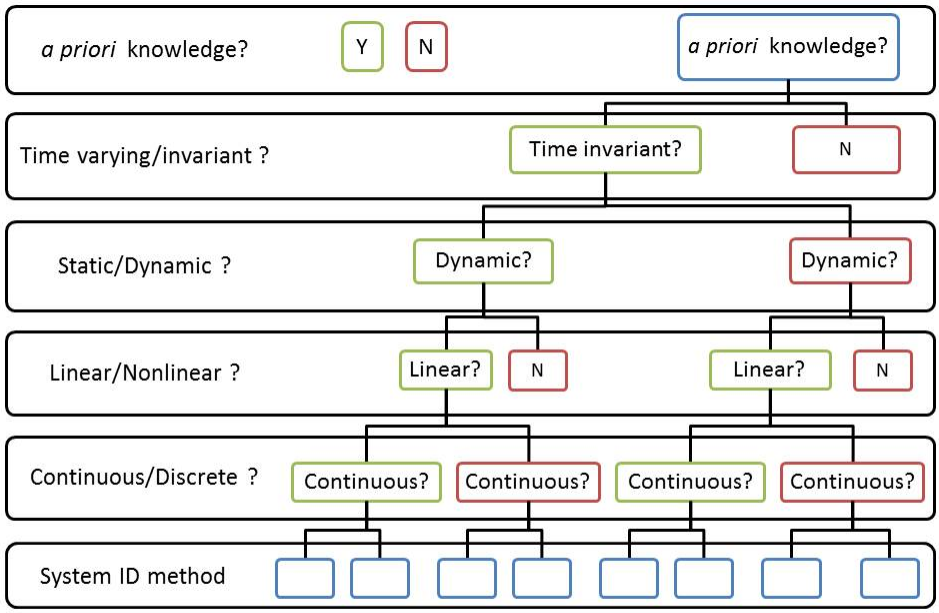

Fig. 2.8: System identification method decision tree

2.1.5 Optimization of the model using the system ID method, model structure, and test data

The best identified model is selected by validating the model's ability to predict the actual flight dynamics from a set of test data. If the model fits well enough then the model can be used to predict the actual system dynamics. If the model does not satisfactorily predict the system dynamics then the model structure, system ID method, or training data collection must be re-evaluated. Ideally this processes should be quantitative, that is if the error between the predicted flight dynamics and the actual flight dynamics is above some threshold then the model is rejected. This does not take into account the errors in measurement and modeling. Thus this process can become qualitative especially for models that make assumptions about structural dynamics.

2.2 UAV System ID Applications Overview

In order to better understand the advantages of each method of system ID, it is important to first understand the application of system ID to UAVs. From the literature, system ID of UAVs includes the following applications:

1. Dynamic model and parameter ID
2. Model validation
3. Control system design
4. Online/real-time system ID
5. Fault detection
6. Comparison of system ID methods
7. Comparison of online vs. offline system ID

Each application is summarized in the following sections.

2.2.1 Dynamic model and parameter ID

A model structure is chosen to represent the relationship between inputs and outputs of a system. *A priori* knowledge about the system can be used to select an appropriate model. This information can include coupling of dynamics, nonlinearities, order of the model. Model parameters can have physical meaning or can be the means for adjusting the model fit to the training data. Once the model structure has been chosen an identification method is used to determine the parameters of the model.

2.2.2 Control system design

System ID is integral to UAV control system design and can provide dynamic system models to be used in simulations to validate UAV control systems. Some control systems (model predictive controllers) require *a priori* knowledge of model parameters and structure, which can be determined using system ID.

2.2.3 Online system ID

In general UAV flight training and test data is recorded and then later analyzed using system ID to select the model and model parameters that best fits (predicts) the training and test data. This is referred to as a batch method. With the increased performance of modern computers it is now possible to identify parameters of some dynamic systems in real time. This has direct application to fault detection and adaptive control.

2.2.4 Fault detection

Online system ID can detect changes between the inputs and the expected and actual outputs of a UAV in flight. These differences can correspond to a failure of some part of the UAV (e.g. failed, failing, or stuck actuator). Once the failure has been detected the flight control system can be adapted to compensate or initiate an emergency landing.

2.2.5 Comparison of system ID methods

There are several methods of system ID. Not all methods are suitable for every UAV type or every end application of the system ID. Some methods are better suited for non-linear system or real-time system ID, while other methods are more suited for determining aerodynamic coefficients or supporting neural net control system design. Thus it is important to compare various techniques so that a researcher with a given UAV and application can appropriately choose a method of system ID.

2.2.6 Comparison of online vs. offline system ID

Online system ID of UAVs is a relatively new research area, and as such it is important to compare the performance of online methods to offline methods. Comparison of system ID should not only be made between methods of system ID but also between different types of UAVs. These types of comparisons can determine how well online methods are suited for cross platform use and if one method is especially useful for a certain type of UAV.

2.3 Current State of System Identification of UAVs

This section details the current state of system ID of UAVs and is divided up into five subsections of UAVs:

1. Helicopter UAVs
2. Fixed-wing UAVs
3. Multirotor UAVs
4. Flapping-wing UAVs
5. Lighter-than-air UAVs

Each section overviews current applications of system ID. Each subsection has corresponding tables that give details on each reference.

2.3.1 System ID of helicopter UAVs

Helicopter dynamics must be discussed in order to understand the importance of system ID of small UAV helicopters. Small UAV helicopter dynamics are characterized by tight coupling of the fuselage, rotor, inflow of air to the rotor, and the engine resulting in a high-order dynamic system. Thus fixed-wing low-order model approximations are generally not applicable when modeling helicopter dynamics. Also helicopter dynamics cannot be decoupled as with fixed-wing aircraft resulting in a hybrid fully coupled model with 13 degrees of freedom. Since helicopter aerodynamics are not fully characterized [20] and cross coupling effects are poorly known [9] (unlike most traditional fixed-wing aircraft), system ID gives needed insight into helicopter nonlinear, coupled dynamics.

It is noted that almost without exception all helicopter UAV system ID literature references the work of Mark B. Tischler [9], [21], [22], and [23]. Tischler developed the software package Comprehensive Identification from Frequency Responses (CIFER®) which is an industry standard for full scale rotorcraft system ID [24] It has successfully been has applied to helicopter UAVs. CIFER® is frequently used in the current literature for helicopter UAV system ID.

Significant work has been done to develop various dynamic models of helicopter UAVs. The helicopter literature divides their applications into control system development, comparison of proposed system ID methods with previously developed methods, online system ID, and unexplored flight maneuvers. Tables 2.1 - 2.3 show the collected references for helicopter system ID.

2.3.2 System ID of fixed-wing UAVs

Fixed-wing dynamic models can be developed from first-principle techniques, wind tunnel data, and computational-fluid-dynamics, however many parameters must be estimated well enough to be useful. These traditional modeling tools also have uncertainties and simplification. The fixed-wing literature uses system ID in tandem with first-principle techniques to better understand flight modes outside of nominal flight e.g. post-stall [15] and [16] and take-off [53] maneuvers where first-principle techniques may not accurately model these dynamics. The fixed-wing literature also uses system ID for controller development, comparison of system ID methods (for a given application), fault detection, and online system ID. Tables 2.4 - 2.6 show the collected references for fixed-wing system ID.

2.3.3 System ID of multirotor UAVs

Multirotors include trirotors, quadrotors, hexarotor, octarotors, etc. They differ from a helicopter in that a helicopter uses a tail-mounted rotor for yaw control. A multirotor uses differential torque of opposing motor rotation to control yaw.

Even though there exists a large volume of multirotor research, there is very little research into system ID of multirotors. This could be due to the fact that PID multirotor controllers can be designed with or without knowledge of the dynamics model. If the model is known then simulation can be performed to analyze the model response and initial gains can be determined. If the model is not known, (which is the case with the current multirotor research), then relay-based tuning or a trial and error method of gain tuning using test stands and a human safety pilot is performed.

Current multirotor literature employs system ID methods for propeller, motor, and mass moment of inertia modeling.

2.3.4 System ID of flapping-wing UAVs

Flapping-wing UAVs, based on biological flight methods, are just emerging. As technologies make these UAVs reliable, system ID can provide insight into unintuitive dynamics, although very little literature exists currently.

2.3.5 System ID of lighter-than-air UAVs

Lighter-than-air UAVs or commonly known as "blimps" have recently been suggested for remote sensing of extraterrestrial planets and moons where traditional Earth atmosphere-based methods would not work [81].

The lighter-than-atmosphere UAV literature uses system ID methods for controller design.

Table 2.1: Summary of UAV system ID methods and applications: single-rotor part 1

Ref.	***Data Source***	***Model***	***System ID***	***Application***
[21]	IMU, GPS, & MC	SS	CIFER	Linear SS model derived for the hover condition
[25]	-	SS	Partitioned TD grey-box: EEM for initial values, OEM for unknown model parameters	LTI MIMO SS model with 13 states
[26]	IMU	Nonlinear SS	TD OEM	ID of inertial properties
[27]	IMU, US, & PT	TF & SS	CIFER	Coupled 6-DOF linear parameter varying mode for CSD
[14]	HILS	MLP combined with NNARXM using LM	PEM	Model-based CSD
[28]	-	SS	PEM	Hover stabilization with LQG control
[29]	INS & GPS	SS	PEM	Multi-loop CSD
[30]	INS & GPS	SS	PEM	CSD
[31]	IMU & GPS	SS	PEM	Nonlinear CSD for landing on moving platforms
[32]	-	SS	PEM	CSD for yaw channel using composite nonlinear feedback control.
[33]	-	Black-box SS	PEM	Practical linear CSD
[34]	IMU & US	Linear SS	PEM	Attitude & altitude CSD.
[35]	-	Linear SS	PEM	CSD
[36]	IMU & LA	ARX, ARMAX, OEM, & BJ	FR & subspace-based method	Position control based on H-infinity control theory
[37]	IMU & GPS	SS using supervised learning	LR	Model for reinforcement learning algorithm applied to automatically learn a controller for autonomous inverted hovering

Table 2.2: Summary of UAV system ID methods and applications: single-rotor part 2

Ref.	***Data Source***	***Model***	***System ID***	***Application***
[38]	-	Apprenticeship learning algorithm	LR	Development of a differential dynamic programming controller for forward flip
[39]	-	Nonlinear SS	CMA-ES	Nonlinear dynamic model used for H-infinity CSD for attitude & heave
[40]	-	MLP	PEM using LM for training NN	Develop NN model for use with a NN based controller
[41]	IMU & GPS	ARX	PEM using LM for training recursive NN	RT sys. ID
[42]	IMU, GPS, & US	ARX	NNARXM	RT ID of longitudinal & lateral dynamics
[43]	IMU, GPS, & US	ARX	NN	Online & offline NN models for CSD
[44]	-	SS	EKF	Online parameter ID
[45]	IMU, GPS, & US	-	OKID	Sensor fault detection
[23]	IMU, GPS, & MC	frequency response to SS	FD using CIFER	Comparison of scale to full-size helicopter flight dynamics. Complete dynamic model derived for hover & cruise flight conditions
[46]	IMU & GPS	SS & acceleration prediction model	LR & CIFER	Comparison of CIFER vs. proposed Sys. ID method that captures inertial properties
[47]	-	SS	EKF, simplified UKF, augmented UKF	Comparison of 3 methods. RT onboard recursive estimation of aerodynamic derivatives.

Table 2.3: Summary of UAV system ID methods and applications: single-rotor part 3

Ref.	***Data Source***	***Model***	***System ID***	***Application***
[48]	IMU & GPS	SS	Adaptive GA & LS	Comparison of GA vs. LS. Realize precise parameter ID for linear SS model for horizontal and vertical dynamics based on test data
[49]	-	SS	LS & TLS	Comparison of LS and TLS in the presence of noise
[22]	-	Frequency response to SS	CIFER	Integrated Sys. ID methods for flight control modeling for flight test examples of the Fire Scout MQ-8B, S-76, & ARH-70A
[24]	IMU & GPS	Frequency response to SS	FD using CIFER	PID autopilot with automated frequency-sweeps for Sys. ID
[50]	-	SS	PE	Development of MATLAB/Simulink rapid software prototyping environment with sys. ID module
[51]	-	SS	TD FD	Overview of rotorcraft development
[52]	-	RFB NARX	OLS	Sys. ID method validation

Table 2.4: Summary of UAV system ID methods and applications: fixed-wing part 1

Ref.	***Data Source***	***Model***	***System ID***	***Application***
[15]	MCS	SS	LS	Post-stall perching dynamics
[16]	MCS	SS	LS	Post stall perching dynamics & quasi-steady longitudinal model for acceleration
[54]	-	Second order ARX	LS	Motor & servo modeling
[55]	IMU, GPS, & DP	linear ss	Recursive FTR (LS in FD)	RT modeling
[56]	-	SS	FD LS	CSD
[57]	IMU	Fourth-order ARX	LS	Loitering flight model for improved CSD
[58]	IMU, GPS, altimeter, & PS	SS	OEM	Nonlinear CSD
[59]	IMU, GPS, & BS	Linear SS	TD OEM & MLM	Framework for flight CSD
[60]	-	Linear ARX	SOM-based local linear modeling scheme	Development of a set of inverse controllers
[61]	IMU, PS, side-slip potentiometer, & angle of attack encoder	ARX	NN	Results validated using the RT hardware in the loop
[62]	IMU	Nonlinear SS	Model ID	CSD
[63]	IMU	SS	Batch LS	Support & validate autopilot hardware & software
[64]	IMU & GPS	FD to SS	CIFER	CSD
[65]	IMU & GPS	Fifth & first order ARX	LS	Fractional order CSD

Table 2.5: Summary of UAV system ID methods and applications: fixed-wing part 2

Ref.	*Data Source*	*Model*	*System ID*	*Application*
[66]	IMU, GPS, ADS, tachometer, potentiometers, & strain gauges	Mu-Markov parametrization	LS	Online sys. ID
[67]	IMU, PS, & wind vane	SS	Square root uKF	Online model ID for control
[68]	IMU, PS, side-slip potentiometer, & angle of attack encoder	ARX	NN	Comparison of RT online and offline NN models
[69]	-	ARX	Multi-network using NN & batch wise LM	Online and offline NN models for CSD
[70]	-	ARX & MPL	Recurrent NN & batch wise LM	Online and offline NN models for CSD
[71]	IMU, GPS, BS, & DP	SS	Online RLS	Control surface fault detection
[72]	-	Fourier transformed SS	RT FTR	Fault detection of the primary control surface, real-time estimation of the longitudinal stability and control derivatives
[73]	Carrier Phase Differential GPS	SS	Moshe Idan maximum likelihood parameter estimation, OKID, & subspace	Comparison of 3 sys. ID methods using carrier-phase differential GPS (DPDGSP) data
[74]	Wind tunnel	SS FD	For SS: EEM LS OEM MLM & for FD: LSR MLM FR	Comparison of ID methods and survey of manned and unmanned aircraft
[20]	IMU	SS	Nonlinear mapping & fuzzy ID	Comparison of ID methods
[53]	IMU, GPS, & PS	ARX, ARMAX, & BJ	PEM	Comparison of 3 models of take-off dynamics

Table 2.6: Summary of UAV system ID methods and applications: fixed-wing part 3

Ref.	***Data Source***	***Model***	***System ID***	***Application***
[75]	IMU, GPS, & PS	SS	GA based parameter ID & PEM	Comparison of the 2 sys. ID methods
[76]	IMU	SS	EKF & EMID	Comparison of the two methods
[77]	IMU & GPS	Fifth & first order ARX	LS	Comparison & fractional order (PI) CSD
[12]	IMU	FD to SS	CIFER	Baseline model used to design informative flight experiments for FD sys. ID
[78]	IMU, GPS, & PS	ARX for discrete-time,inverse Z-transform convert to continuous-time & FD for small order model	LS	Sys. ID method proposal
[79]	IMU, GPS, & PS	SS	Nonlinear constrained optimization algorithm	Undergraduate education in UAVs
[80]	-	ARX	-	Autopilot tuning

Table 2.7: Summary of UAV system ID methods and applications: multirotor and other

Ref.	***UAV Source***	***Data Type***	***Model***	***System ID***	***Application***
[82]	Multirotor	Speed sensor, & voltage sensor	TF	Step response	Sys. ID of drive system
[83]	Multirotor	-	Learned model	Coevolution of models	Automatic modeling & control
[84]	Multirotor	IMU & US	SS	LM optimization, quadratic optimization	Model of propeller, motor, and mass moment of inertia
[85]	Multirotor	-	-	Parameter ID	Comprehensive nonlinear modeling
[86]	Flapping-Wing	Capacitive displacement sensor & non-contact charge-coupled device laser displacement sensor	TF	Linear discrete-time, subspace algorithm	Verification of theoretical model
[81]	Lighter-than-air	IMU & GPS	-	PE	CSD
[87]	Lighter-than-air	MCS	Learning predictive models	GP	Reinforcement learning CSD

Chapter 3

Thesis and Research Objectives

3.1 Thesis Statement

The primary objective of this research is to evaluate the suitability of a Recursive Least Squares algorithm with an Error Filtering Online Learning scheme for identifying online the aerodynamic force and moment coefficients of the linear longitudinal equations of motion with current low-cost sensor data of a small fixed-wing unmanned aerial vehicle.

3.2 Research Objectives

1. Develop a Batch Least Squares (BLS) algorithm to identify the aerodynamic coefficients of the linear longitudinal equations of motion using flight data from low-cost sensors.

2. Develop a Recursive Least Squares (RLS) algorithm to identify the aerodynamic coefficients of the linear longitudinal equations of motion using flight data from low-cost sensors.

3. Evaluate the accuracy of the identified model from BLS and RLS compared to flight data.

4. Add the Error Filtering Online Learning (EFOL) scheme to the RLS algorithm and identify the aerodynamic coefficients of the linear longitudinal equations of motion using flight data from low-cost sensors.

5. Compare the identified models from the BLS, RLS, and the RLS with EFOL scheme, and their ability to predict flight data for various maneuvers.

6. Evaluate RLS EFOL scheme's suitability to identify aerodynamic coefficients online.

7. Outline how any shortcomings of the RLS EFOL scheme can be resolved and provide a future research direction.

Chapter 4
Aerodynamic and Mechanical Models for System Identification

4.1 Overview

This section presents the derivation of the linear longitudinal equations of motion of a general aircraft from the nonlinear equations of motion. The linear longitudinal equations of motion apply directly to small UAVs. Also the state space model of the linear longitudinal equation of motion used for system ID is presented.

4.2 Derivation of the 6 Degree of Freedom Nonlinear Equations of Motion

The equations of motion of an aircraft can be split into translational motion and rotational motion. Newton's second law for rigid-body dynamics can be used to describe both the translational and rotational motion [7] and will be used here to develop the equations of motion of the UAV. Note that for the rigid body assumption to apply, the system's mass must not change in time as is the case for this electric powered UAV. Gas powered UAVs fall under the category of a continuously varying mass system [88] and require special care when deriving the equations of motion [89].

4.2.1 Coordinate system

For clarification the coordinate system sign convention of the equations of motion is given in Fig. 4.1. This coordinate system describes the sign convention of the accelerations, velocities, positions, and angles used in the equations of motion. The control surface sign convention for the UAV is shown in Fig. 4.2.

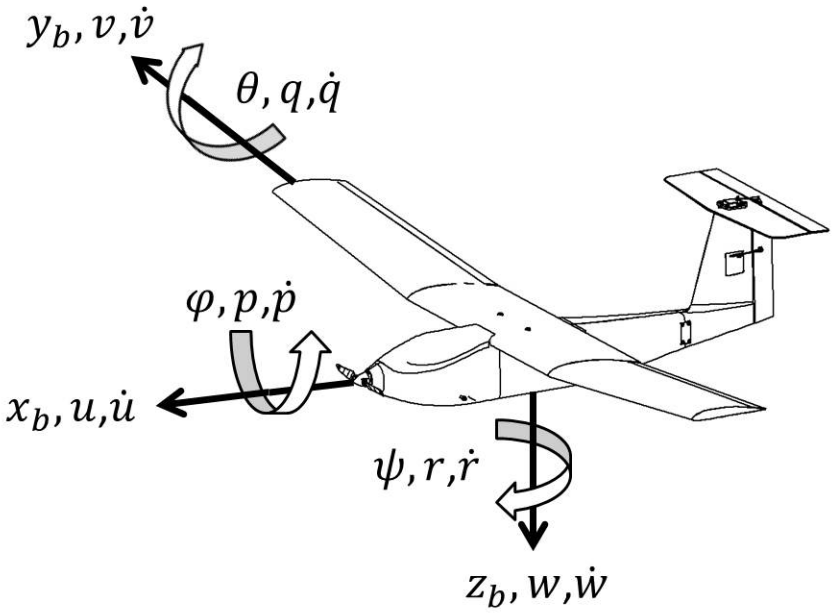

Fig. 4.1: Eq. of motion coordinate system sign convention with accelerations, velocities, positions, and angles.

4.2.2 Derivation of the 6 degree of freedom nonlinear equations of motion: translational motion

Beginning with translational motion in an inertial frame the time rate of change of the translational momentum is equal to the sum of the forces exerted on the rigid-body.

$$\Sigma \mathbf{F}_i = \frac{d\mathbf{P}_i}{dt} \tag{4.1}$$

P_i is the inertial translational momentum expressed as

$$\mathbf{P}_i = m\mathbf{V}_i \tag{4.2}$$

Substituting Eq. (4.2) into Eq. (4.1) yields the following formulation for translational motion

$$\Sigma \mathbf{F}_i = \frac{d(m\mathbf{V}_i)}{dt} \tag{4.3}$$

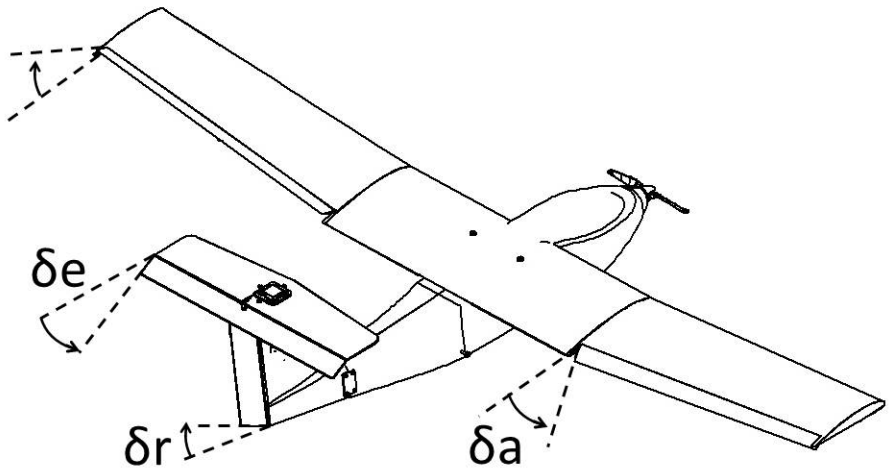

Fig. 4.2: Control surface deflection sign convention (aileron, elevator, rudder)

Again Newton's Second Law for Rigid-Body Dynamics only applies to constant mass systems. This is not to say that Newton's Second Law cannot ever be applied to a body that is loosing or gaining mass. It simply means that Newton's Second Law requires that the mass and the momentum of the entire system must be accounted for. Since m is constant and to avoid confusion with a mass varying systems, m is taken out of the time derivative using the constant factor rule in differentiation.

$$\Sigma \mathbf{F}_i = m \frac{d\mathbf{V}_i}{dt} \tag{4.4}$$

For convenience in expressing and measuring velocities and angular rates of the UAV, the inertial frame velocity vector is expressed in body-fixed frame through a transformation. This is important since most of the UAV sensors output data in the body-fixed frame. The transformation introduces additional terms into the translational and rotational equations of motion. The additional terms are due to the body-fixed rotating with respect to the inertial frame. The full derivation, as found in [90], of the transformation from inertial to body frame for the velocity vector follows. First the velocity vector is expressed in its body components.

$$\mathbf{V}_b = V_{x_b}\mathbf{i}_b + V_{y_b}\mathbf{j}_b + V_{z_b}\mathbf{k}_b \tag{4.5}$$

Then the time derivative of the velocity vector $\mathbf{V}_b$ with respect to the inertial frame is found by differentiating Eq. (4.5) as

$$\frac{d\mathbf{V}_b}{dt_i} = \frac{dV_{x_b}}{dt_b}\mathbf{i}_b + \frac{dV_{y_b}}{dt_b}\mathbf{j}_b + \frac{dV_{z_b}}{dt_b}\mathbf{k}_b + V_{x_b}\frac{d\mathbf{i}_b}{dt_i} + V_{y_b}\frac{d\mathbf{j}_b}{dt_i} + V_{z_b}\frac{d\mathbf{k}_b}{dt_i}, \tag{4.6}$$

where $\frac{d}{dt_i}$ is the time derivative with respect to the inertial frame. The first three terms of the right hand side of Eq. (4.6) are the change in $\mathbf{V}_b$ as viewed from the body frame. These three terms can be combined into the time derivative of $\mathbf{V}_b$ in the body frame by

$$\frac{d\mathbf{V}_b}{dt_b} = \frac{dV_{x_b}}{dt_b}\mathbf{i}_b + \frac{dV_{y_b}}{dt_b}\mathbf{j}_b + \frac{dV_{z_b}}{dt_b}\mathbf{k}_b. \tag{4.7}$$

The last three terms of the right-hand side of Eq. (4.6) are the change in V_b from the rotation of the body frame with respect to the inertial frame. The angular velocity of the body frame with respect to the inertial frame is expressed as ω_b. The derivatives of $\mathbf{i}_b$, $\mathbf{j}_b$, and $\mathbf{k}_b$ can be found by

$$\frac{d}{dt_i}\mathbf{i}_b = \omega_b \times \mathbf{i}_b \qquad \frac{d}{dt_i}\mathbf{j}_b = \omega_b \times \mathbf{j}_b \qquad \frac{d}{dt_i}\mathbf{k}_b = \omega_b \times \mathbf{k}_b. \tag{4.8}$$

Substituting Eq.(4.7) and Eq. (4.8) into right hand side of Eq. (4.6) yields

$$\frac{d\mathbf{V}_i}{dt_i} = \frac{d\mathbf{V}_b}{dt_b} + V_{x_b}(\omega_b \times \mathbf{i}_b) + V_{y_b}(\omega_b \times \mathbf{j}_b) + V_{z_b}(\omega_b \times \mathbf{k}_b). \tag{4.9}$$

Manipulating the last three terms of the right hand side further by

$$\frac{d\mathbf{V}_i}{dt_i} = \frac{d\mathbf{V}_b}{dt_b} + \omega_b \times (V_{x_b}\mathbf{i}_b) + \omega_b \times (V_{y_b}\mathbf{j}_b) + \omega_b \times (V_{z_b}\mathbf{k}_b) \tag{4.10}$$

$$\frac{d\mathbf{V}_i}{dt_i} = \frac{d\mathbf{V}_b}{dt_b} + \omega_b \times (V_{x_b}\mathbf{i}_b + V_{y_b}\mathbf{j}_b + V_{z_b}\mathbf{k}_b) \tag{4.11}$$

gives the desired relationship

$$\frac{d\mathbf{V}_i}{dt_i} = \frac{d\mathbf{V}_b}{dt_b} + \omega_b \times \mathbf{V}_b. \tag{4.12}$$

This relationship can now be used in Eq. (4.4) to express the time derivative of the velocity vector in terms of the body-fixed frame, which gives

$$\Sigma \mathbf{F}_b = m\frac{d\mathbf{V}_b}{dt} + \omega_b \times (m\mathbf{V}_b). \tag{4.13}$$

Keeping the equations of motion in body-fixed coordinate systems the force can be separated into surface and body forces as

$$\mathbf{F}_S + \mathbf{W} = m\frac{d\mathbf{V}_b}{dt} + \omega_b \times (m\mathbf{V}_b). \tag{4.14}$$

This is done for ease of derivation. Now the equations of translational motion are expressed in terms of their vector components starting with the terms associated with angular velocity on the right of the Eq. (4.14) as

$$\omega_b \times (m\mathbf{V}_b) = m\begin{vmatrix} i_{x_b} & i_{y_b} & i_{z_b} \\ \omega_{x_b} & \omega_{y_b} & \omega_{z_b} \\ V_{x_b} & V_{y_b} & V_{z_b} \end{vmatrix} = m\begin{bmatrix} \omega_{y_b}V_{z_b} - \omega_{z_b}V_{y_b} \\ \omega_{z_b}V_{x_b} - \omega_{x_b}V_{z_b} \\ \omega_{x_b}V_{y_b} - \omega_{y_b}V_{x_b} \end{bmatrix}. \tag{4.15}$$

Substituting Eq. (4.15) into Eq. (4.14) and expanding the rest of the terms into vector components yields

$$\begin{Bmatrix} F_{S_{x_b}} \\ F_{S_{y_b}} \\ F_{S_{z_b}} \end{Bmatrix} + \begin{Bmatrix} W_{x_b} \\ W_{y_b} \\ W_{z_b} \end{Bmatrix} = m\frac{d}{dt}\begin{Bmatrix} V_{x_b} \\ V_{y_b} \\ V_{z_b} \end{Bmatrix} + m\begin{bmatrix} \omega_{y_b}V_{z_b} - \omega_{z_b}V_{y_b} \\ \omega_{z_b}V_{x_b} - \omega_{x_b}V_{z_b} \\ \omega_{x_b}V_{y_b} - \omega_{y_b}V_{x_b} \end{bmatrix}. \tag{4.16}$$

The equations of motion are expressed here in terms of their vector components so that later the equations of motion can be split into longitudinal and lateral dynamics. Eq. (4.16)

can be rearranged as

$$m\frac{d}{dt}\begin{Bmatrix} V_{x_b} \\ V_{y_b} \\ V_{z_b} \end{Bmatrix} = \begin{bmatrix} F_{S_{x_b}} + W_{x_b} - m\omega_{y_b}V_{z_b} + m\omega_{z_b}V_{y_b} \\ F_{S_{y_b}} + W_{y_b} - m\omega_{z_b}V_{x_b} + m\omega_{x_b}V_{z_b} \\ F_{S_{z_b}} + W_{z_b} - m\omega_{x_b}V_{y_b} + m\omega_{y_b}V_{x_b} \end{bmatrix}. \tag{4.17}$$

It should be noted that this derivation of the equations of motion is for a constant mass UAV. Some UAVs change mass with time as a result of burning fuel. The equations of motion need to take into account this momentum flux. The derivation for the mass changing system can be found in [7]. Since this UAV does not change mass with time the time rate of change of the velocity is simply

$$m\begin{Bmatrix} \dot{V}_{x_b} \\ \dot{V}_{y_b} \\ \dot{V}_{z_b} \end{Bmatrix} = \begin{bmatrix} F_{x_b} + W_{x_b} - m\omega_{y_b}V_{z_b} + m\omega_{z_b}V_{y_b} \\ F_{y_b} + W_{y_b} - m\omega_{z_b}V_{x_b} + m\omega_{x_b}V_{z_b} \\ F_{z_b} + W_{z_b} - m\omega_{x_b}V_{y_b} + m\omega_{y_b}V_{x_b} \end{bmatrix}, \tag{4.18}$$

where F_b is the pseudo aerodynamic force thrust. The classical dynamics notation is replaced with the following flight dynamics notation

$$V = \begin{Bmatrix} V_{x_b} \\ V_{y_b} \\ V_{z_b} \end{Bmatrix} = \begin{Bmatrix} u \\ v \\ w \end{Bmatrix} = \begin{Bmatrix} \text{axial velocity} \\ \text{sideslip velocity} \\ \text{normal velocity} \end{Bmatrix} \tag{4.19}$$

$$\omega_b = \begin{Bmatrix} \omega_{x_b} \\ \omega_{y_b} \\ \omega_{z_b} \end{Bmatrix} = \begin{Bmatrix} p \\ q \\ r \end{Bmatrix} = \begin{Bmatrix} \text{rolling rate} \\ \text{pitching rate} \\ \text{yawing rate} \end{Bmatrix}, \tag{4.20}$$

$$m = W/g \tag{4.21}$$

and substituting in the flight dynamics notation in to Eq. (4.18) gives

$$\begin{bmatrix} W/g & 0 & 0 \\ 0 & W/g & 0 \\ 0 & 0 & W/g \end{bmatrix} \begin{Bmatrix} \dot{u} \\ \dot{v} \\ \dot{w} \end{Bmatrix} = \begin{Bmatrix} F_{xb} + W_{xb} + (rv - qw)W/g \\ F_{yb} + W_{yb} + (pw - ru)W/g \\ F_{zb} + W_{zb} + (qu - pv)W/g \end{Bmatrix} \tag{4.22}$$

4.2.3 Derivation of the 6 degree of freedom nonlinear equations of motion: rotational motion

Rotational motion can also be described in similar manner to the translational motion. From Newton's Second Law the time rate of change of the rotational momentum is equal to the sum of the moments exerted on the rigid-body in the inertial frame expressed as

$$\Sigma \mathbf{M}_i = \frac{d\mathbf{H}_i}{dt}, \tag{4.23}$$

where H_i is the inertial rotational momentum given by

$$\mathbf{H}_i = [\mathbf{I}]\omega_i. \tag{4.24}$$

Substituting Eq. (4.24) into Eq. (4.23) yields the following formulation for rotational motion

$$\Sigma \mathbf{M}_i = \frac{d([\mathbf{I}]\omega_i)}{dt}. \tag{4.25}$$

Again Newton's Second Law applies to rigid-bodies. For rotational motion this means the products of inertia are constant and can be taken out of the time derivative resulting in

$$\Sigma \mathbf{M}_i = [\mathbf{I}]\frac{d(\omega_i)}{dt}. \tag{4.26}$$

The angular velocity vector is transformed from inertial to body-fixed frame in the same manner as the translation velocity vector. The derivation for this transformation is found

in [91]. The transformation yields

$$\frac{d\omega_i}{dt_i} = \frac{d\omega_b}{dt_b} + \omega_b \times \omega_b. \tag{4.27}$$

The rotational motion can now be written in terms of the body-fixed frame as

$$\mathbf{M}_b = [\mathbf{I}]\frac{d(\omega_b)}{dt} + \omega_b \times ([\mathbf{I}]\omega_b). \tag{4.28}$$

The inertial tensor is expressed in terms of its components as

$$[\mathbf{I}] = \begin{bmatrix} I_{xx_b} & -I_{xy_b} & -I_{xz_b} \\ -I_{yx_b} & I_{yy_b} & -I_{yz_b} \\ -I_{zx_b} & -I_{zy_b} & I_{zz_b} \end{bmatrix}. \tag{4.29}$$

Since the body-fixed coordinate system is used, the product of inertia are zero due to symmetry about the y_b plane.

$$[\mathbf{I}] = \begin{bmatrix} I_{xx_b} & 0 & -I_{xz_b} \\ 0 & I_{yy_b} & 0 \\ -I_{zx_b} & 0 & I_{zz_b} \end{bmatrix} \tag{4.30}$$

If the UAV was asymmetrical about the y_b plane then the inertial tensor would be full with no zeros. Thus the angular momentum vector, $\mathbf{H}$, is

$$\mathbf{H} = [\mathbf{I}]\omega_b = \begin{bmatrix} I_{xx_b} & 0 & -I_{xz_b} \\ 0 & I_{yy_b} & 0 \\ -I_{zx_b} & 0 & I_{zz_b} \end{bmatrix} \begin{Bmatrix} \omega_{x_b} \\ \omega_{y_b} \\ \omega_{z_b} \end{Bmatrix} = \begin{Bmatrix} I_{xx_b}\omega_{x_b} - I_{xz_b}\omega_{z_b} \\ I_{yy_b}\omega_{y_b} \\ I_{zz_b}\omega_{z_b} - I_{zx_b}\omega_{x_b} \end{Bmatrix} \tag{4.31}$$

$$\omega_b \times ([\mathbf{I}]\omega) = \omega \times \mathbf{H} = \begin{vmatrix} i_{x_b} & i_{y_b} & i_{z_b} \\ \omega_{x_b} & \omega_{y_b} & \omega_{z_b} \\ H_{x_b} & H_{y_b} & H_{z_b} \end{vmatrix} = \begin{Bmatrix} \omega_{y_b} H_{z_b} - \omega_{z_b} H_{y_b} \\ \omega_{z_b} H_{x_b} - \omega_{x_b} H_{z_b} \\ \omega_{x_b} H_{y_b} - \omega_{y_b} H_{x_b} \end{Bmatrix} = \begin{Bmatrix} (I_{zz_b} - I_{yy_b})\omega_{y_b}\omega_{z_b} - I_{xz_b}\omega_{x_b}\omega_{y_b} \\ (I_{xx_b} - I_{zz_b})\omega_{x_b}\omega_{z_b} - I_{xz_b}(\omega_{x_b}^2 - \omega_{y_b}^2) \\ (I_{yy_b} - I_{xx_b})\omega_{x_b}\omega_{y_b} - I_{xz_b}\omega_{y_b}\omega_{z_b} \end{Bmatrix} \tag{4.32}$$

Substituting Eqs. (4.31) and (4.32) into Eq. (4.28)

$$\begin{bmatrix} M_{S_{x_b}} \\ M_{S_{y_b}} \\ M_{S_{z_b}} \end{bmatrix} = \begin{bmatrix} I_{xx_b} & 0 & -I_{xz_b} \\ 0 & I_{yy_b} & 0 \\ -I_{zx_b} & 0 & I_{zz_b} \end{bmatrix} \frac{d}{dt} \begin{Bmatrix} \omega_{x_b} \\ \omega_{y_b} \\ \omega_{z_b} \end{Bmatrix} + \begin{Bmatrix} (I_{zz_b} - I_{yy_b})\omega_{y_b}\omega_{z_b} - I_{xz_b}\omega_{x_b}\omega_{y_b} \\ (I_{xx_b} - I_{zz_b})\omega_{x_b}\omega_{z_b} - I_{xz_b}(\omega_{x_b}^2 - \omega_{y_b}^2) \\ (I_{yy_b} - I_{xx_b})\omega_{x_b}\omega_{y_b} - I_{xz_b}\omega_{y_b}\omega_{z_b} \end{Bmatrix} \tag{4.33}$$

Rearranging the equation

$$\begin{bmatrix} I_{xx_b} & 0 & -I_{xz_b} \\ 0 & I_{yy_b} & 0 \\ -I_{zx_b} & 0 & I_{zz_b} \end{bmatrix} \begin{Bmatrix} \dot{\omega}_{x_b} \\ \dot{\omega}_{y_b} \\ \dot{\omega}_{z_b} \end{Bmatrix} = \begin{Bmatrix} M_{x_b} + (I_{yy_b} - I_{zz_b})\omega_{y_b}\omega_{z_b} + I_{xz_b}\omega_{x_b}\omega_{y_b} \\ M_{y_b} + (I_{zz_b} - I_{xx_b})\omega_{x_b}\omega_{z_b} + I_{xz_b}(\omega_{x_b}^2 - \omega_{y_b}^2) \\ M_{z_b} + (I_{xx_b} - I_{yy_b})\omega_{x_b}\omega_{y_b} + I_{xz_b}\omega_{y_b}\omega_{z_b} \end{Bmatrix}, \tag{4.34}$$

where M_b is the pseudo moments. Applying flight dynamic notation to Eq. (4.34) gives

$$\begin{bmatrix} I_{xx_b} & 0 & -I_{xz_b} \\ 0 & I_{yy_b} & 0 \\ -I_{xz_b} & 0 & I_{zz_b} \end{bmatrix} \begin{Bmatrix} \dot{p} \\ \dot{q} \\ \dot{r} \end{Bmatrix} = \begin{Bmatrix} M_{xb} + (I_{yy_b} - I_{zz_b})qr + I_{xz_b}pq \\ M_{yb} + (I_{zz_b} - I_{xx_b})pr + I_{xz_b}(r^2 - p^2) \\ M_{zb} + (I_{xx_b} - I_{yy_b})pq - I_{xz_b}qr \end{Bmatrix} \tag{4.35}$$

4.2.4 Derivation of the 6 degree of freedom nonlinear equations of motion: translational and rotational motion combined

Combining Eqs. (4.22) and (4.35) and putting the two equations into matrix form yields the 6 DOF nonlinear equations of motion

$$\begin{bmatrix} W/g & 0 & 0 & 0 & 0 & 0 \\ 0 & W/g & 0 & 0 & 0 & 0 \\ 0 & 0 & W/g & 0 & 0 & 0 \\ 0 & 0 & 0 & I_{xx_b} & 0 & -I_{xz_b} \\ 0 & 0 & 0 & 0 & I_{yy_b} & 0 \\ 0 & 0 & 0 & -I_{xz_b} & 0 & I_{zz_b} \end{bmatrix} \begin{Bmatrix} \dot{u} \\ \dot{v} \\ \dot{w} \\ \dot{p} \\ \dot{q} \\ \dot{r} \end{Bmatrix} = \begin{Bmatrix} F_{xb} + W_{xb} + (rv - qw)W/g \\ F_{yb} + W_{yb} + (pw - ru)W/g \\ F_{zb} + W_{zb} + (qu - pv)W/g \\ M_{xb} + (I_{yy_b} - I_{zz_b})qr + I_{xz_b}pq \\ M_{yb} + (I_{zz_b} - I_{xx_b})pr + I_{xz_b}(r^2 - p^2) \\ M_{zb} + (I_{xx_b} - I_{yy_b})pq - I_{xz_b}qr \end{Bmatrix} \tag{4.36}$$

4.3 Linearized Equations of Motion

The nonlinear equations of motion for the UAV are now linearized. Given a general second-order nonlinear system given by the following differential equation

$$\ddot{x} = f(\dot{x}, x, t) \tag{4.37}$$

where $\dot{x}$ is the rate of change of the state and x is the state, it is assumed that there exists a particular solution to the differential equation, in this case a trim input of $x_0(t)$. The differential equation can be expanded in a Taylor series around the particular solution

(trim) and yields

$$\ddot{x} = f(\dot{x}_0, x_0, t) + \left.\frac{\partial f}{\partial \dot{x}}\right|_{\dot{x}=\dot{x}_0, x=x_0} (\dot{x} - \dot{x}_0) + \left.\frac{\partial f}{\partial x}\right|_{\dot{x}=\dot{x}_0, x=x_0} (x - x_0) + \cdots \tag{4.38}$$

The higher order terms of the Taylor series expansion can be ignored by assuming that the general solution does not deviate far from the particular solution. The particular solutions satisfies

$$\ddot{x}_0 = f(\dot{x}_0, x_0, t) \tag{4.39}$$

and making the substitution for deviation from particular solution of the form

$$\Delta\dot{x} = \dot{x} - \dot{x}_0 \tag{4.40}$$

$$\Delta x = x - x_0 \tag{4.41}$$

Using (4.39), (4.40) and, (4.41) in (4.38) yields

$$\ddot{x} = \ddot{x}_0 + \left.\frac{\partial f}{\partial \dot{x}}\right|_{\dot{x}=\dot{x}_0, x=x_0} \Delta\dot{x} + \left.\frac{\partial f}{\partial x}\right|_{\dot{x}=\dot{x}_0, x=x_0} \Delta x \tag{4.42}$$

which can be expressed as the particular solution plus the deviation from the particular solution

$$\ddot{x} = \ddot{x}_0 + \Delta\ddot{x} \tag{4.43}$$

Thus a small deviation or disturbance from the particular solution must satisfy

$$\Delta\ddot{x} = \left.\frac{\partial f}{\partial \dot{x}}\right|_{\dot{x}=\dot{x}_0, x=x_0} \Delta\dot{x} + \left.\frac{\partial f}{\partial \dot{x}}\right|_{\dot{x}=\dot{x}_0, x=x_0} \Delta x \tag{4.44}$$

Note that this equation is linear in Δx as a result of evaluating the derivatives for the known particular solution and is known as *small-disturbance theory.*

Now applying small-disturbance theory to the rigid-body 6 degree of freedom (DOF) equations of motion (4.36) and each of its variables as an equilibrium state value plus some

small disturbance from the equilibrium state. The equilibrium state is steady level flight.

$$\begin{array}{ccc}
u = u_0 + \Delta u & v = v_0 + \Delta v & w = w_0 + \Delta w \\
p = p_0 + \Delta p & q = q_0 + \Delta q & r = r_0 + \Delta r \\
x_f = x_0 + \Delta x_f & y_f = y_0 + \Delta y_f & z_f = z_0 + \Delta z_f \\
\phi = \phi_0 + \Delta\phi & \theta = \theta_0 + \Delta\theta & \psi = \psi_0 + \Delta\psi \\
F_{x_b} = F_{x_b 0} + \Delta F_{x_b} & F_{y_b} = F_{y_b 0} + \Delta F_{y_b} & F_{z_b} = F_{z_b 0} + \Delta F_{z_b} \\
W_{x_b} = W_{x_b 0} + \Delta W_{x_b} & W_{y_b} = W_{y_b 0} + \Delta W_{y_b} & W_{z_b} = W_{z_b 0} + \Delta W_{z_b} \\
M_{x_b} = M_{x_b 0} + \Delta M_{x_b} & M_{y_b} = M_{y_b 0} + \Delta M_{y_b} & M_{z_b} = M_{z_b 0} + \Delta M_{z_b} \\
\delta a = \delta a_0 + \Delta\delta a & \delta e = \delta e_0 + \Delta\delta e & \delta r = \delta r_0 + \Delta\delta r
\end{array} \tag{4.45}$$

The sum of the moments and forces must balance to produce the equilibrium state of steady level flight. Thus

$$\begin{gathered}
u_0 = V_0,\ x_0 = (V_{wx_f} + V_0 \cos\theta_0)t,\ y_0 = V_{wy_f} t,\ z_0 = (V_{wz_f} - V_0 \sin\theta_0)t \\
F_{x_b 0} = -W_{x_b 0},\ F_{z_b 0} = -W_{z_b 0} \\
v_0 = w_0 = p_0 = q_0 = r_0 = \phi_0 = \psi_0 = F_{y_b 0} = W_{y_b 0} = \mathbf{M}_0 = 0
\end{gathered} \tag{4.46}$$

Substituting the results from balancing the forces and moments in Eq. (4.46) for the equilibrium state into Eq. (4.45) gives

$$\begin{array}{ccc}
u = V_0 + \Delta u & v = \Delta v & w = \Delta w \\
p = \Delta p & q = \Delta q & r = \Delta r \\
x_f = (V_{wx_f} + V_0 \cos\theta_0)t + \Delta x_f & y_f = V_{wy_f} t + \Delta y_f & z_f = (V_{wz_f} - V_0 \sin\theta_0)t + \Delta z_f \\
\phi = \Delta\phi & \theta = \theta_0 + \Delta\theta & \psi = \Delta\psi \\
F_{x_b} = -W_{x_b 0} + \Delta F_{x_b} & F_{y_b} = \Delta F_{y_b} & F_{z_b} = -W_{z_b 0} + \Delta F_{z_b} \\
W_{x_b} = W_{x_b 0} + \Delta W_{x_b} & W_{y_b} = \Delta W_{y_b} & W_{z_b} = W_{z_b 0} + \Delta W_{z_b} \\
M_{x_b} = \Delta M_{x_b} & M_{y_b} = \Delta M_{y_b} & M_{z_b} = \Delta M_{z_b} \\
\delta a = \delta a_0 + \Delta\delta a & \delta e = \delta e_0 + \Delta\delta e & \delta r = \delta r_0 + \Delta\delta r
\end{array} \tag{4.47}$$

Substituting in the small-disturbance variables, Eq. (4.36) becomes

$$\begin{bmatrix} W/g & 0 & 0 & 0 & 0 & 0 \\ 0 & W/g & 0 & 0 & 0 & 0 \\ 0 & 0 & W/g & 0 & 0 & 0 \\ 0 & 0 & 0 & I_{xx_b} & 0 & -I_{xz_b} \\ 0 & 0 & 0 & 0 & I_{yy_b} & 0 \\ 0 & 0 & 0 & -I_{xz_b} & 0 & I_{zz_b} \end{bmatrix} \begin{Bmatrix} \Delta\dot{u} \\ \Delta\dot{v} \\ \Delta\dot{w} \\ \Delta\dot{p} \\ \Delta\dot{q} \\ \Delta\dot{r} \end{Bmatrix} = \begin{Bmatrix} -W_{x_b0} + \Delta F_{x_b} + W_{x_b0} + \Delta W_{x_b} + (\Delta r\Delta v - \Delta q\Delta w)W/g \\ \Delta F_{y_b} + \Delta W_{y_b} + (\Delta p\Delta w - \Delta r(V_0 + \Delta u))W/g \\ -W_{z_b0} + \Delta F_{z_b} + W_{z_b0} + \Delta W_{z_b} + (\Delta q(V_0 + \Delta u) - \Delta p\Delta v)W/g \\ \Delta M_{x_b} + (I_{yy_b} - I_{zz_b})\Delta q\Delta r + I_{xz_b}\Delta p\Delta q \\ \Delta M_{y_b} + (I_{zz_b} - I_{xx_b})\Delta p\Delta r + I_{xz_b}(\Delta r^2 - \Delta p^2) \\ \Delta M_{z_b} + (I_{xx_b} - I_{yy_b})\Delta p\Delta q - I_{xz_b}\Delta q\Delta r \end{Bmatrix} \tag{4.48}$$

Canceling out terms and neglecting the product of small disturbances gives

$$\begin{bmatrix} W/g & 0 & 0 & 0 & 0 & 0 \\ 0 & W/g & 0 & 0 & 0 & 0 \\ 0 & 0 & W/g & 0 & 0 & 0 \\ 0 & 0 & 0 & I_{xx_b} & 0 & -I_{xz_b} \\ 0 & 0 & 0 & 0 & I_{yy_b} & 0 \\ 0 & 0 & 0 & -I_{xz_b} & 0 & I_{zz_b} \end{bmatrix} \begin{Bmatrix} \Delta\dot{u} \\ \Delta\dot{v} \\ \Delta\dot{w} \\ \Delta\dot{p} \\ \Delta\dot{q} \\ \Delta\dot{r} \end{Bmatrix} = \begin{Bmatrix} \Delta F_{x_b} + \Delta W_{x_b} \\ \Delta F_{y_b} + \Delta W_{y_b} - \Delta r(V_0)W/g \\ \Delta F_{z_b} + \Delta W_{z_b} + \Delta q(V_0)W/g \\ \Delta M_{x_b} \\ \Delta M_{y_b} \\ \Delta M_{z_b} \end{Bmatrix} \tag{4.49}$$

The small-disturbance aerodynamic forces are functions of translational and rotational velocities, translational accelerations, and the deflection of the control surfaces. These aerodynamic forces can be approximated as

$$\begin{Bmatrix} \Delta F_{x_b} \\ \Delta F_{y_b} \\ \Delta F_{z_b} \end{Bmatrix} = \begin{bmatrix} \frac{\partial F_{x_b}}{\partial u} & \frac{\partial F_{x_b}}{\partial v} & \frac{\partial F_{x_b}}{\partial w} \\ \frac{\partial F_{y_b}}{\partial u} & \frac{\partial F_{y_b}}{\partial v} & \frac{\partial F_{y_b}}{\partial w} \\ \frac{\partial F_{z_b}}{\partial u} & \frac{\partial F_{z_b}}{\partial v} & \frac{\partial F_{z_b}}{\partial w} \end{bmatrix} \begin{Bmatrix} \Delta u \\ \Delta v \\ \Delta w \end{Bmatrix} + \begin{bmatrix} \frac{\partial F_{x_b}}{\partial p} & \frac{\partial F_{x_b}}{\partial q} & \frac{\partial F_{x_b}}{\partial r} \\ \frac{\partial F_{y_b}}{\partial p} & \frac{\partial F_{y_b}}{\partial q} & \frac{\partial F_{y_b}}{\partial r} \\ \frac{\partial F_{z_b}}{\partial p} & \frac{\partial F_{z_b}}{\partial q} & \frac{\partial F_{z_b}}{\partial r} \end{bmatrix} \begin{Bmatrix} \Delta p \\ \Delta q \\ \Delta r \end{Bmatrix}$$
$$+ \begin{bmatrix} \frac{\partial F_{x_b}}{\partial \dot{u}} & \frac{\partial F_{x_b}}{\partial \dot{v}} & \frac{\partial F_{x_b}}{\partial \dot{w}} \\ \frac{\partial F_{y_b}}{\partial \dot{u}} & \frac{\partial F_{y_b}}{\partial \dot{v}} & \frac{\partial F_{y_b}}{\partial \dot{w}} \\ \frac{\partial F_{z_b}}{\partial \dot{u}} & \frac{\partial F_{z_b}}{\partial \dot{v}} & \frac{\partial F_{z_b}}{\partial \dot{w}} \end{bmatrix} \begin{Bmatrix} \Delta \dot{u} \\ \Delta \dot{v} \\ \Delta \dot{w} \end{Bmatrix} + \begin{bmatrix} \frac{\partial F_{x_b}}{\partial \delta a} & \frac{\partial F_{x_b}}{\partial \delta e} & \frac{\partial F_{x_b}}{\partial \delta r} \\ \frac{\partial F_{y_b}}{\partial \delta a} & \frac{\partial F_{y_b}}{\partial \delta e} & \frac{\partial F_{y_b}}{\partial \delta r} \\ \frac{\partial F_{z_b}}{\partial \delta a} & \frac{\partial F_{z_b}}{\partial \delta e} & \frac{\partial F_{z_b}}{\partial \delta r} \end{bmatrix} \begin{Bmatrix} \Delta \delta a \\ \Delta \delta e \\ \Delta \delta r \end{Bmatrix} \tag{4.50}$$

The small-disturbance aerodynamic moments are also functions of translational and rotational velocities, translational accelerations, and the deflection of the control surfaces. These aerodynamic moments can be approximated as

$$\begin{Bmatrix} \Delta M_{x_b} \\ \Delta M_{y_b} \\ \Delta M_{z_b} \end{Bmatrix} = \begin{bmatrix} \frac{\partial M_{x_b}}{\partial u} & \frac{\partial M_{x_b}}{\partial v} & \frac{\partial M_{x_b}}{\partial w} \\ \frac{\partial M_{y_b}}{\partial u} & \frac{\partial M_{y_b}}{\partial v} & \frac{\partial M_{y_b}}{\partial w} \\ \frac{\partial M_{z_b}}{\partial u} & \frac{\partial M_{z_b}}{\partial v} & \frac{\partial M_{z_b}}{\partial w} \end{bmatrix} \begin{Bmatrix} \Delta u \\ \Delta v \\ \Delta w \end{Bmatrix} + \begin{bmatrix} \frac{\partial M_{x_b}}{\partial p} & \frac{\partial M_{x_b}}{\partial q} & \frac{\partial M_{x_b}}{\partial r} \\ \frac{\partial M_{y_b}}{\partial p} & \frac{\partial M_{y_b}}{\partial q} & \frac{\partial M_{y_b}}{\partial r} \\ \frac{\partial M_{z_b}}{\partial p} & \frac{\partial M_{z_b}}{\partial q} & \frac{\partial M_{z_b}}{\partial r} \end{bmatrix} \begin{Bmatrix} \Delta p \\ \Delta q \\ \Delta r \end{Bmatrix}$$
$$+ \begin{bmatrix} \frac{\partial M_{x_b}}{\partial \dot{u}} & \frac{\partial M_{x_b}}{\partial \dot{v}} & \frac{\partial M_{x_b}}{\partial \dot{w}} \\ \frac{\partial M_{y_b}}{\partial \dot{u}} & \frac{\partial M_{y_b}}{\partial \dot{v}} & \frac{\partial M_{y_b}}{\partial \dot{w}} \\ \frac{\partial M_{z_b}}{\partial \dot{u}} & \frac{\partial M_{z_b}}{\partial \dot{v}} & \frac{\partial M_{z_b}}{\partial \dot{w}} \end{bmatrix} \begin{Bmatrix} \Delta \dot{u} \\ \Delta \dot{v} \\ \Delta \dot{w} \end{Bmatrix} + \begin{bmatrix} \frac{\partial M_{x_b}}{\partial \delta a} & \frac{\partial M_{x_b}}{\partial \delta e} & \frac{\partial M_{x_b}}{\partial \delta r} \\ \frac{\partial M_{y_b}}{\partial \delta a} & \frac{\partial M_{y_b}}{\partial \delta e} & \frac{\partial M_{y_b}}{\partial \delta r} \\ \frac{\partial M_{z_b}}{\partial \delta a} & \frac{\partial M_{z_b}}{\partial \delta e} & \frac{\partial M_{z_b}}{\partial \delta r} \end{bmatrix} \begin{Bmatrix} \Delta \delta a \\ \Delta \delta e \\ \Delta \delta r \end{Bmatrix} \tag{4.51}$$

These derivatives are all evaluated at the equilibrium flight condition of steady level flight. Equations (4.50) and (4.51) only depend on the motion of the aircraft relative to the surrounding air and not on the orientation relative to the Earth's surface. This is the reasoning for choosing the atmosphere-fixed coordinates. Side slip acceleration terms have little effect on lift or vorticity and can be neglected. Symmetry also cancels out some of the derivative

terms. Thus the following derivatives shall be used in the linearized equations of motion.

$$\begin{gathered}\frac{\partial F_{y_b}}{\partial \dot{u}} = \frac{\partial F_{x_b}}{\partial \dot{v}} = \frac{\partial F_{y_b}}{\partial \dot{v}} = \frac{\partial F_{z_b}}{\partial \dot{v}} = \frac{\partial F_{y_b}}{\partial \dot{w}} = 0 \\ \frac{\partial M_{x_b}}{\partial \dot{u}} = \frac{\partial M_{z_b}}{\partial \dot{u}} = \frac{\partial M_{x_b}}{\partial \dot{v}} = \frac{\partial M_{y_b}}{\partial \dot{v}} = \frac{\partial M_{z_b}}{\partial \dot{v}} = \frac{\partial M_{x_b}}{\partial \dot{w}} = \frac{\partial M_{z_b}}{\partial \dot{w}} = 0\end{gathered} \tag{4.52}$$

All of the following derivatives evaluated at the equilibrium flight condition of steady level flight can also be eliminated based on symmetry of axial forces [7].

$$\begin{gathered}\frac{\partial F_{x_b}}{\partial v} = \frac{\partial F_{y_b}}{\partial u} = \frac{\partial F_{y_b}}{\partial w} = \frac{\partial F_{z_b}}{\partial v} = 0 \\ \frac{\partial F_{x_b}}{\partial p} = \frac{\partial F_{x_b}}{\partial r} = \frac{\partial F_{y_b}}{\partial q} = \frac{\partial F_{z_b}}{\partial p} = \frac{\partial F_{z_b}}{\partial r} = 0 \\ \frac{\partial F_{x_b}}{\partial \delta a} = \frac{\partial F_{x_b}}{\partial \delta r} = \frac{\partial F_{y_b}}{\partial \delta e} = \frac{\partial F_{z_b}}{\partial \delta a} = \frac{\partial F_{z_b}}{\partial \delta r} = 0 \\ \frac{\partial M_{x_b}}{\partial u} = \frac{\partial M_{x_b}}{\partial w} = \frac{\partial M_{y_b}}{\partial v} = \frac{\partial M_{z_b}}{\partial u} = \frac{\partial M_{z_b}}{\partial w} = 0 \\ \frac{\partial M_{x_b}}{\partial p} = \frac{\partial M_{x_b}}{\partial r} = \frac{\partial M_{y_b}}{\partial q} = \frac{\partial M_{z_b}}{\partial p} = \frac{\partial M_{z_b}}{\partial r} = 0 \\ \frac{\partial M_{x_b}}{\partial \delta e} = \frac{\partial M_{y_b}}{\partial \delta a} = \frac{\partial M_{y_b}}{\partial \delta r} = \frac{\partial M_{z_b}}{\partial \delta e} = 0\end{gathered} \tag{4.53}$$

Gravitational force components are only dependent on the Euler angles as shown.

$$\begin{Bmatrix} W_{x_b} \\ W_{y_b} \\ W_{z_b} \end{Bmatrix} = W \begin{Bmatrix} -\sin(\theta_0) \\ \sin(\phi_0)\cos(\theta_0) \\ \cos(\phi_0)\cos(\theta_0) \end{Bmatrix} \tag{4.54}$$

For the equilibrium flight condition of steady level flight, the gravitational force derivatives are

$$\begin{Bmatrix} \Delta W_{x_b} \\ \Delta W_{y_b} \\ \Delta W_{z_b} \end{Bmatrix} = \begin{bmatrix} \frac{\partial W_{x_b}}{\partial \phi} & \frac{\partial W_{x_b}}{\partial \theta} & \frac{\partial W_{x_b}}{\partial \psi} \\ \frac{\partial W_{y_b}}{\partial \phi} & \frac{\partial W_{y_b}}{\partial \theta} & \frac{\partial W_{y_b}}{\partial \psi} \\ \frac{\partial W_{z_b}}{\partial \phi} & \frac{\partial W_{z_b}}{\partial \theta} & \frac{\partial W_{z_b}}{\partial \psi} \end{bmatrix} \begin{Bmatrix} \Delta \phi \\ \Delta \theta \\ \Delta \psi \end{Bmatrix}$$
$$= \begin{bmatrix} 0 & -W\cos(\theta_0) & 0 \\ W\cos(\phi_0)\cos(\theta_0) & -W\sin(\phi_0)\sin(\theta_0) & 0 \\ W\sin(\phi_0)\cos(\theta_0) & -W\cos(\phi_0)\sin(\theta_0) & 0 \end{bmatrix} \begin{Bmatrix} \Delta \phi \\ \Delta \theta \\ \Delta \psi \end{Bmatrix} \tag{4.55}$$
$$= \begin{bmatrix} 0 & -W\cos(\theta_0) & 0 \\ W\cos(\theta_0) & 0 & 0 \\ 0 & -W\sin(\theta_0) & 0 \end{bmatrix} \begin{Bmatrix} \Delta \phi \\ \Delta \theta \\ \Delta \psi \end{Bmatrix}$$

where $\phi_0 = 0$. Now using all previous approximations and assumptions for the forces and moments gives

$$\begin{Bmatrix} \Delta F_{x_b} + \Delta W_{x_b} \\ \Delta F_{y_b} + \Delta W_{y_b} \\ \Delta F_{z_b} + \Delta W_{z_b} \end{Bmatrix} = \begin{bmatrix} F_{x_b,u} & 0 & F_{x_b,w} \\ 0 & F_{y_b,v} & 0 \\ F_{z_b,u} & 0 & F_{z_b,w} \end{bmatrix} \begin{Bmatrix} \Delta u \\ \Delta v \\ \Delta w \end{Bmatrix} + \begin{bmatrix} 0 & F_{x_b,q} & 0 \\ F_{y_b,p} & 0 & F_{y_b,r} \\ 0 & F_{z_b,q} & 0 \end{bmatrix} \begin{Bmatrix} \Delta p \\ \Delta q \\ \Delta r \end{Bmatrix}$$
$$+ \begin{bmatrix} F_{x_b,\dot{u}} & 0 & F_{x_b,\dot{w}} \\ 0 & 0 & 0 \\ F_{z_b,\dot{u}} & 0 & F_{z_b,\dot{w}} \end{bmatrix} \begin{Bmatrix} \Delta \dot{u} \\ \Delta \dot{v} \\ \Delta \dot{w} \end{Bmatrix} + \begin{bmatrix} 0 & F_{x_b,\delta e} & 0 \\ F_{y_b},\delta a & 0 & F_{y_b,\delta r} \\ 0 & F_{z_b,\delta e} & 0 \end{bmatrix} \begin{Bmatrix} \Delta \delta a \\ \Delta \delta e \\ \Delta \delta r \end{Bmatrix} + \tag{4.56}$$
$$\begin{bmatrix} 0 & -W\cos(\theta_0) & 0 \\ W\cos(\theta_0) & 0 & 0 \\ 0 & -W\sin(\theta_0) & 0 \end{bmatrix} \begin{Bmatrix} \Delta \phi \\ \Delta \theta \\ \Delta \psi \end{Bmatrix}$$

$$\begin{Bmatrix} \Delta M_{x_b} \\ \Delta M_{y_b} \\ \Delta M_{z_b} \end{Bmatrix} = \begin{bmatrix} 0 & M_{x_b,v} & 0 \\ M_{y_b,u} & 0 & M_{y_b,w} \\ 0 & M_{z_b,v} & 0 \end{bmatrix} \begin{Bmatrix} \Delta u \\ \Delta v \\ \Delta w \end{Bmatrix} + \begin{bmatrix} M_{x_b,p} & 0 & M_{x_b,r} \\ 0 & M_{y_b,q} & 0 \\ M_{z_b,p} & 0 & M_{z_b,r} \end{bmatrix} \begin{Bmatrix} \Delta p \\ \Delta q \\ \Delta r \end{Bmatrix}$$
$$+ \begin{bmatrix} 0 & 0 & 0 \\ M_{y_b,\dot{u}} & 0 & M_{y_b,\dot{w}} \\ 0 & 0 & 0 \end{bmatrix} \begin{Bmatrix} \Delta \dot{u} \\ \Delta \dot{v} \\ \Delta \dot{w} \end{Bmatrix} + \begin{bmatrix} M_{x_b,\delta a} & 0 & M_{x_b,\delta r} \\ 0 & M_{y_b}, \delta e & 0 \\ M_{z_b,\delta a} & 0 & M_{z_b,\delta r} \end{bmatrix} \begin{Bmatrix} \Delta \delta a \\ \Delta \delta e \\ \Delta \delta r \end{Bmatrix} \tag{4.57}$$

Note that the force and moment notation ($\frac{\partial F_{x_b}}{\partial u}$) has been simplified ($F_{x_b,u}$). Also note that control inputs: $\Delta\delta a$, $\Delta\delta e$, and $\Delta\delta r$ are respectively the change in the aileron, elevator, and rudder deflection.

Now small-disturbance theory can also be applied to the six first-order differential equations relating time rate of change of position and orientation yielding,

$$\begin{Bmatrix} \dot{x}_f \\ \dot{y}_f \\ \dot{z}_f \end{Bmatrix} = \begin{bmatrix} C_\theta C_\psi & S_\phi S_\theta C_\psi - C_\phi S_\psi & C_\phi S_\theta C_\psi + S_\phi S_\psi \\ C_\theta S_\psi & S_\phi S_\theta S_\psi + C_\phi C_\psi & C_\phi S_\theta S_\psi - S_\phi C_\psi \\ -S_\theta & S_\phi C_\theta & C_\phi C_\theta \end{bmatrix} \begin{Bmatrix} u \\ v \\ w \end{Bmatrix} + \begin{Bmatrix} V_{wx_f} \\ V_{wy_f} \\ V_{wz_f} \end{Bmatrix}$$
$$\begin{Bmatrix} \dot{\phi} \\ \dot{\theta} \\ \dot{\psi} \end{Bmatrix} = \begin{bmatrix} 1 & S_\phi S_\theta / C_\theta & C_\phi S_\theta / C_\theta \\ 0 & C_\phi & -S_\phi \\ 0 & S_\phi / C_\theta & C_\phi / C_\theta \end{bmatrix} \begin{Bmatrix} p \\ q \\ r \end{Bmatrix} \tag{4.58}$$

where V_{wx_f}, V_{wy_f}, and V_{wz_f} are the wind velocity vectors. Using small angle approximations and small-disturbance variables,

$$\begin{array}{lll} \sin(\phi) \cong \Delta\phi & \sin(\theta) \cong \sin(\theta_0) + \cos(\theta_0)\Delta\theta & \sin(\psi) \cong \Delta\psi \\ \cos(\phi) \cong 1 & \cos(\theta) \cong \cos(\theta_0) - \sin(\theta_0)\Delta\theta & \cos(\psi) \cong 1 \end{array} \tag{4.59}$$

Eq. (4.58) becomes

$$\begin{aligned}
&\begin{Bmatrix} V_{wx_f} + V_0 C_{\theta_0} + \Delta\dot{x}_f \\ V_{wy_f} + \Delta\dot{y}_f \\ V_{wz_f} - V_0 S_{\theta_0} + \Delta\dot{z}_f \end{Bmatrix} \\
&= \begin{bmatrix} C_{\theta_0} - S_{\theta_0}\Delta\theta & S_{\theta_0}\Delta\phi - \Delta\psi & S_{\theta_0} + C_{\theta_0}\Delta\theta \\ C_{\theta_0}\Delta\psi & 1 & S_{\theta_0}\Delta\psi - \Delta\phi \\ -S_{\theta_0} - C_{\theta_0}\Delta\theta & C_{\theta_0}\Delta\phi & C_{\theta_0} - S_{\theta_0}\Delta\theta \end{bmatrix} \begin{Bmatrix} V_0 + \Delta u \\ \Delta v \\ \Delta w \end{Bmatrix} + \begin{Bmatrix} V_{wx_f} \\ V_{wy_f} \\ V_{wz_f} \end{Bmatrix} \qquad (4.60) \\
&\begin{Bmatrix} \Delta\dot{\phi} \\ \Delta\dot{\theta} \\ \Delta\dot{\psi} \end{Bmatrix} = \begin{bmatrix} 1 & S_\phi\Delta\phi/C_{\theta_0} & S_{\theta_0}/C_{\theta_0} + \Delta\theta/C_{\theta_0}^2 \\ 0 & 1 & -\Delta\phi \\ 0 & \Delta\phi/C_{\theta_0} & 1/C_\theta + S_{\theta_0}\Delta\theta/C_{\theta_0}^2 \end{bmatrix} \begin{Bmatrix} \Delta p \\ \Delta q \\ \Delta r \end{Bmatrix}
\end{aligned}$$

Neglecting second-order terms (any small angle multiplied by another small angle) and assuming a zero wind velocity, Eq. (4.60) becomes

$$\begin{aligned}
\begin{Bmatrix} \Delta\dot{x}_f \\ \Delta\dot{y}_f \\ \Delta\dot{z}_f \\ \Delta\dot{\phi} \\ \Delta\dot{\theta} \\ \Delta\dot{\psi} \end{Bmatrix} &= \begin{bmatrix} \cos(\theta_0) & 0 & \sin(\theta_0) & 0 & 0 & 0 \\ 0 & 1 & 0 & 0 & 0 & 0 \\ -\sin(\theta_0) & 0 & \cos(\theta_0) & 0 & 0 & 0 \\ 0 & 0 & 0 & 1 & 0 & \tan(\theta_0) \\ 0 & 0 & 0 & 0 & 1 & 0 \\ 0 & 0 & 0 & 0 & 0 & \sec(\theta_0) \end{bmatrix} \begin{Bmatrix} \Delta u \\ \Delta v \\ \Delta w \\ \Delta p \\ \Delta q \\ \Delta r \end{Bmatrix} \\
&+ \begin{bmatrix} 0 & -V_0\sin(\theta_0) & 0 \\ 0 & 0 & V_0\cos(\theta_0) \\ 0 & -V_0\cos(\theta_0) & 0 \\ 0 & 0 & 0 \\ 0 & 0 & 0 \\ 0 & 0 & 0 \end{bmatrix} \begin{Bmatrix} \Delta\phi \\ \Delta\theta \\ \Delta\psi \end{Bmatrix}
\end{aligned} \qquad (4.61)$$

Applying these results to the rigid-body 6-DOF equations of motion gives

$$\begin{bmatrix} W/g - F_{x_b,\dot{u}} & 0 & -F_{x_b,\dot{w}} & 0 & 0 & 0 & 0 & 0 & 0 & 0 & 0 & 0 \\ 0 & W/g & 0 & 0 & 0 & 0 & 0 & 0 & 0 & 0 & 0 & 0 \\ -F_{z_b,\dot{u}} & 0 & W/g - F_{z_b,\dot{w}} & 0 & 0 & 0 & 0 & 0 & 0 & 0 & 0 & 0 \\ 0 & 0 & 0 & I_{xx_b} & 0 & -I_{xz_b} & 0 & 0 & 0 & 0 & 0 & 0 \\ -M_{y_b,\dot{u}} & 0 & -M_{y_b,\dot{w}} & 0 & I_{yy_b} & 0 & 0 & 0 & 0 & 0 & 0 & 0 \\ 0 & 0 & 0 & -I_{xz_b} & 0 & I_{zz_b} & 0 & 0 & 0 & 0 & 0 & 0 \\ 0 & 0 & 0 & 0 & 0 & 0 & 1 & 0 & 0 & 0 & 0 & 0 \\ 0 & 0 & 0 & 0 & 0 & 0 & 0 & 1 & 0 & 0 & 0 & 0 \\ 0 & 0 & 0 & 0 & 0 & 0 & 0 & 0 & 1 & 0 & 0 & 0 \\ 0 & 0 & 0 & 0 & 0 & 0 & 0 & 0 & 0 & 1 & 0 & 0 \\ 0 & 0 & 0 & 0 & 0 & 0 & 0 & 0 & 0 & 0 & 1 & 0 \\ 0 & 0 & 0 & 0 & 0 & 0 & 0 & 0 & 0 & 0 & 0 & 1 \end{bmatrix} \begin{Bmatrix} \Delta\dot{u} \\ \Delta\dot{v} \\ \Delta\dot{w} \\ \Delta\dot{p} \\ \Delta\dot{q} \\ \Delta\dot{r} \\ \Delta\dot{x}_f \\ \Delta\dot{y}_f \\ \Delta\dot{z}_f \\ \Delta\dot{\phi} \\ \Delta\dot{\theta} \\ \Delta\dot{\psi} \end{Bmatrix} = \begin{bmatrix} 0 & F_{x_b,\delta e} & 0 \\ F_{y_b,\delta a} & 0 & F_{y_b,\delta r} \\ 0 & F_{z_b,\delta e} & 0 \\ M_{x_b,\delta a} & 0 & M_{x_b,\delta r} \\ 0 & M_{y_b,\delta e} & 0 \\ M_{z_b,\delta a} & 0 & M_{z_b,\delta r} \\ 0 & 0 & 0 \\ 0 & 0 & 0 \\ 0 & 0 & 0 \\ 0 & 0 & 0 \\ 0 & 0 & 0 \\ 0 & 0 & 0 \end{bmatrix} \begin{Bmatrix} \Delta\delta a \\ \Delta\delta e \\ \Delta\delta r \end{Bmatrix} \quad (4.62)$$

$$
+\begin{bmatrix}
F_{x_b,u} & 0 & F_{x_b,w} & 0 & F_{x_b,q} & 0 & 0 & 0 & 0 & 0 & -W\cos(\theta_0) & 0 \\
0 & F_{y_b,v} & 0 & F_{y_b,p} & 0 & F_{y_b,r} - V_0 W/g & 0 & 0 & 0 & W\cos(\theta_0) & 0 & 0 \\
F_{z_b,u} & 0 & F_{z_b,w} & 0 & F_{z_b,q} + V_0 W/g & 0 & 0 & 0 & 0 & 0 & -W\sin(\theta_0) & 0 \\
0 & M_{x_b,v} & 0 & M_{x_b,p} & 0 & M_{x_b,r} & 0 & 0 & 0 & 0 & 0 & 0 \\
M_{y_b,u} & 0 & M_{y_b,w} & 0 & M_{y_b,q} & 0 & 0 & 0 & 0 & 0 & 0 & 0 \\
0 & M_{z_b,v} & 0 & M_{z_b,p} & 0 & M_{z_b,r} & 0 & 0 & 0 & 0 & 0 & 0 \\
\cos(\theta_0) & 0 & \sin(\theta_0) & 0 & 0 & 0 & 0 & 0 & 0 & 0 & -V_0\sin(\theta_0) & 0 \\
0 & 1 & 0 & 0 & 0 & 0 & 0 & 0 & 0 & 0 & 0 & V_0\cos(\theta_0) \\
-\sin(\theta_0) & 0 & \cos(\theta_0) & 0 & 0 & 0 & 0 & 0 & 0 & 0 & -V_0\cos(\theta_0) & 0 \\
0 & 0 & 0 & 1 & 0 & \tan(\theta_0) & 0 & 0 & 0 & 0 & 0 & 0 \\
0 & 0 & 0 & 0 & 1 & 0 & 0 & 0 & 0 & 0 & 0 & 0 \\
0 & 0 & 0 & 0 & 0 & \sec(\theta_0) & 0 & 0 & 0 & 0 & 0 & 0
\end{bmatrix}
\begin{Bmatrix}
\Delta u \\ \Delta v \\ \Delta w \\ \Delta p \\ \Delta q \\ \Delta r \\ \Delta x_f \\ \Delta y_f \\ \Delta z_f \\ \Delta \phi \\ \Delta \theta \\ \Delta \psi
\end{Bmatrix} \tag{4.63}
$$

4.4 Force and Moment Derivatives

Now the equations for the derivatives of the forces and moments will be derived beginning by expressing the total airspeed in terms of its components u, v, and w.

$$V = \sqrt{u^2 + v^2 + w^2} \tag{4.64}$$

The aerodynamic angles α, angle of attack and β, side slip angle and their approximations in terms of components of velocity are given as

$$\alpha = \tan^{-1}(\frac{w}{u}) \cong \frac{w}{u} \tag{4.65}$$

$$\beta = \tan^{-1}(\frac{v}{u}) \cong \frac{v}{u} \tag{4.66}$$

Now consider a function $\mathscr{F}$ which is defined in terms of total velocity, aerodynamic angle and, side slip angle: $\mathscr{F}(V, \alpha, \beta)$. The change in the function with respect to axial velocity is

$$\frac{\partial \mathscr{F}}{\partial u} = \frac{\partial \mathscr{F}}{\partial V}\frac{\partial V}{\partial u} + \frac{\partial \mathscr{F}}{\partial \alpha}\frac{\partial \alpha}{\partial u} + \frac{\partial \mathscr{F}}{\partial \beta}\frac{\partial \beta}{\partial u} \tag{4.67}$$

Angle of attack is not a function of side slip velocity, so the change of the function with respect to side slip velocity is

$$\frac{\partial \mathscr{F}}{\partial v} = \frac{\partial \mathscr{F}}{\partial V}\frac{\partial V}{\partial v} + \cancelto{0}{\frac{\partial \mathscr{F}}{\partial \alpha}\frac{\partial \alpha}{\partial v}} + \frac{\partial \mathscr{F}}{\partial \beta}\frac{\partial \beta}{\partial v} = \frac{\partial \mathscr{F}}{\partial V}\frac{\partial V}{\partial v} + \frac{\partial \mathscr{F}}{\partial \beta}\frac{\partial \beta}{\partial v} \tag{4.68}$$

Similarly sideslip angle is not a function of normal velocity using the approximation for sideslip angle given in Eq. (4.66), thus the change of the function with respect to normal velocity is

$$\frac{\partial \mathscr{F}}{\partial w} = \frac{\partial \mathscr{F}}{\partial V}\frac{\partial V}{\partial w} + \frac{\partial \mathscr{F}}{\partial \alpha}\frac{\partial \alpha}{\partial w} + \cancelto{0}{\frac{\partial \mathscr{F}}{\partial \beta}\frac{\partial \beta}{\partial w}} = \frac{\partial \mathscr{F}}{\partial V}\frac{\partial V}{\partial w} + \frac{\partial \mathscr{F}}{\partial \alpha}\frac{\partial \alpha}{\partial w} \tag{4.69}$$

Finding the components of the partials of V with respect to u, v, w gives

$$\frac{\partial V}{\partial u} = \frac{u}{\sqrt{u^2 + v^2 + w^2}} \qquad \frac{\partial V}{\partial v} = \frac{v}{\sqrt{u^2 + v^2 + w^2}} \qquad \frac{\partial V}{\partial w} = \frac{w}{\sqrt{u^2 + v^2 + w^2}} \tag{4.70}$$

and the small angle approximation for the partials of the aerodynamic angles gives

$$\frac{\partial \alpha}{\partial u} \cong -\frac{w}{u^2} \qquad \frac{\partial \alpha}{\partial v} \cong 0 \qquad \frac{\partial \alpha}{\partial w} \cong \frac{1}{u} \tag{4.71}$$

$$\frac{\partial \beta}{\partial u} \cong -\frac{v}{u^2} \qquad \frac{\partial \beta}{\partial v} \cong \frac{1}{u} \qquad \frac{\partial \beta}{\partial v} \cong 0 \tag{4.72}$$

Applying the equilibrium state of steady level flight of the components of velocity

$$\begin{Bmatrix} u \\ v \\ w \end{Bmatrix} = \begin{Bmatrix} V_0 \\ 0 \\ 0 \end{Bmatrix} \tag{4.73}$$

to Eq. (4.70), (4.71), and (4.72) yields

$$\frac{\partial V}{\partial u} = 1 \tag{4.74}$$

$$\frac{\partial V}{\partial v} = \frac{\partial V}{\partial w} = \frac{\partial \alpha}{\partial u} = \frac{\partial \beta}{\partial u} = 0 \tag{4.75}$$

$$\frac{\partial \alpha}{\partial w} \cong \frac{\partial \beta}{\partial v} \cong \frac{1}{V_0} \tag{4.76}$$

Thus

$$\frac{\partial \mathscr{F}}{\partial u} = \frac{\partial \mathscr{F}}{\partial V} \tag{4.77}$$

$$\frac{\partial \mathscr{F}}{\partial v} = \frac{1}{V_0}\frac{\partial \mathscr{F}}{\partial \beta} \tag{4.78}$$

$$\frac{\partial \mathscr{F}}{\partial w} = \frac{1}{V_0}\frac{\partial \mathscr{F}}{\partial \alpha} \tag{4.79}$$

Now the sum of the forces and moments will be shown and used to define the partial derivatives developed in the previous sets of equations. The forces and moments acting on the aircraft are due to; gravity, aerodynamic loading, and thrust. Starting with the force

balance

$$\boldsymbol{F}+\boldsymbol{W}=\frac{1}{2}\rho V^2 S_w \begin{Bmatrix} C_X \\ C_Y \\ C_Z \end{Bmatrix} + T \begin{Bmatrix} \cos(\alpha_{T0}) \\ 0 \\ -\sin(\alpha_{T0}) \end{Bmatrix} + W \begin{Bmatrix} -\sin(\theta) \\ \sin(\phi)\cos(\theta) \\ \cos(\phi)\cos(\theta) \end{Bmatrix} \tag{4.80}$$

and moment balance

$$\boldsymbol{M}=\frac{1}{2}\rho V^2 S_w \begin{Bmatrix} b_w C_\ell \\ \bar{c}_w C_m \\ b_w C_n \end{Bmatrix} + \begin{Bmatrix} 0 \\ z_T T\cos(\alpha_{T0}) + x_T T\sin(\alpha_{T0}) \\ 0 \end{Bmatrix} \tag{4.81}$$

where ρ is the air density, S_w is the wing planform area, α_{T0} is the thrust angle of attack, C_X, C_Y, and C_Z are the x, y, and z components of aerodynamic force coefficients, T is the thrust force, x_T and z_T are the x and z components of the center of thrust, b_w is the main wing span, $\bar{c}_w$ and C_ℓ, C_m, and C_n are the roll, pitch, and yaw moment coefficients . The sum of the forces and moments can be expressed in terms of lift and drag and applying the equilibrium state of steady level flight yields

$$\frac{1}{2}\rho V^2 S_w \begin{Bmatrix} C_X \\ C_Y \\ C_Z \\ b_w C_\ell \\ \bar{c}_w C_m \\ b_w C_n \end{Bmatrix} = \frac{1}{2}\rho V^2 S_w \begin{Bmatrix} -C_D \\ 0 \\ -C_L \\ 0 \\ \bar{c}_w C_m \\ 0 \end{Bmatrix} = \begin{Bmatrix} -T\cos(\alpha_{T0}) + W\sin(\theta_0) \\ 0 \\ T\sin(\alpha_{T0}) - W\cos(\theta_0) \\ 0 \\ -z_T T\cos(\alpha_{T0}) - x_T T\sin(\alpha_{T0}) \\ 0 \end{Bmatrix} \tag{4.82}$$

where C_L is the lift coefficient and C_D is the drag coefficient. Assuming the thrust vector is aligned with the center of gravity and the direction of flight the partials of the forces with

respect to velocity are

$$\begin{aligned}\frac{\partial F_{x_b}}{\partial V} &= \frac{\partial}{\partial V}\left[\tfrac{1}{2}\rho V^2 S_w C_X + T\cos(\alpha_{T0}) - W\sin(\theta_0)\right] \\ &= \rho V S_w\left(C_X + \tfrac{V}{2}\tfrac{\partial C_X}{\partial V}\right) + \tfrac{\partial T}{\partial V}\cos(\alpha_{T0}) \\ &= \rho V S_w\left[\left(C_L + \tfrac{V}{2}\tfrac{\partial C_L}{\partial V}\right)\cos(\alpha) - \left(C_D + \tfrac{V}{2}\tfrac{\partial C_D}{\partial V}\right)\sin(\alpha)\right] + \tfrac{\partial T}{\partial V}\cos(\alpha_{T0})\end{aligned} \tag{4.83}$$

$$\frac{\partial F_{y_b}}{\partial V} = \frac{\partial}{\partial V}\left[\tfrac{1}{2}\rho V^2 S_w C_Y + W\sin(\phi)\cos(\theta)\right] = \rho V S_w\left(C_Y + \tfrac{V}{2}\tfrac{\partial C_Y}{\partial V}\right) \tag{4.84}$$

$$\begin{aligned}\frac{\partial F_{z_b}}{\partial V} &= \frac{\partial}{\partial V}\left[\tfrac{1}{2}\rho V^2 S_w C_Z - T\sin(\alpha_{T0}) - W\cos(\phi)cos(\theta)\right] \\ &= \rho V S_w\left(C_Z + \tfrac{V}{2}\tfrac{\partial C_Z}{\partial V}\right) - \tfrac{\partial T}{\partial V}\sin(\alpha_{T0}) \\ &= \rho V S_w\left[-\left(C_L + \tfrac{V}{2}\tfrac{\partial C_L}{\partial V}\right)\cos(\alpha) - \left(C_D + \tfrac{V}{2}\tfrac{\partial C_D}{\partial V}\right)\sin(\alpha)\right] - \tfrac{\partial T}{\partial V}\sin(\alpha_{T0})\end{aligned} \tag{4.85}$$

and the partials of the moments with respect to velocity are

$$\frac{\partial M_{x_b}}{\partial V} = \frac{\partial}{\partial V}\left(\tfrac{1}{2}\rho V^2 S_w b_w C_\ell\right) = \rho V S_w b_w\left(C_\ell + \tfrac{V}{2}\tfrac{\partial C_\ell}{\partial V}\right) \tag{4.86}$$

$$\begin{aligned}\frac{\partial M_{y_b}}{\partial V} &= \frac{\partial}{\partial V}\left[\tfrac{1}{2}\rho V^2 S_w \bar{c}_w C_m + z_T T\cos(\alpha_{T0}) - x_T T\sin(\alpha_{T0})\right] \\ &= \rho V S_w \bar{c}_w\left(C_m + \tfrac{V}{2}\tfrac{\partial C_m}{\partial V}\right) + \tfrac{\partial T}{\partial V}\left[z_T T\cos(\alpha_{T0}) - x_T T\sin(\alpha_{T0})\right]\end{aligned} \tag{4.87}$$

$$\frac{\partial M_{z_b}}{\partial V} = \frac{\partial}{\partial V}\left(\tfrac{1}{2}\rho V^2 S_w b_w C_n\right) = \rho V S_w b_w\left(C_n + \tfrac{V}{2}\tfrac{\partial C_n}{\partial V}\right) \tag{4.88}$$

Again these partial derivatives are evaluated at the equilibrium flight condition of steady level flight. Only axial force, normal force and pitching moment depend on angle of attack,

the derivatives with respect to α are

$$\begin{aligned}\frac{\partial F_{x_b}}{\partial \alpha} &= \frac{\partial}{\partial \alpha}\left[\tfrac{1}{2}\rho V^2 S_w C_X + T\cos(\alpha_{T0}) - W\sin(\theta_0)\right] = \tfrac{1}{2}\rho V^2 S_w \tfrac{\partial C_X}{\partial \alpha} \\ &= \tfrac{1}{2}\rho V^2 S_w \left[\tfrac{\partial C_L}{\partial \alpha}\sin(\alpha) + C_L\cos(\alpha) - \tfrac{\partial C_D}{\partial \alpha}\cos(\alpha) + C_D\sin(\alpha)\right]\end{aligned} \tag{4.89}$$

$$\begin{aligned}\frac{\partial F_{z_b}}{\partial \alpha} &= \frac{\partial}{\partial \alpha}\left[\tfrac{1}{2}\rho V^2 S_w C_Z - T\sin(\alpha_{T0}) + W\cos(\phi)\cos(\theta_0)\right] = \tfrac{1}{2}\rho V^2 S_w \tfrac{\partial C_Z}{\partial \alpha} \\ &= \tfrac{1}{2}\rho V^2 S_w \left[-\tfrac{\partial C_L}{\partial \alpha}\cos(\alpha) + C_L\sin(\alpha) - \tfrac{\partial C_D}{\partial \alpha}\sin(\alpha) - C_D\cos(\alpha)\right]\end{aligned} \tag{4.90}$$

$$\frac{\partial M_{y_b}}{\partial \alpha} = \frac{\partial}{\partial \alpha}\left[\tfrac{1}{2}\rho V^2 S_w \bar{c}_w C_m + z_T T\cos(\alpha_{T0}) + x_T T\sin(\alpha_{T0})\right] = \tfrac{1}{2}\rho V^2 S_w \bar{c}_w \tfrac{\partial C_m}{\partial \alpha} \tag{4.91}$$

With respect to axial velocity u

$$F_{x_b,u} = \frac{\partial F_{x_b}}{\partial V} = \rho V_0 S_w \left(C_X + \tfrac{V_0}{2} C_{X,u}\right) + T_{,V}\cos(\alpha) \tag{4.92}$$

$$F_{y_b,u} = \frac{\partial F_{y_b}}{\partial V} = \rho V_0 S_w \left(C_Y + \tfrac{V_0}{2} C_{Y,u}\right) = 0 \tag{4.93}$$

$$F_{z_b,u} = \frac{\partial F_{z_b}}{\partial V} = \rho V_0 S_w \left(C_Z + \tfrac{V_0}{2} C_{Z,u}\right) - T_{,V}\sin(\alpha) \tag{4.94}$$

$$M_{x_b,u} = \frac{\partial M_{x_b}}{\partial V} = \rho V_0 S_w b_w \left(C_\ell + \tfrac{V_0}{2} C_{\ell,u}\right) = 0 \tag{4.95}$$

$$\begin{aligned} M_{y_b,u} &= \tfrac{\partial M_{y_b}}{\partial V} = \rho V_0 S_w \bar{c}_w \left(C_m + \tfrac{V_0}{2} C_{m,u} \right) + T_{,V} \left[z_T \cos(\alpha_{T0}) + x_T \sin(\alpha_{T0}) \right] \\ &= \rho V_0 S_w \bar{c}_w \left(C_m + \tfrac{V_0}{2} C_{m,u} \right) + z_{T0} T_{,V} \end{aligned} \tag{4.96}$$

$$M_{z_b,u} = \frac{\partial M_{z_b}}{\partial V} = \rho V_0 S_w b_w \left(C_n + \tfrac{V_0}{2} C_{n,u} \right) = 0 \tag{4.97}$$

Derivatives with respect to normal velocity w

$$\begin{aligned} F_{x_b,w} &\equiv \tfrac{\partial F_{x_b}}{\partial w} = \tfrac{1}{V_0} \tfrac{\partial F_{x_b}}{\partial \alpha} = \tfrac{1}{2} \rho V_0 S_w C_{X,\alpha} \\ F_{z_b,w} &\equiv \tfrac{\partial F_{z_b}}{\partial w} = \tfrac{1}{V_0} \tfrac{\partial F_{z_b}}{\partial \alpha} = \tfrac{1}{2} \rho V_0 S_w C_{Z,\alpha} \\ M_{y_b,w} &\equiv \tfrac{\partial M_{y_b}}{\partial w} = \tfrac{1}{V_0} \tfrac{\partial M_{y_b}}{\partial \alpha} = \tfrac{1}{2} \rho V_0 S_w \bar{c}_w C_{m,\alpha} \\ F_{y_b,w} &= M_{x_b,w} = M_{z_b,w} = 0 \end{aligned} \tag{4.98}$$

Derivatives with respect to side slip velocity v

$$\begin{aligned} F_{y_b,v} &\equiv \tfrac{\partial F_{y_b}}{\partial v} = \tfrac{1}{V_0} \tfrac{\partial F_{y_b}}{\partial \beta} = \tfrac{1}{2} \rho V_0 S_w C_{Y,\beta} \\ M_{x_b,v} &\equiv \tfrac{\partial M_{x_b}}{\partial v} = \tfrac{1}{V_0} \tfrac{\partial M_{x_b}}{\partial \beta} = \tfrac{1}{2} \rho V_0 S_w b_w C_{\ell,\beta} \\ M_{z_b,v} &\equiv \tfrac{\partial M_{z_b}}{\partial v} = \tfrac{1}{V_0} \tfrac{\partial M_{z_b}}{\partial \beta} = \tfrac{1}{2} \rho V_0 S_w b_w C_{n,\beta} \\ F_{x_b,v} &= F_{z_b,v} = M_{y_b,v} = 0 \end{aligned} \tag{4.99}$$

Derivatives with respect to roll rate p

$$\begin{aligned} F_{y_b,p} &\equiv \tfrac{\partial F_{y_b}}{\partial p} = \tfrac{1}{2} \rho V_0^2 S_w C_{Y,p} \\ M_{x_b,p} &\equiv \tfrac{\partial M_{x_b}}{\partial p} = \tfrac{1}{2} \rho V_0^2 S_w b_w C_{\ell,p} \\ M_{z_b,p} &\equiv \tfrac{\partial M_{z_b}}{\partial p} = \tfrac{1}{2} \rho V_0^2 S_w b_w C_{n,p} \\ F_{x_b,p} &= F_{z_b,p} = M_{y_b,p} = 0 \end{aligned} \tag{4.100}$$

Derivatives with respect to pitch rate q

$$\begin{aligned} F_{x_b,q} &\equiv \tfrac{\partial F_{x_b}}{\partial q} = \tfrac{1}{2}\rho V_0^2 S_w C_{X,q} \\ F_{z_b,q} &\equiv \tfrac{\partial F_{z_b}}{\partial q} = \tfrac{1}{2}\rho V_0^2 S_w C_{Z,q} \\ M_{y_b,q} &\equiv \tfrac{\partial M_{y_b}}{\partial q} = \tfrac{1}{2}\rho V_0^2 S_w \bar{c}_w C_{m,q} \\ F_{y_b,q} &= M_{x_b,q} = M_{z_b,q} = 0 \end{aligned} \tag{4.101}$$

Derivatives with respect to pitch rate r

$$\begin{aligned} F_{y_b,r} &\equiv \tfrac{\partial F_{y_b}}{\partial r} = \tfrac{1}{2}\rho V_0^2 S_w C_{Y,r} \\ M_{x_b,r} &\equiv \tfrac{\partial M_{x_b}}{\partial r} = \tfrac{1}{2}\rho V_0^2 S_w b_w C_{\ell,r} \\ M_{z_b,r} &\equiv \tfrac{\partial M_{z_b}}{\partial r} = \tfrac{1}{2}\rho V_0^2 S_w b_w C_{n,r} \\ F_{x_b,r} &= F_{z_b,r} = M_{y_b,r} = 0 \end{aligned} \tag{4.102}$$

Longitudinal derivatives with respect to translational acceleration $\dot{u}$ and $\dot{w}$

$$\begin{aligned} F_{x_b,\dot{u}} &\cong F_{z_b,\dot{u}} \cong M_{y_b,\dot{u}} \cong F_{x_b,\dot{w}} \cong 0 \\ F_{z_b,\dot{w}} &\equiv \tfrac{\partial F_{z_b}}{\partial \dot{w}} = \tfrac{1}{V_0}\tfrac{\partial F_{z_b}}{\partial \dot{\alpha}} = \tfrac{1}{2}\rho V_0 S_w C_{Z,\dot{\alpha}} \\ M_{y_b,\dot{w}} &\equiv \tfrac{\partial M_{y_b}}{\partial \dot{w}} = \tfrac{1}{V_0}\tfrac{\partial M_{y_b}}{\partial \dot{\alpha}} = \tfrac{1}{2}\rho V_0 S_w \bar{c}_w C_{m,\dot{\alpha}} \end{aligned} \tag{4.103}$$

The lateral derivatives with respect to translational acceleration are either zero or negligible and will be treated as such.

The following section give the equations for the derivatives with respect to control surface deflection starting with aileron deflection, δa

$$\begin{aligned} F_{y_b,\delta a} &\equiv \tfrac{\partial F_{y_b}}{\partial \delta a} = \tfrac{1}{2}\rho V_0^2 S_w C_{Y,\delta a} \\ M_{x_b,\delta a} &\equiv \tfrac{\partial M_{x_b}}{\partial \delta a} = \tfrac{1}{2}\rho V_0^2 S_w b_w C_{\ell,\delta a} \\ M_{z_b,\delta a} &\equiv \tfrac{\partial M_{z_b}}{\partial \delta a} = \tfrac{1}{2}\rho V_0^2 S_w b_w C_{n,\delta a} \\ F_{x_b,\delta a} &= F_{z_b,\delta a} = M_{y_b,\delta a} = 0 \end{aligned} \tag{4.104}$$

Derivatives with respect to elevator deflection, δe

$$\begin{aligned} F_{x_b,\delta e} &\equiv \tfrac{\partial F_{x_b}}{\partial \delta e} = \tfrac{1}{2}\rho V_0^2 S_w C_{X,\delta e} \\ F_{z_b,\delta e} &\equiv \tfrac{\partial F_{z_b}}{\partial \delta e} = \tfrac{1}{2}\rho V_0^2 S_w C_{Z,\delta e} \\ M_{y_b,\delta e} &\equiv \tfrac{\partial M_{y_b}}{\partial \delta e} = \tfrac{1}{2}\rho V_0^2 S_w \bar{c}_w C_{m,\delta e} \\ F_{y_b,\delta e} &= M_{x_b,\delta e} = M_{z_b,\delta e} = 0 \end{aligned} \tag{4.105}$$

Derivatives with respect to rudder deflection, δr

$$\begin{aligned} F_{y_b,\delta r} &\equiv \tfrac{\partial F_{y_b}}{\partial \delta r} = \tfrac{1}{2}\rho V_0^2 S_w C_{Y,\delta r} \\ M_{x_b,\delta r} &\equiv \tfrac{\partial M_{x_b}}{\partial \delta r} = \tfrac{1}{2}\rho V_0^2 S_w b_w C_{\ell,\delta r} \\ M_{z_b,\delta r} &\equiv \tfrac{\partial M_{z_b}}{\partial \delta r} = \tfrac{1}{2}\rho V_0^2 S_w b_w C_{n,\delta r} \\ F_{x_b,\delta r} &= F_{z_b,\delta r} = M_{y_b,\delta r} = 0 \end{aligned} \tag{4.106}$$

The partial derivatives of the forces and moments are grouped together to provide a reference for dimensional derivatives of the 6 DOF equations of motion.

$$
\begin{array}{lll}
F_{x_b,\dot{u}} \cong 0 & F_{z_b,\dot{u}} \cong 0 & M_{y_b,\dot{u}} \cong 0 \\
F_{x_b,\dot{w}} \cong 0 & F_{z_b,\dot{w}} = \frac{1}{2}\rho V_0 S_w C_{Z,\dot{\alpha}} & M_{y_b,\dot{w}} = \frac{1}{2}\rho V_0 S_w \bar{c}_w C_{m,\dot{\alpha}}
\end{array}
\tag{4.107}
$$

$$
\begin{aligned}
F_{x_b,u} &= \rho V_0 S_w \left(C_X + \tfrac{V_0}{2} C_{X,u} \right) + T_{,V} \cos(\alpha_{T0}) \\
F_{z_b,u} &= \rho V_0 S_w \left(C_Z + \tfrac{V_0}{2} C_{Z,u} \right) - T_{,V} \sin(\alpha_{T0}) \\
M_{y_b,u} &= \rho V_0 S_w \bar{c}_w \left(C_m + \tfrac{V_0}{2} C_{m,u} \right) + z_{T0} T_{,V}
\end{aligned}
\tag{4.108}
$$

$$
\begin{array}{lll}
F_{x_b,w} = \frac{1}{2}\rho V_0 S_w C_{X,\alpha} & F_{z_b,w} = \frac{1}{2}\rho V_0 S_w C_{Z,\alpha} & M_{y_b,w} = \frac{1}{2}\rho V_0 S_w \bar{c}_w C_{m,\alpha} \\
F_{y_b,v} = \frac{1}{2}\rho V_0 S_w C_{Y,\beta} & M_{x_b,v} = \frac{1}{2}\rho V_0 S_w b_w C_{\ell,\beta} & M_{z_b,v} = \frac{1}{2}\rho V_0 S_w b_w C_{n,\beta} \\
F_{y_b,p} = \frac{1}{2}\rho V_0^2 S_w C_{Y,p} & M_{x_b,p} = \frac{1}{2}\rho V_0^2 S_w b_w C_{\ell,p} & M_{z_b,p} = \frac{1}{2}\rho V_0^2 S_w b_w C_{n,p} \\
F_{x_b,q} = \frac{1}{2}\rho V_0^2 S_w C_{X,q} & F_{z_b,q} = \frac{1}{2}\rho V_0^2 S_w C_{Z,q} & M_{y_b,q} = \frac{1}{2}\rho V_0^2 S_w \bar{c}_w C_{m,q} \\
F_{y_b,r} = \frac{1}{2}\rho V_0^2 S_w C_{Y,r} & M_{x_b,r} = \frac{1}{2}\rho V_0^2 S_w b_w C_{\ell,r} & M_{z_b,r} = \frac{1}{2}\rho V_0^2 S_w b_w C_{n,r} \\
F_{y_b,\delta a} = \frac{1}{2}\rho V_0^2 S_w C_{Y,\delta a} & M_{x_b,\delta a} = \frac{1}{2}\rho V_0^2 S_w b_w C_{\ell,\delta a} & M_{z_b,\delta a} = \frac{1}{2}\rho V_0^2 S_w b_w C_{n,\delta a} \\
F_{x_b,\delta e} = \frac{1}{2}\rho V_0^2 S_w C_{X,\delta e} & F_{z_b,\delta e} = \frac{1}{2}\rho V_0^2 S_w C_{Z,\delta e} & M_{y_b,\delta e} = \frac{1}{2}\rho V_0^2 S_w \bar{c}_w C_{m,\delta e} \\
F_{y_b,\delta r} = \frac{1}{2}\rho V_0^2 S_w C_{Y,\delta r} & M_{x_b,\delta r} = \frac{1}{2}\rho V_0^2 S_w b_w C_{\ell,\delta r} & M_{z_b,\delta r} = \frac{1}{2}\rho V_0^2 S_w b_w C_{n,\delta r}
\end{array}
\tag{4.109}
$$

4.5 Linearized Uncoupled Equations of Motion

The linearized equations of motion, Eq. (4.62), can be decoupled in to longitudinal and lateral dynamics [7]. The linearized longitudinal equations of motion are

$$\begin{bmatrix} W/g - F_{x_b,\dot{u}} & -F_{x_b,\dot{w}} & 0 & 0 & 0 & 0 \\ -F_{z_b,\dot{u}} & W/g - F_{z_b,\dot{w}} & 0 & 0 & 0 & 0 \\ -M_{y_b,\dot{u}} & -M_{y_b,\dot{w}} & I_{yy_b} & 0 & 0 & 0 \\ 0 & 0 & 0 & 1 & 0 & 0 \\ 0 & 0 & 0 & 0 & 1 & 0 \\ 0 & 0 & 0 & 0 & 0 & 1 \end{bmatrix} \begin{Bmatrix} \Delta\dot{u} \\ \Delta\dot{w} \\ \Delta\dot{q} \\ \Delta\dot{x}_f \\ \Delta\dot{z}_f \\ \Delta\dot{\theta} \end{Bmatrix} = \begin{bmatrix} F_{x_b,\delta e} \\ F_{z_b,\delta e} \\ M_{y_b,\delta e} \\ 0 \\ 0 \\ 0 \end{bmatrix} \Delta\delta e$$
$$+ \begin{bmatrix} F_{x_b,u} & F_{x_b,w} & F_{x_b,q} & 0 & 0 & -W\cos(\theta_0) \\ F_{z_b,u} & F_{z_b,w} & F_{z_b,q} + V_0 W/g & 0 & 0 & -W\sin(\theta_0) \\ M_{y_b,u} & M_{y_b,w} & M_{y_b,q} & 0 & 0 & 0 \\ \cos(\theta_0) & \sin(\theta_0) & 0 & 0 & 0 & -V_0\sin(\theta_0) \\ -\sin(\theta_0) & \cos(\theta_0) & 0 & 0 & 0 & -V_0\cos(\theta_0) \\ 0 & 0 & 1 & 0 & 0 & 0 \end{bmatrix} \begin{Bmatrix} \Delta u \\ \Delta w \\ \Delta q \\ \Delta x_f \\ \Delta z_f \\ \Delta\theta \end{Bmatrix} \tag{4.110}$$

where the force and moment derivatives are defined in Eqs. (4.107)-(4.109). The linear longitudinal equations of motion can be further simplified by removing the rows and columns associated with Δx_f and Δz_f. This is due to the translation and rotational being independent of Δx_f and Δz_f. The linear longitudinal equations of motion can now be expressed

as

$$\begin{bmatrix} W/g - F_{x_b,\dot{u}} & -F_{x_b,\dot{w}} & 0 & 0 \\ -F_{z_b,\dot{u}} & W/g - F_{z_b,\dot{w}} & 0 & 0 \\ -M_{y_b,\dot{u}} & -M_{y_b,\dot{w}} & I_{yy_b} & 0 \\ 0 & 0 & 0 & 1 \end{bmatrix} \begin{Bmatrix} \Delta\dot{u} \\ \Delta\dot{w} \\ \Delta\dot{q} \\ \Delta\dot{\theta} \end{Bmatrix} = \begin{bmatrix} F_{x_b,\delta e} \\ F_{z_b,\delta e} \\ M_{y_b,\delta e} \\ 0 \end{bmatrix} \Delta\delta e + \begin{bmatrix} F_{x_b,u} & F_{x_b,w} & F_{x_b,q} & -W\cos(\theta_0) \\ F_{z_b,u} & F_{z_b,w} & F_{z_b,q} + V_0 W/g & -W\sin(\theta_0) \\ M_{y_b,u} & M_{y_b,w} & M_{y_b,q} & 0 \\ 0 & 0 & 1 & 0 \end{bmatrix} \begin{Bmatrix} \Delta u \\ \Delta w \\ \Delta q \\ \Delta\theta \end{Bmatrix} \tag{4.111}$$

4.6 State Space Model for System Identification

In this section the state space model for system ID is derived from Eq. (4.111). The force and moment derivatives on the left side of the equation are assumed to be small and are neglected [7]. This leaves a diagonal matrix of mass and mass moment of inertia. Then both sides of the equation are divided by the mass or mass moment of inertia, leaving an identity matrix that multiplies the state derivatives. The state space model of the linear longitudinal equations of motion is

$$\begin{Bmatrix} \Delta\dot{u} \\ \Delta\dot{w} \\ \Delta\dot{q} \\ \Delta\dot{\theta} \end{Bmatrix} = \begin{bmatrix} \frac{F_{x_b,\delta e}}{W/g} \\ \frac{F_{z_b,\delta e}}{W/g} \\ \frac{M_{y_b,\delta e}}{I_{yy_b}} \\ 0 \end{bmatrix} \Delta\delta e + \begin{bmatrix} \frac{F_{x_b,u}}{W/g} & \frac{F_{x_b,w}}{W/g} & \frac{F_{x_b,q}}{W/g} & \frac{-W\cos(\theta_0)}{W/g} \\ \frac{F_{z_b,u}}{W/g} & \frac{F_{z_b,w}}{W/g} & \frac{F_{z_b,q}+V_0 W/g}{W/g} & \frac{-W\sin(\theta_0)}{W/g} \\ \frac{M_{y_b,u}}{I_{yy_b}} & \frac{M_{y_b,w}}{I_{yy_b}} & \frac{M_{y_b,q}}{I_{yy_b}} & 0 \\ 0 & 0 & 1 & 0 \end{bmatrix} \begin{Bmatrix} \Delta u \\ \Delta w \\ \Delta q \\ \Delta\theta \end{Bmatrix} \tag{4.112}$$

4.7 Chapter Summary

The derivation from Newton's Second Law to nonlinear equations of motion, linearized

equations of motion, linearized longitudinal equation of motion, and the state space model for system ID was presented. The main equations are summarized here.

Newton's Second Law for translational and rotational dynamics.

$$\Sigma F_i = \frac{dP_i}{dt} \tag{4.113}$$

$$\Sigma M_i = \frac{dH_i}{dt} \tag{4.114}$$

Translational and rotational eqution of motion.

$$F_S + W = m\frac{dV_b}{dt} + \omega_b \times (mV_b) \tag{4.115}$$

$$M_b = [I]\frac{d(\omega_b)}{dt} + \omega_b \times ([I]\omega_b) \tag{4.116}$$

6 degree of freedom nonlinear equations of motion.

$$\begin{bmatrix} W/g & 0 & 0 & 0 & 0 & 0 \\ 0 & W/g & 0 & 0 & 0 & 0 \\ 0 & 0 & W/g & 0 & 0 & 0 \\ 0 & 0 & 0 & I_{xx_b} & 0 & -I_{xz_b} \\ 0 & 0 & 0 & 0 & I_{yy_b} & 0 \\ 0 & 0 & 0 & -I_{xz_b} & 0 & I_{zz_b} \end{bmatrix} \begin{Bmatrix} \dot{u} \\ \dot{v} \\ \dot{w} \\ \dot{p} \\ \dot{q} \\ \dot{r} \end{Bmatrix} = \begin{Bmatrix} F_{xb} + W_{xb} + (rv - qw)W/g \\ F_{yb} + W_{yb} + (pw - ru)W/g \\ F_{zb} + W_{zb} + (qu - pv)W/g \\ M_{xb} + (I_{yy_b} - I_{zz_b})qr + I_{xz_b}pq \\ M_{yb} + (I_{zz_b} - I_{xx_b})pr + I_{xz_b}(r^2 - p^2) \\ M_{zb} + (I_{xx_b} - I_{yy_b})pq - I_{xz_b}qr \end{Bmatrix} \tag{4.117}$$

Linear longitudinal equations of motion.

$$\begin{bmatrix} W/g - F_{x_b,\dot{u}} & -F_{x_b,\dot{w}} & 0 & 0 & 0 & 0 \\ -F_{z_b,\dot{u}} & W/g - F_{z_b,\dot{w}} & 0 & 0 & 0 & 0 \\ -M_{y_b,\dot{u}} & -M_{y_b,\dot{w}} & I_{yy_b} & 0 & 0 & 0 \\ 0 & 0 & 0 & 1 & 0 & 0 \\ 0 & 0 & 0 & 0 & 1 & 0 \\ 0 & 0 & 0 & 0 & 0 & 1 \end{bmatrix} \begin{Bmatrix} \Delta\dot{u} \\ \Delta\dot{w} \\ \Delta\dot{q} \\ \Delta\dot{x}_f \\ \Delta\dot{z}_f \\ \Delta\dot{\theta} \end{Bmatrix} = \begin{bmatrix} F_{x_b,\delta e} \\ F_{z_b,\delta e} \\ M_{y_b,\delta e} \\ 0 \\ 0 \\ 0 \end{bmatrix} \Delta\delta e$$
$$+ \begin{bmatrix} F_{x_b,u} & F_{x_b,w} & F_{x_b,q} & 0 & 0 & -W\cos(\theta_0) \\ F_{z_b,u} & F_{z_b,w} & F_{z_b,q} + V_0 W/g & 0 & 0 & -W\sin(\theta_0) \\ M_{y_b,u} & M_{y_b,w} & M_{y_b,q} & 0 & 0 & 0 \\ \cos(\theta_0) & \sin(\theta_0) & 0 & 0 & 0 & -V_0\sin(\theta_0) \\ -\sin(\theta_0) & \cos(\theta_0) & 0 & 0 & 0 & -V_0\cos(\theta_0) \\ 0 & 0 & 1 & 0 & 0 & 0 \end{bmatrix} \begin{Bmatrix} \Delta u \\ \Delta w \\ \Delta q \\ \Delta x_f \\ \Delta z_f \\ \Delta\theta \end{Bmatrix} \tag{4.118}$$

Simplified linear longitudinal state space model for system ID.

$$\begin{Bmatrix} \Delta\dot{u} \\ \Delta\dot{w} \\ \Delta\dot{q} \\ \Delta\dot{\theta} \end{Bmatrix} = \begin{bmatrix} \frac{F_{x_b,\delta e}}{W/g} \\ \frac{F_{z_b,\delta e}}{W/g} \\ \frac{M_{y_b,\delta e}}{I_{yy_b}} \\ 0 \end{bmatrix} \Delta\delta e$$
$$+ \begin{bmatrix} \frac{F_{x_b,u}}{W/g} & \frac{F_{x_b,w}}{W/g} & \frac{F_{x_b,q}}{W/g} & \frac{-W\cos(\theta_0)}{W/g} \\ \frac{F_{z_b,u}}{W/g} & \frac{F_{z_b,w}}{W/g} & \frac{F_{z_b,q}+V_0 W/g}{W/g} & \frac{-W\sin(\theta_0)}{W/g} \\ \frac{M_{y_b,u}}{I_{yy_b}} & \frac{M_{y_b,w}}{I_{yy_b}} & \frac{M_{y_b,q}}{I_{yy_b}} & 0 \\ 0 & 0 & 1 & 0 \end{bmatrix} \begin{Bmatrix} \Delta u \\ \Delta w \\ \Delta q \\ \Delta\theta \end{Bmatrix} \tag{4.119}$$

Chapter 5

System Identification Method

5.1 UAV System ID Method Overview

The method of system ID used here in is a variation on the recursive linear least squares approximation. Recall that least squares is the mathematically optimal method of selecting unknown parameters that minimize the sum square of the residual errors. This minimization, described in [10], is shown by

$$J = \frac{1}{2} e^T e \tag{5.1}$$

Given the differential equation

$$\dot{x} = ax + bu, \tag{5.2}$$

the recursive linear least squares uses measured values for the state, x, state derivative, $\dot{x}$, and input, u, in order to estimate the parameters, a and b, of the equations of motion. Measurements for the state derivatives are not always available as is partially the case here. In order to estimate the state derivative, the state could be differentiated. This however is not desirable as it amplifies noise in the measurements. The Error Filtering Online Learning (EFOL) scheme provides a filtering technique using the Laplace domain to find the state derivative while filtering out high frequency noise [11]. The following sections describe the derivation and implementation of the recursive linear least squares algorithm using the EFOL scheme to find the aerodynamic parameters for the linear longitudinal dynamics of the Minion class UAV.

5.2 Derivation of the Recursive Linear Least Squares Algorithm Using the Error Filtering Online Learning (EFOL) Scheme

Starting with the differential equation in scalar form

$$\dot{x} = ax + bu, \tag{5.3}$$

where $\dot{x}$ is the state derivative, x is the state, and u is the input to the system. For the specific case of the UAV, some of $\dot{x}$ and all of x and u can be measured. The measured values are denoted as $\dot{\tilde{x}}$, $\tilde{x}$, and $\tilde{u}$. Estimated values are denoted as $\hat{a}$ and $\hat{b}$. Due to some of the state derivatives being measurable, there are two different cases for the EFOL scheme.

1. $\dot{x}$ is measured ($\dot{\tilde{x}}$)
2. $\dot{x}$ is determined using filtering ($\dot{\hat{x}}$)

5.2.1 Case 1: Measured $\dot{\mathbf{x}}$

The differential equation is given with measurement and parameter estimation error, estimated parameters, measured states, and measured state differentials.

$$\dot{\tilde{x}} = \hat{a}\tilde{x} + \hat{b}\tilde{u} + (a - \hat{a})\tilde{x} + (b - \hat{b})\tilde{u} + e_{measured} \tag{5.4}$$

The measurement error, $e_{measurement}$, and the difference between estimated and true parameters, $(a - \hat{a})$ and $(b - \hat{b})$, are combined into one error, e_f, as

$$\dot{\tilde{x}} = \hat{a}\tilde{x} + \hat{b}\tilde{u} + e_f \tag{5.5}$$

where $\hat{a}$ and $\hat{b}$ are the estimated parameters. A first-order filter is applied to both sides of the equation

$$\frac{\lambda}{s+\lambda}\dot{\tilde{x}} = \hat{a}\frac{\lambda}{s+\lambda}\tilde{x} + \hat{b}\frac{\lambda}{s+\lambda}\tilde{u} + \frac{\lambda}{s+\lambda}e_f \tag{5.6}$$

Then a change of variables is used to make the differential equation a linearly parametrized model yielding

$$\tilde{\chi} = \hat{\theta}_1\tilde{\zeta_1} + \hat{\theta}_2\tilde{\zeta_2} + \delta. \tag{5.7}$$

Combining terms into vector notation gives

$$\tilde{\chi} = \hat{\theta}^T\tilde{\zeta} + \delta. \tag{5.8}$$

Solving the equation for the filtered error, δ gives

$$\delta = \tilde{\chi} - \hat{\theta}^T\tilde{\zeta} \tag{5.9}$$

5.2.2 Case 2: Determined $\dot{\mathbf{x}}$

For case 2 the differential equation is given with the measurement and parameter estimation error, estimated parameters, and measured states. However the state differentials are not measured. Instead a filtering techniques using the Laplace domain will be used to determine the state differentials. Thus the state differentials are currently denoted as estimates in

$$\dot{\hat{x}} = \hat{a}\tilde{x} + \hat{b}\tilde{u} + (a - \hat{a})\tilde{x} + (b - \hat{b})\tilde{u} + e_{measurement} \tag{5.10}$$

The measurement errors, $e_{measurement}$, and the difference in estimated and true parameters, $(a - \hat{a})$ and $(b - \hat{b})$, are combined into one error, e_f, as with case 1

$$\dot{\tilde{x}} = \hat{a}\tilde{x} + \hat{b}\tilde{u} + e_f, \tag{5.11}$$

where $\hat{a}$ and $\hat{b}$ are the estimated parameters. Now before applying the first-order filter, Eq. (5.42) is changed to the Laplace domain using the Laplace transform. The state derivative is changed to the Laplace domain using the following transform

$$\mathcal{L}[\dot{\hat{x}}(s)] = s[\tilde{x}(s)] - \tilde{x}_0 \tag{5.12}$$

Applying the Laplace transform to Eq. (5.42) yields

$$s[\tilde{x}(s)] - \tilde{x}_0 = \hat{a}\tilde{x}(s) + \hat{b}\tilde{u}(s) + e_f(s) \tag{5.13}$$

The initial condition $\tilde{x}_0$ is moved to the right side of the equation.

$$s[\tilde{x}(s)] = \tilde{x}_0 + \hat{a}\tilde{x}(s) + \hat{b}\tilde{u}(s) + e_f(s) \tag{5.14}$$

Now the first-order filter can be applied to both sides of the equation

$$\frac{\lambda s}{s+\lambda}[\tilde{x}(s)] = \tilde{x}_0\frac{\lambda}{s+\lambda} + \hat{a}\frac{\lambda}{s+\lambda}\tilde{x}(s) + \hat{b}\frac{\lambda}{s+\lambda}\tilde{u}(s) + \frac{\lambda}{s+\lambda}e_f(s) \tag{5.15}$$

The Laplace domain differentiation with a lowpass filter, $\frac{\lambda s}{s+\lambda}$, is replaced with the transformation $\lambda(1 - \frac{\lambda}{s+\lambda})$, eliminating the differentiation.

$$\lambda(1 - \frac{\lambda}{s+\lambda})[\tilde{x}(s)] = \tilde{x}_0\frac{\lambda}{s+\lambda} + \hat{a}\frac{\lambda}{s+\lambda}\tilde{x}(s) + \hat{b}\frac{\lambda}{s+\lambda}\tilde{u}(s) + \frac{\lambda}{s+\lambda}e_f(s) \tag{5.16}$$

Since $\tilde{x}$ and $\tilde{u}$ are in the time domain, Eq. (5.16) is changed back into the time domain using the inverse Laplace transforms. It is noted that the inverse Laplace transform of $\frac{\lambda}{s+\lambda}$ is $\lambda(e^{-\lambda t})$. The time domain equation of motion is

$$\lambda(1 - \frac{\lambda}{s+\lambda})[\tilde{x}(t)] = \tilde{x}_0\lambda(e^{-\lambda t}) + \hat{a}\frac{\lambda}{s+\lambda}\tilde{x}(t) + \hat{b}\frac{\lambda}{s+\lambda}\tilde{u}(t) + \frac{\lambda}{s+\lambda}e_f(t) \tag{5.17}$$

Again a change of variables is used to make the differential equation a linearly parametrized model yielding

$$\tilde{\chi} = \tilde{\theta}_1\tilde{\zeta}_1 + \hat{\theta}_2\tilde{\zeta}_2 + \hat{\theta}_3\tilde{\zeta}_3 + \delta. \tag{5.18}$$

Combining terms into vector notation gives

$$\tilde{\chi} = \hat{\theta}^T\tilde{\zeta} + \delta. \tag{5.19}$$

Solving the equation for the filtered error, δ gives

$$\delta = \tilde{\chi} - \hat{\theta}^T \tilde{\zeta} \tag{5.20}$$

Now recursive least squares can be applied to the differential equation in linear form with the addition of the covariance matrix, P. The update equation for the parameter estimate, [10] is

$$\dot{\hat{\theta}} = -P(t)\zeta(t)\delta, \qquad \theta(0) = \theta_0, \tag{5.21}$$

and the update equation for the covariance is

$$\dot{P} = -P(t)\zeta(t)\zeta(t)^T P(t), \qquad P(0) = P_0. \tag{5.22}$$

$\dot{\hat{\theta}}$ and $\dot{P}$ are integrated to get $\hat{\theta}$ and P by

$$\hat{\theta} = \int \dot{\hat{\theta}} dt \tag{5.23}$$

and

$$P = \int \dot{P} dt. \tag{5.24}$$

5.3 Implementation of the Recursive Linear Least Squares Algorithm Using the Error Filtering Online Learning (EFOL) Scheme

The derivation of recursive least squares algorithm using the EFOL scheme has been shown. Now the algorithm is applied to the specific case of the Minion class UAV. Detailed steps are shown herein to avoid any confusion. Starting with the linear longitudinal

equations of motion using the state space representation

$$\begin{Bmatrix} \Delta\dot{u} \\ \Delta\dot{w} \\ \Delta\dot{q} \\ \Delta\dot{\theta} \end{Bmatrix} = \begin{bmatrix} \frac{F_{x_b,\delta e}}{W/g} \\ \frac{F_{z_b,\delta e}}{W/g} \\ \frac{M_{y_b,\delta e}}{I_{yy_b}} \\ 0 \end{bmatrix} \Delta\delta e + \begin{bmatrix} \frac{F_{x_b,u}}{W/g} & \frac{F_{x_b,w}}{W/g} & \frac{F_{x_b,q}}{W/g} & \frac{-W\cos(\theta_0)}{W/g} \\ \frac{F_{z_b,u}}{W/g} & \frac{F_{z_b,w}}{W/g} & \frac{F_{z_b,q}+V_0W/g}{W/g} & \frac{-W\sin(\theta_0)}{W/g} \\ \frac{M_{y_b,u}}{I_{yy_b}} & \frac{M_{y_b,w}}{I_{yy_b}} & \frac{M_{y_b,q}}{I_{yy_b}} & 0 \\ 0 & 0 & 1 & 0 \end{bmatrix} \begin{Bmatrix} \Delta u \\ \Delta w \\ \Delta q \\ \Delta\theta \end{Bmatrix} \tag{5.25}$$

The elements within the A and B matrices are represented in the following way

$$\begin{Bmatrix} \Delta\dot{u} \\ \Delta\dot{w} \\ \Delta\dot{q} \\ \Delta\dot{\theta} \end{Bmatrix} = \begin{bmatrix} \hat{A}_{11} & \hat{A}_{12} & \hat{A}_{13} & A_{14} \\ \hat{A}_{21} & \hat{A}_{22} & \hat{A}_{23} & A_{24} \\ \hat{A}_{31} & \hat{A}_{32} & \hat{A}_{33} & 0 \\ 0 & 0 & 1 & 0 \end{bmatrix} \begin{Bmatrix} \Delta u \\ \Delta w \\ \Delta q \\ \Delta\theta \end{Bmatrix} + \begin{bmatrix} \hat{B}_1 \\ \hat{B}_2 \\ \hat{B}_3 \\ 0 \end{bmatrix} \Delta\delta e. \tag{5.26}$$

This representation will simplify the derivation of the recursive least squares using the Error Filter Online Learning (EFOL) Scheme. The error associated with measurements and parameter estimates can be represented by a column vector of errors corresponding to each change in the state as is represented here in Eq. 5.43

$$\begin{Bmatrix} \Delta\dot{u} \\ \Delta\dot{w} \\ \Delta\dot{q} \\ \Delta\dot{\theta} \end{Bmatrix} = \begin{bmatrix} \hat{A}_{11} & \hat{A}_{12} & \hat{A}_{13} & A_{14} \\ \hat{A}_{21} & \hat{A}_{22} & \hat{A}_{23} & A_{24} \\ \hat{A}_{31} & \hat{A}_{32} & \hat{A}_{33} & 0 \\ 0 & 0 & 1 & 0 \end{bmatrix} \begin{Bmatrix} \Delta u \\ \Delta w \\ \Delta q \\ \Delta\theta \end{Bmatrix} + \begin{bmatrix} \hat{B}_1 \\ \hat{B}_2 \\ \hat{B}_3 \\ 0 \end{bmatrix} \Delta\delta e + \begin{Bmatrix} e_{f_1} \\ e_{f_2} \\ e_{f_3} \\ e_{f_4} \end{Bmatrix} \tag{5.27}$$

Now the EFOL scheme will be applied. The purpose of the EFOL is two fold: first to filter the data using a low pass filter, and second to avoid the use of differentiation. Differentiation of noisy data causes the noise to be amplified. The EFOL scheme uses a

filtering approach in the Laplace domain which is as follows. Before filtering, the changes in the states will be transformed in to the Laplace domain using the Laplace transform.

$$\mathcal{L}[\dot{x}(s)] = s[x(s)] - x_0 \tag{5.28}$$

Applying the Laplace transform to the equations of motion yields.

$$\begin{Bmatrix} s\Delta u(s) - u_0 \\ s\Delta w(s) - w_0 \\ s\Delta q(s) - q_0 \\ s\Delta\theta(s) - \theta_0 \end{Bmatrix} = \begin{bmatrix} \hat{A}_{11} & \hat{A}_{12} & \hat{A}_{13} & A_{14} \\ \hat{A}_{21} & \hat{A}_{22} & \hat{A}_{23} & A_{24} \\ \hat{A}_{31} & \hat{A}_{32} & \hat{A}_{33} & 0 \\ 0 & 0 & 1 & 0 \end{bmatrix} \begin{Bmatrix} \Delta u(s) \\ \Delta w(s) \\ \Delta q(s) \\ \Delta\theta(s) \end{Bmatrix} + \begin{bmatrix} \hat{B}_1 \\ \hat{B}_2 \\ \hat{B}_3 \\ 0 \end{bmatrix} \Delta\delta e(s) + \begin{Bmatrix} e_{f_1}(s) \\ e_{f_2}(s) \\ e_{f_3}(s) \\ e_{f_4}(s) \end{Bmatrix} \tag{5.29}$$

Now both sides of the equations of motion are filtered using a stable first-order lowpass filter.

$$\begin{aligned} \tfrac{\lambda}{s+\lambda} \begin{Bmatrix} s\Delta u(s) - u_0 \\ s\Delta w(s) - w_0 \\ s\Delta q(s) - q_0 \\ s\Delta\theta(s) - \theta_0 \end{Bmatrix} &= \tfrac{\lambda}{s+\lambda} \begin{bmatrix} \hat{A}_{11} & \hat{A}_{12} & \hat{A}_{13} & A_{14} \\ \hat{A}_{21} & \hat{A}_{22} & \hat{A}_{23} & A_{24} \\ \hat{A}_{31} & \hat{A}_{32} & \hat{A}_{33} & 0 \\ 0 & 0 & 1 & 0 \end{bmatrix} \begin{Bmatrix} \Delta u(s) \\ \Delta w(s) \\ \Delta q(s) \\ \Delta\theta(s) \end{Bmatrix} \\ &+ \tfrac{\lambda}{s+\lambda} \begin{bmatrix} \hat{B}_1 \\ \hat{B}_2 \\ \hat{B}_3 \\ 0 \end{bmatrix} \Delta\delta e(s) + \tfrac{\lambda}{s+\lambda} \begin{Bmatrix} e_{f_1}(s) \\ e_{f_2}(s) \\ e_{f_3}(s) \\ e_{f_4}(s) \end{Bmatrix} \end{aligned} \tag{5.30}$$

The filtered initial conditions are moved to the right had side of the equation.

$$\begin{aligned}
&\tfrac{\lambda}{s+\lambda}\begin{Bmatrix} s\Delta u(s) \\ s\Delta w(s) \\ s\Delta q(s) \\ s\Delta\theta(s) \end{Bmatrix} = \\
&\tfrac{\lambda}{s+\lambda}\begin{Bmatrix} u_0 \\ w_0 \\ q_0 \\ \theta_0 \end{Bmatrix} + \tfrac{\lambda}{s+\lambda}\begin{bmatrix} \hat{A}_{11} & \hat{A}_{12} & \hat{A}_{13} & A_{14} \\ \hat{A}_{21} & \hat{A}_{22} & \hat{A}_{23} & A_{24} \\ \hat{A}_{31} & \hat{A}_{32} & \hat{A}_{33} & 0 \\ 0 & 0 & 1 & 0 \end{bmatrix}\begin{Bmatrix} \Delta u(s) \\ \Delta w(s) \\ \Delta q(s) \\ \Delta\theta(s) \end{Bmatrix} \\
&+\tfrac{\lambda}{s+\lambda}\begin{bmatrix} \hat{B}_1 \\ \hat{B}_2 \\ \hat{B}_3 \\ 0 \end{bmatrix}\Delta\delta e(s) + \tfrac{\lambda}{s+\lambda}\begin{Bmatrix} e_{f_1}(s) \\ e_{f_2}(s) \\ e_{f_3}(s) \\ e_{f_4}(s) \end{Bmatrix}.
\end{aligned} \tag{5.31}$$

Since the A and B matrices are to be estimated, the filter is grouped with the states and state derivatives. The Laplace domain differentiation with lowpass filter, $\frac{\lambda s}{s+\lambda}$, is replaced with the transformation $\lambda(1-\frac{\lambda}{s+\lambda})$, eliminating the differentiation. The A and B matrices

and the initial conditions are also combined together shown in Eq. 5.32,

$$\begin{Bmatrix} \lambda(1-\frac{\lambda}{s+\lambda})\Delta u(s) \\ \lambda(1-\frac{\lambda}{s+\lambda})\Delta w(s) \\ \lambda(1-\frac{\lambda}{s+\lambda})\Delta q(s) \\ \lambda(1-\frac{\lambda}{s+\lambda})\Delta\theta(s) \end{Bmatrix} = \begin{bmatrix} \hat{A}_{11} & \hat{A}_{12} & \hat{A}_{13} & A_{14} & \hat{B}_1 & u_0 \\ \hat{A}_{21} & \hat{A}_{22} & \hat{A}_{23} & A_{24} & \hat{B}_2 & w_0 \\ \hat{A}_{31} & \hat{A}_{32} & \hat{A}_{33} & 0 & \hat{B}_3 & q_0 \\ 0 & 0 & 1 & 0 & 0 & \theta_0 \end{bmatrix} \begin{Bmatrix} \frac{\lambda}{s+\lambda}\Delta u(s) \\ \frac{\lambda}{s+\lambda}\Delta w(s) \\ \frac{\lambda}{s+\lambda}\Delta q(s) \\ \frac{\lambda}{s+\lambda}\Delta\theta(s) \\ \frac{\lambda}{s+\lambda}\Delta\delta e(s) \\ \frac{\lambda}{s+\lambda} \end{Bmatrix} + \begin{Bmatrix} \frac{\lambda}{s+\lambda}e_{f_1}(s) \\ \frac{\lambda}{s+\lambda}e_{f_2}(s) \\ \frac{\lambda}{s+\lambda}e_{f_3}(s) \\ \frac{\lambda}{s+\lambda}e_{f_4}(s) \end{Bmatrix}. \tag{5.32}$$

The equations of motion are transformed back into the time domain using the inverse

Laplace transforms. Noting that the inverse Laplace transform of $\frac{\lambda}{s+\lambda}$ is $\lambda(e^{-\lambda t})$, the equation of motion in the time domain is

$$\begin{Bmatrix} \lambda(1-\frac{\lambda}{s+\lambda})\Delta u(t) \\ \lambda(1-\frac{\lambda}{s+\lambda})\Delta w(t) \\ \lambda(1-\frac{\lambda}{s+\lambda})\Delta q(t) \\ \lambda(1-\frac{\lambda}{s+\lambda})\Delta\theta(t) \end{Bmatrix} = \begin{bmatrix} \hat{A}_{11} & \hat{A}_{12} & \hat{A}_{13} & A_{14} & \hat{B}_1 & u_0 \\ \hat{A}_{21} & \hat{A}_{22} & \hat{A}_{23} & A_{24} & \hat{B}_2 & w_0 \\ \hat{A}_{31} & \hat{A}_{32} & \hat{A}_{33} & 0 & \hat{B}_3 & q_0 \\ 0 & 0 & 1 & 0 & 0 & \theta_0 \end{bmatrix} \begin{Bmatrix} \frac{\lambda}{s+\lambda}\Delta u(t) \\ \frac{\lambda}{s+\lambda}\Delta w(t) \\ \frac{\lambda}{s+\lambda}\Delta q(t) \\ \frac{\lambda}{s+\lambda}\Delta\theta(t) \\ \frac{\lambda}{s+\lambda}\Delta\delta e(t) \\ \lambda(e^{-\lambda t}) \end{Bmatrix} + \begin{Bmatrix} \frac{\lambda}{s+\lambda}e_{f_1}(t) \\ \frac{\lambda}{s+\lambda}e_{f_2}(t) \\ \frac{\lambda}{s+\lambda}e_{f_3}(t) \\ \frac{\lambda}{s+\lambda}e_{f_4}(t) \end{Bmatrix}. \tag{5.33}$$

Now the equations of motion can be rewritten from the state space model to a linearly parametrized model which coincides with the EFOL and general least squares form,

$$\begin{Bmatrix} \chi_1(t) \\ \chi_2(t) \\ \chi_3(t) \\ \chi_4(t) \end{Bmatrix} = \begin{bmatrix} \hat{A}_{11} & \hat{A}_{12} & \hat{A}_{13} & A_{14} & \hat{B}_1 & u_0 \\ \hat{A}_{21} & \hat{A}_{22} & \hat{A}_{23} & A_{24} & \hat{B}_2 & w_0 \\ \hat{A}_{31} & \hat{A}_{32} & \hat{A}_{33} & 0 & \hat{B}_3 & q_0 \\ 0 & 0 & 1 & 0 & 0 & \theta_0 \end{bmatrix} \begin{Bmatrix} \zeta_1(t) \\ \zeta_2(t) \\ \zeta_3(t) \\ \zeta_4(t) \\ \zeta_5(t) \\ \zeta_6(t) \end{Bmatrix} + \begin{Bmatrix} \delta_1(t) \\ \delta_2(t) \\ \delta_3(t) \\ \delta_4(t) \end{Bmatrix}. \tag{5.34}$$

where there is a change of variables for the filtered state derivative, state, and filtered error. The equation is now put into vector notation for the remainder of the derivation as

$$\chi = \hat{\theta}\zeta + \delta. \tag{5.35}$$

Solving for δ, the filtered error, gives

$$\delta = \chi - \hat{\theta}\zeta. \tag{5.36}$$

Using the filtered error, δ, the filtered states, ζ, and a covariance matrix, P, recursive least squares can be used to give the change in the parameter estimates and the change in the covariance. The change is the parameter estimates are computed by

$$\dot{\hat{\theta}} = -P(t)\zeta(t)\delta \qquad \theta(0) = \theta_0, \tag{5.37}$$

and the change in the covariance is computed by

$$\dot{P} = -P(t)\zeta(t)\zeta(t)^T P(t) \qquad P(0) = P_0 \tag{5.38}$$

Then $\dot{\hat{\theta}}$ and $\dot{P}$ are integrated giving

$$\hat{\theta} = \int \dot{\hat{\theta}} dt \tag{5.39}$$

$$P = \int \dot{P} dt. \tag{5.40}$$

This is the full derivation of recursive least squares algorithm with the EFOL scheme. The EFOL scheme assumes that the state derivatives are not available for measuring. This is true only for the pitch angular acceleration, $\dot{q}$, for the UAV. Axial acceleration, $\dot{u}$, vertical acceleration, $\dot{w}$, and the pitch angular velocity, $\dot{\theta}$, are measured and available for use in the system ID. The state derivatives can be included in the EFOL simply by filtering them, just as the states are filtered. If the measured stated derivatives are used the χ vector becomes

$$\chi = \begin{Bmatrix} \frac{\lambda}{s+\lambda}\Delta\dot{u}(t) \\ \frac{\lambda}{s+\lambda}\Delta\dot{w}(t) \\ \frac{\lambda s}{s+\lambda}\Delta q(t) \\ \frac{\lambda}{s+\lambda}\Delta\dot{\theta}(t) \end{Bmatrix} \tag{5.41}$$

5.4 Chapter Summary

The Error Filtering Online Learning Scheme was derived first in scalar form and then in full matrix form specifically for the UAV. The main equations are summarized here.

General state space form of the equations of motion

$$\dot{\tilde{x}} = \hat{a}\tilde{x} + \hat{b}\tilde{u} + e_f, \tag{5.42}$$

and for the specific case of the UAV

$$\begin{Bmatrix} \Delta\dot{u} \\ \Delta\dot{w} \\ \Delta\dot{q} \\ \Delta\dot{\theta} \end{Bmatrix} = \begin{bmatrix} \hat{A}_{11} & \hat{A}_{12} & \hat{A}_{13} & A_{14} \\ \hat{A}_{21} & \hat{A}_{22} & \hat{A}_{23} & A_{24} \\ \hat{A}_{31} & \hat{A}_{32} & \hat{A}_{33} & 0 \\ 0 & 0 & 1 & 0 \end{bmatrix} \begin{Bmatrix} \Delta u \\ \Delta w \\ \Delta q \\ \Delta\theta \end{Bmatrix} + \begin{bmatrix} \hat{B}_1 \\ \hat{B}_2 \\ \hat{B}_3 \\ 0 \end{bmatrix} \Delta\delta e + \begin{Bmatrix} e_{f_1} \\ e_{f_2} \\ e_{f_3} \\ e_{f_4} \end{Bmatrix} \tag{5.43}$$

EFOL linearized parameter model in expanded format

$$\begin{Bmatrix} \lambda(1-\frac{\lambda}{s+\lambda})\Delta u(t) \\ \lambda(1-\frac{\lambda}{s+\lambda})\Delta w(t) \\ \lambda(1-\frac{\lambda}{s+\lambda})\Delta q(t) \\ \lambda(1-\frac{\lambda}{s+\lambda})\Delta\theta(t) \end{Bmatrix} = \begin{bmatrix} \hat{A}_{11} & \hat{A}_{12} & \hat{A}_{13} & A_{14} & \hat{B}_1 & u_0 \\ \hat{A}_{21} & \hat{A}_{22} & \hat{A}_{23} & A_{24} & \hat{B}_2 & w_0 \\ \hat{A}_{31} & \hat{A}_{32} & \hat{A}_{33} & 0 & \hat{B}_3 & q_0 \\ 0 & 0 & 1 & 0 & 0 & \theta_0 \end{bmatrix} \begin{Bmatrix} \frac{\lambda}{s+\lambda}\Delta u(t) \\ \frac{\lambda}{s+\lambda}\Delta w(t) \\ \frac{\lambda}{s+\lambda}\Delta q(t) \\ \frac{\lambda}{s+\lambda}\Delta\theta(t) \\ \frac{\lambda}{s+\lambda}\Delta\delta e(t) \\ \lambda(e^{-\lambda t}) \end{Bmatrix} + \begin{Bmatrix} \frac{\lambda}{s+\lambda}e_{f_1}(t) \\ \frac{\lambda}{s+\lambda}e_{f_2}(t) \\ \frac{\lambda}{s+\lambda}e_{f_3}(t) \\ \frac{\lambda}{s+\lambda}e_{f_4}(t) \end{Bmatrix}. \tag{5.44}$$

and in vector format

$$\chi = \hat{\theta}\zeta + \delta \tag{5.45}$$

Filtered error between the identified model and the data

$$\delta = \chi - \hat{\theta}\zeta. \tag{5.46}$$

Recursive least squares update equations

$$\dot{\hat{\theta}} = -P(t)\zeta(t)\delta \qquad \theta(0) = \theta_0, \tag{5.47}$$

and

$$\dot{P} = -P(t)\zeta(t)\zeta(t)^T P(t) \qquad P(0) = P_0 \tag{5.48}$$

Recursive least squares estimated parameters

$$\hat{\theta} = \int \dot{\hat{\theta}} dt \tag{5.49}$$

and covariance

$$P = \int \dot{P} dt. \tag{5.50}$$

Chapter 6

Experiment Setup

This chapter gives a brief overview of the Minion class UAV on which system ID is preformed. Each sensor used to collect data for system ID is detailed. The flight testing procedure and maneuvers for the system ID are discussed.

6.1 The AggieAir Minion Personal Remote Sensing UAV Overview

The AggieAir service center at the Utah Water Research Laboratory provides scientific grade data for civilian research. The Minion UAV serves as the primary platform for data collection at the AggieAir service center. The Minion UAV, shown in Figure 6.1, is a traditional fixed-wing aircraft with a T-tail and is designed for launch and retrieval without the use of a runway. Additionally the UAV breaks down to meet international check on luggage size requirement of 60 total inches. A summary of the configuration parameters are given in Table 6.1

Fig. 6.1: Minion class personal remote sensing unmanned aerial vehicle

Table 6.1: Summary of the Minion class UAV system ID configuration parameters

Parameter	***Value***	***Units***
System ID configuration weight	4.1	kg
Maximum weight	6.35	kg
Maximum payload weight	1.81	kg
Wing span	2.29	m
Fuselage length	1.08	m
Range	48	km
Flight time	1	hr
Cruse speed	15	m/s

6.2 Low-cost Sensors for Data Acquisition

AggieAir systems use low-cost sensors for autonomous flight. In general a UAV requires four types of sensor for autonomous flight: triaxial accelerometer, triaxial gyroscope, triaxial magnetometer, and a Global Positioning Unit (GPS). Often the accelerometer, gyroscope, and magnetometer are combined into a single sensor housing. Sensors such as differential and absolute pressures sensors and angle of attach and side slip sensors can provide additional measurements. These additional sensors are not required for autonomous flight but do allow for increased autopilot performance. A main point of this thesis is to asses how well system ID can be performed with sensors already flown on the Minion UAV. The Minion class UAV was equipped with a MicroStrain 3DM GX3-25 OEM Attitude Heading and Reference System (AHRS), u-blox LEA-6h GPS, and a Freescale Semiconductor MPXV7002DP piezoresistive transducer differential pressure sensor. The UAV was later equip with a VectorNav VN-200 Rugged. The following sections detail each sensor and the measurements it provides.

6.2.1 MicroStrain 3DM GX3 AHRS

The MicroStrain 3DM GX3-25 OEM AHRS, shown in Fig. 6.2, contains a triaxial accelerometer, triaxial gyroscope, and triaxial magnetometer. The 3DM GX3-25 OEM AHRS can provide measurement data on:

- Linear accelerations in the x, y, & z body axis ($\dot{u}$, $\dot{v}$, & $\dot{w}$)

- Angular rates around the x, y, & z body axis (p, q, & r)
- Orientation matrix in Euler angles ϕ, θ, & , ψ relative to its initial orientation
- Heading in relation to magnetic north

Fig. 6.2: MicroStrain 3DM GX3 AHRS

The GX3 has a maximum data rate of 1000 Hz for raw acceleration and angular rate data. For orientation matrix with acceleration and angular rate data the maximum data rate is 500 Hz. For the system ID flight testing the AHRS is set at 500 Hz. The specifications for the GX3 are given in Table 6.2

Table 6.2: GX3 Specifications

Parameter	***Accels***	***Gyros***	***Mags***
Measurement Range	±5 g	±300 deg/sec	±2.5 Gauss
Non-linearity	±0.1 % fs	±0.03 % fs	±0.4 % fs
In-run bias stability	±0.04 mg	±18 deg/hr	-
Initial bias error	±0.002 g	±0.25 deg/sec	±0.003 Gauss
Scale factor stability	±0.05 %	±0.05 %	±0.1 %
Noise density	80 $\mu g/\sqrt{Hz}$	0.03 deg/sec/$\sqrt{Hz}$	100 μGauss/$\sqrt{Hz}$
Alignment error	±0.05 deg	±0.05 deg	±0.05 deg
User adjustable bandwidth	225 Hz max	440 Hz max	230 Hz max
Sampling rate	±30 kHz	±30 kHz	±7.5 kHz max

6.2.2 u-blox LEA-6h GPS

The u-blox LEA-6h GPS, shown in Fig. 6.3, provides the following measurements:

Fig. 6.3: u-blox LEA-6h GPS

- Magnitude of the velocity parallel to the Earth's surface referred to as ground speed ($V_{ground} = \sqrt{u^2 + v^2}$)
- Magnitude of the velocity perpendicular to the Earth's surface referred to as vertical speed (w)
- Position in Earth Centered Earth Fixed coordinate system (x_f, y_f, & z_f)

The GPS updates at 4 Hz. Each measurement has some delay due to the time it takes to generate an accurate position and velocity measurement. Thus the delay must be accounted for in the data post processing. The specifications for the GPS are given in Table 6.3.

Table 6.3: GPS Specifications

Parameter	***Specification***
Max navigation update rate	2 Hz
Horizontal position accuracy	2.5 m
Velocity accuracy	0.1 m/s
Heading accuracy	0.5 deg

6.2.3 Freescale semiconductor MPXV7002DP piezoresistive transducer differential pressure sensor

The Freescale Semiconductor MPXV7002DP piezoresistive transducer differential pressure sensor, shown in Fig. 6.4, provides a measurement for differential pressure, ΔP, which is directly used to calculate airspeed, V. The sensor has an update rate of 20 Hz. The sensor is calibrated on the ground by changing an air density gain until it reads zero airspeed, however this calibration is insufficient for an accurate airspeed measurement.

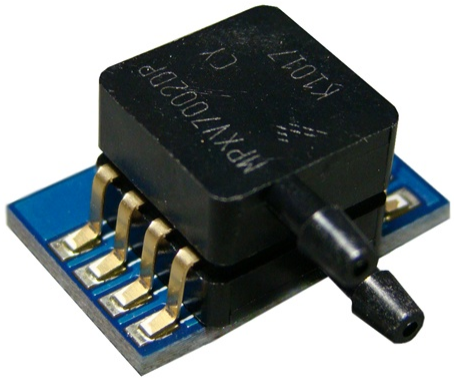

Fig. 6.4: Differential pressure sensor

The airspeed measurement is calculated from the differential pressure reading and air density. Airspeed can be calculated from differential pressure using the formula

$$V_{airspeed} = \sqrt{\frac{2\Delta P}{\rho}}, \tag{6.1}$$

where ΔP is the differential air pressure and ρ is the air density. Equation (6.1) shows that the airspeed is inversely proportional to the air density. Air density varies with altitude and temperature. Thus for a constant airspeed using only the differential pressure without updating the air density will give biased airspeed measurements. This bias can be corrected using a static pressure and temperature sensor, however the Minion UAV does not currently have an integrated static pressure sensor or temperature sensor. Thus the airspeed data is

not used for system ID. The specifications for the differential pressure sensor are given in Table 6.4.

Table 6.4: Differential Pressure Sensor Specifications

Parameter	***Specification***
Pressure range	±2 kPa
Full scale output (FS0)	4.25-4.75 Vdc
Full scale span (FSS)	3.5-4.5 Vdc
Accuracy	±6.25 %FSS
Sensitivity	1.0 V/kPa
Update rate	A/D dependent (20 Hz)

6.2.4 VectorNav VN-200 rugged GPS/INS

The VectorNav VN-200 GPS/INS, shown in Fig. 6.5, contains a triaxial accelerometer, triaxial gyroscope, and triaxial magnetometer, pressure sensor, and GPS. The navigation solution uses an Extended Kalman filter. The VN-200 can provide measurement data on:

- Linearized accelerations in the x, y, & z body axis ($\dot{u}$, $\dot{v}$, & $\dot{w}$)
- Angular rates around the x, y, & z body axis (p, q, & r)
- Orientation matrix in Euler angles ϕ, θ, & ψ
- Velocities in the x, y, & z body axis (u, v, & w)

Fig. 6.5: VectorNav VN-200 rugged GPS-aided inertial navigation system

The specifications for the VN-200 are given in Table 6.5.

Table 6.5: VN-200 Specifications

Parameter	***Specification***
Dynamic Accuracy (Heading, True Inertial)	0.3 deg RMS
Dynamic Accuracy (Pitch/Roll)	0.1 deg RMS
Angular Resolution	<0.05 deg
Angular Repeatability	<0.1 deg
Horizontal Position Accuracy	2.0 m RMS
Vertical Position Accuracy	2.5 m RMS
Position Resolution	1 mm
Velocity Accuracy	±0.05 m/s
Velocity Resolution	1 mm/s
Output rate	400 Hz

6.3 Control Inputs

Four types of inputs are used to excite the dynamics of the Minion UAV: sine wave, frequency sweep (chirp), doublet, and singlet.

6.3.1 Sine wave

The sine wave maneuver, shown in Fig. 6.6, is a constant sine wave input for approximately 20 seconds for each set. Three different periods are used for the sine input wave: 0.25 Hz, 0.5 Hz, and 1.0 Hz.

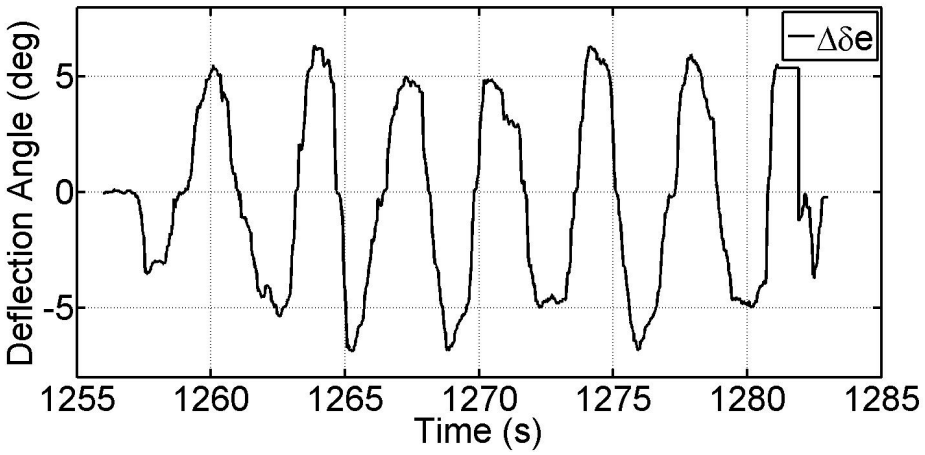

Fig. 6.6: Sine wave elevator input

6.3.2 Frequency sweep

The frequency sweep maneuver or chirp, shown in Fig. 6.7, provides frequency rich data which is essential for system ID. Each sweep starts at a frequency of 0.25 Hz and is progressively ramped up to 1.0 Hz over 10 to 20 seconds.

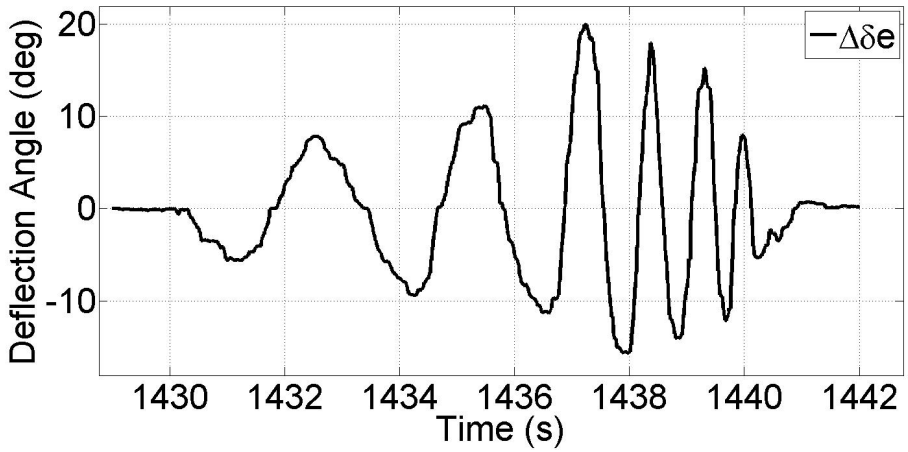

Fig. 6.7: Frequency sweep (Chirp) elevator input

6.3.3 Doublet

A doublet, shown in Fig. 6.8, is a quick elevator up, elevator down maneuver that has similar qualities as a step input. Doublet data is used for model validation After the doublet input the aircraft is allowed to oscillate freely for as long as possible while still maintaining visual contact and control.

6.3.4 Singlet

A singlet, shown in Fig. 6.9 is a short elevator up or elevator down maneuver that has similar qualities as to a impulse. The singlet data also provides data used for model validation.s. After the singlet input the aircraft is allowed to oscillate freely for as long as possible while still maintaining visual contact and control.

6.4 Flight Testing Procedure

The flight test procedure is as follows. The avionics are turned on and sensors are

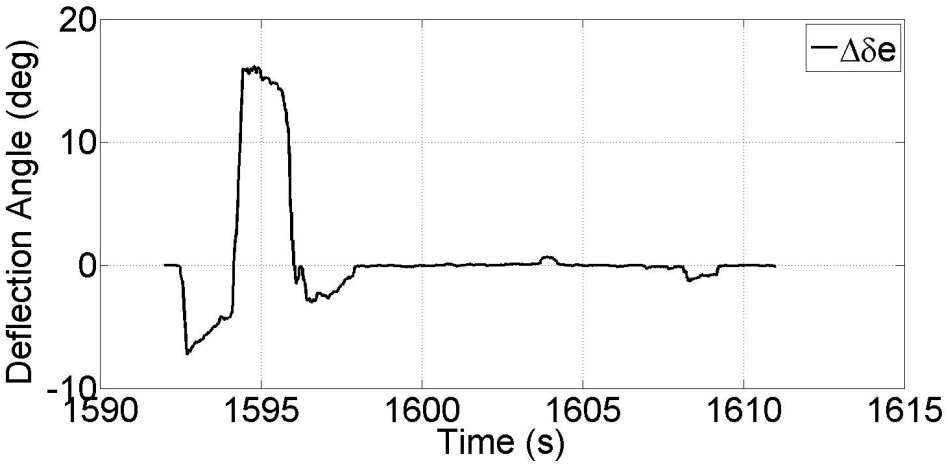

Fig. 6.8: Doublet elevator input

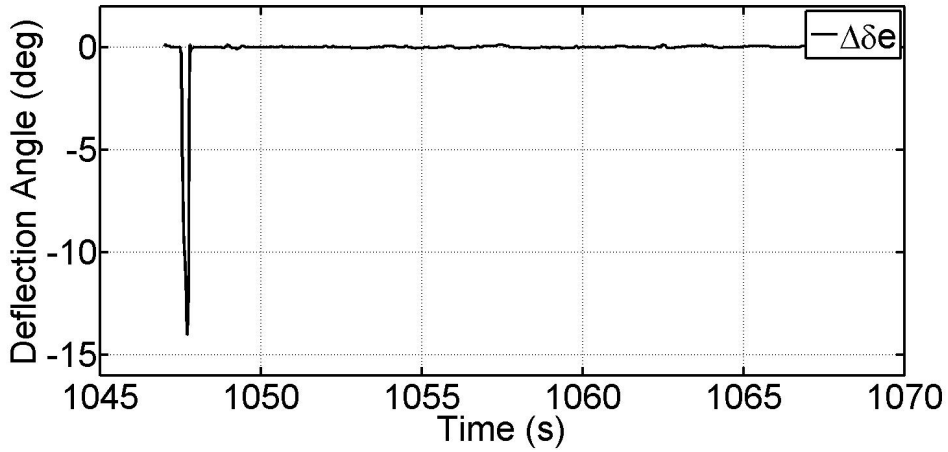

Fig. 6.9: Singlet elevator input

allowed to warm up for several minutes (5-15 min). The UAV is launched and the flight controls (ailerons, rudder, and elevator) are timed so that the UAV will fly straight and level without pilot input. The trim settings are recorded. A metronome is used to keep the test pilot in time and consistent with the maneuvers. Sine wave maneuvers are preformed at quarter elevator defection at 0.25 Hz, 0.5 Hz, and 1.0 Hz. Each sine wave is repeated for approximately 20 seconds. Before and after each maneuver the aircraft is returned to trim for 3 sec. Four sets of frequency sweeps are performed in the same manner as the sine waves. Frequency sweeps start at 0.25 Hz and ramps to 1.0 Hz over a 20 second period using

a maximum of quarter elevator deflection. Doublet maneuvers are performed in the same manner as the sine wave and frequency sweep. Each doublet is a quarter up elevator input for 1 second, down elevator for 1 second and return to trim. After the doublet the UAV is allowed to oscillate for as long as possible without any pilot input. Singlet maneuvers are performed in the same manner as the doublets. Each singlet is a quick quarter down elevator input. Then the plane is landed and the data is allowed to buffer for several minutes after landing.

6.5 Chapter Summary

Characteristics of the Minion UAV have been given. Sensors and their characteristics have been detailed. Maneuver input and test flight procedures have discussed.

Chapter 7

Data Processing

In an ideal experiment the data is noiseless, captures all dynamics, has no lag, and is already in the correct coordinate system. This is not the case with real world flight data. Flight data is often very noisy due to propulsion system vibrations, air turbulence, and inherent sensor noise. Even more not all sensors give data in the same coordinate system. For example a GPS gives data in an inertial frame whereas an IMU gives measurements in a body frame. Thus it is necessary to process and check data for consistency prior to conducting the system ID.

The following sections detail the data processing procedure used prior to carrying out system ID on the UAV flight data. Within these sections is a detailed progression of how each data set is processed to ensure that none of the flight dynamics are lost. Graphs are provided to visually verifying the consistency between raw data and processed data.

7.1 Raw Data

There are two set of flight data collected for system identification. Flight one contains sine wave, frequency sweep, and doublet system ID maneuvers. Flight two contains sine wave, frequency sweep, and singlet system ID maneuvers, These maneuvers are detailed in 6.3. The system ID maneuvers are defined as follows:

- Sine wave: at 0.25, 0.5, and 1 Hz
- Frequency sweeps: from 0.25 to 1 Hz
- Doublets: holding elevator deflection for 1 seconds
- Singlets: a quick full deflection of the elevator

Only the frequency sweeps are used as training data for system ID of nominal model parameters. Sine waves, doublets, and singlets are used for testing and validating the model developed from the system ID. Since the UAV model being identified is a linear longitudinal model only data sections consisting of longitudinal flight are used.

Four sensors on the Minion UAV have been described in Chapter 6. The following list details the data variables from each sensor that can be used in the system ID, elevator input being the input from the autopilot and not a sensor.

- 3DM GX3 IMU
  - x acceleration
  - z acceleration
  - q rotational rate
  - θ Euler angle
- GPS
  - N velocity
  - E velocity
  - D velocity
- Differential pressure pitot tube
  - Airspeed
- Autopilot
  - Elevator input signal
- VN-200
  - x velocity
  - z velocity
  - q rotational rate
  - θ Euler angle

7.2 Linearly Interpolate Between Data Dropouts

During the data storage process, occasionally data is lost from one or more sensors. Unlike a Kalman filter, batch least squares requires data from all sensors at each complete measurement and is unable to handle data dropouts. Thus the data is resampled at 400 Hz with the gaps filled through linear interpolation. Figures 7.2, 7.3, 7.4, 7.5, and 7.9 show the states and control input that have been resampled.

7.3 Low-pass Filter Data at 4 Hz

The flight data is low-pass filtered at 4 Hz to remove noise from sensors and propulsion vibration. Figures 7.4, 7.6, 7.7, and 7.7 clearly show the filtering of the state and state derivatives. Filtering flight data can alter the flight dynamics if not done properly. Filtering can produce phase lag in the data or change the amplitude of oscillations. To ensure data fidelity and consistency a phase neutral backwards-forwards filter can be used which does not introduce lag into the filtered data. Low-pass filtering cuts out high frequency noise and smooth out discrete data. Each filtered data set is examined visually to ensure that the flight dynamics are retained. The data is low-passed at 4 Hz, and all maneuvers are at 1 Hz or less so the low-pass filter will not filter out any dynamics of interest.

7.4 Differentiate Velocity and Rotational Velocity Data

System ID of the linear longitudinal equations of motion for the Minion UAV requires data from the state, u, w, q, and θ, the state derivatives $\dot{u}$, $\dot{w}$, $\dot{q}$, and $\dot{\theta}$, and the input δe. In practice the state, and the input can be observed. As for the state derivatives, $\dot{u}$, $\dot{w}$, and $\dot{\theta}$ are observable by the MEMS sensors and have data sets. The MEMS sensors aboard the Minion UAV do not record rotational acceleration in pitch, $\dot{q}$, data. This presents an issue for the system ID, which is overcome by taking the derivative of the states.

While performing system ID, it became apparent that the accelerometer data $\dot{u}$ and $\dot{w}$ could not be used due to an uncompensated bias. Both the GX3 and VN-200 have filters which are designed to remove the bias in real-time. However, when the data is integrated and compared to body velocities, the integrated acceleration does not have a zero-mean

velocity, whereas the velocity data u and w have a zero-mean or close to zero-mean velocity. Thus u and w data are both differentiated and used instead of the accelerometer data. This uncompensated bias is especially observable in the comparison of integrated acceleration and velocity flight data shown in Fig. 7.1. The state derivatives are shown in figs. 7.6, 7.7, and 7.7.

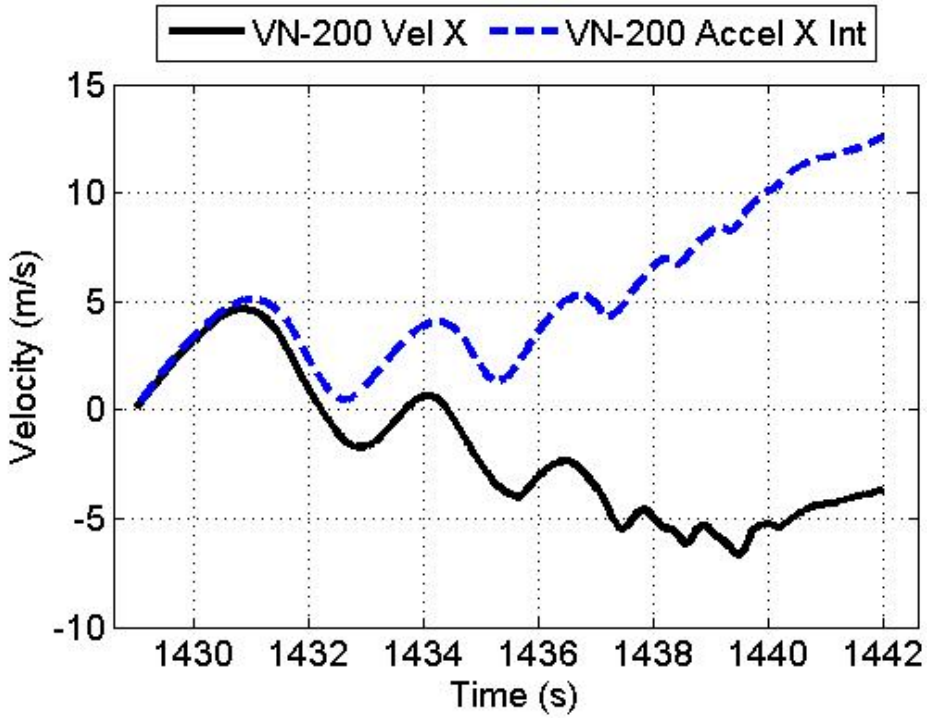

Fig. 7.1: Comparison of VN-200 velocity vs. integrated acceleration data, showing acceleration has a bias that causes velocity drift. Note: the nominal velocity of 22 m/s has been removed.

7.5 Remove Steady State Values

Linearized Longitudinal equations of motion assume that the UAV is in steady level flight and that deviations from that state are small. To satisfy this condition the steady state values are removed from the velocity u, fig. 7.2, Euler angle θ, fig. 7.5, and elevator deflection $\Delta\delta e$, fig. 7.9. All other states are a deviation from a steady state value of zero during steady level flight.

7.6 Separate System ID Flight Maneuvers

Once the data has been processed for system ID, the next step is to separate the data into each maneuver. This is done to separate out longitudinal maneuvers from lateral data. Data is selected three seconds before and after each maneuver. These three second of data correspond to when the UAV is in trimmed steady level flight.

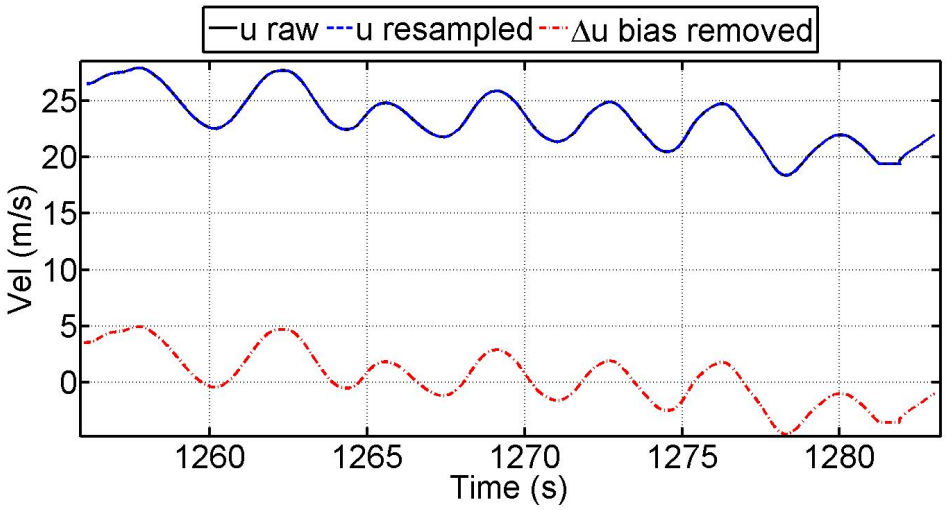

Fig. 7.2: The raw, resampled, and steady state removed u velocity data. The u velocity data from the VN-200 is already smooth due to the extended Kalman filter and does not need to be low-pass filtered, where data from a GPS does.

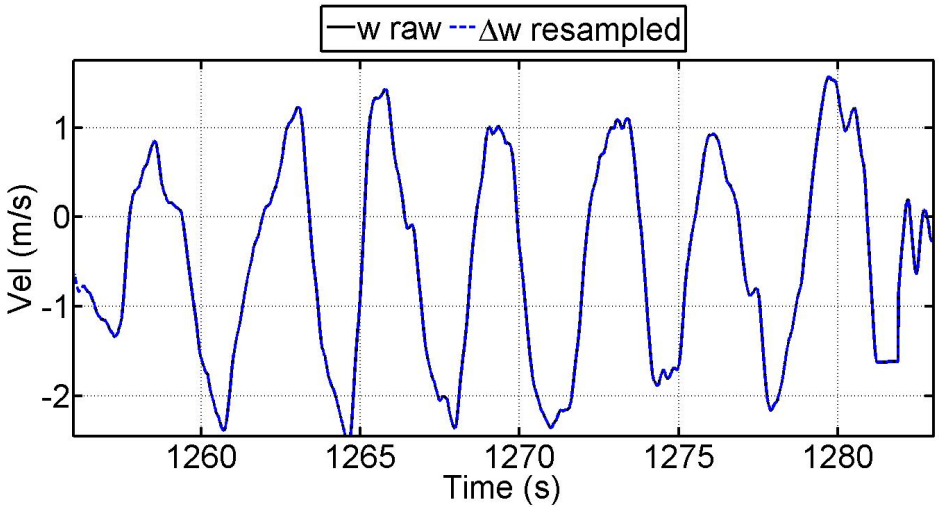

Fig. 7.3: The raw, and resampled w velocity data. The w velocity data from the VN-200 is already smooth due to the extended Kalman filter and does not need to be low-pass filtered, where data from a GPS does. Also the w velocity data does not need to be normalized. At steady state the w velocity is zero and when the aircraft is performing system ID maneuvers the oscillations are deviations from zero velocity.

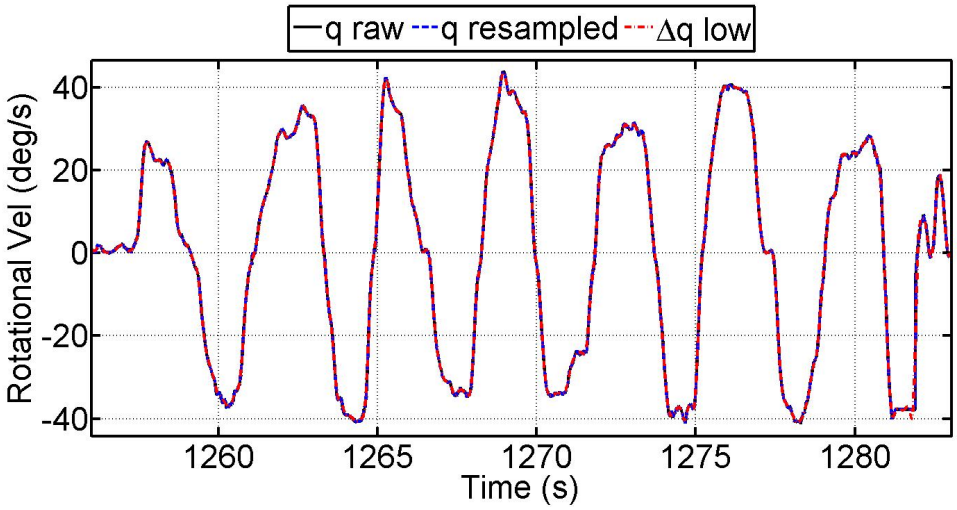

Fig. 7.4: The raw, resampled, and low-pass filtered q rotational rate data.

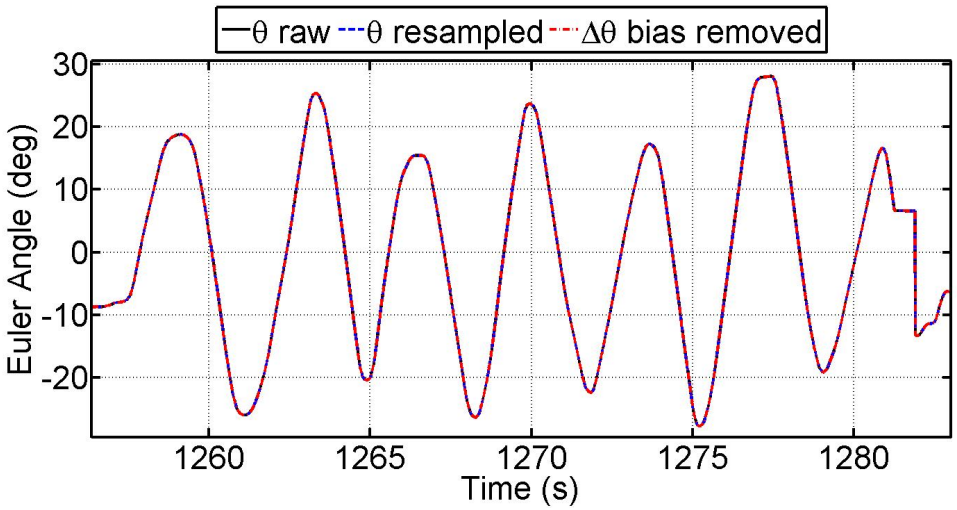

Fig. 7.5: The raw, resampled, and normalized θ Euler angle data.

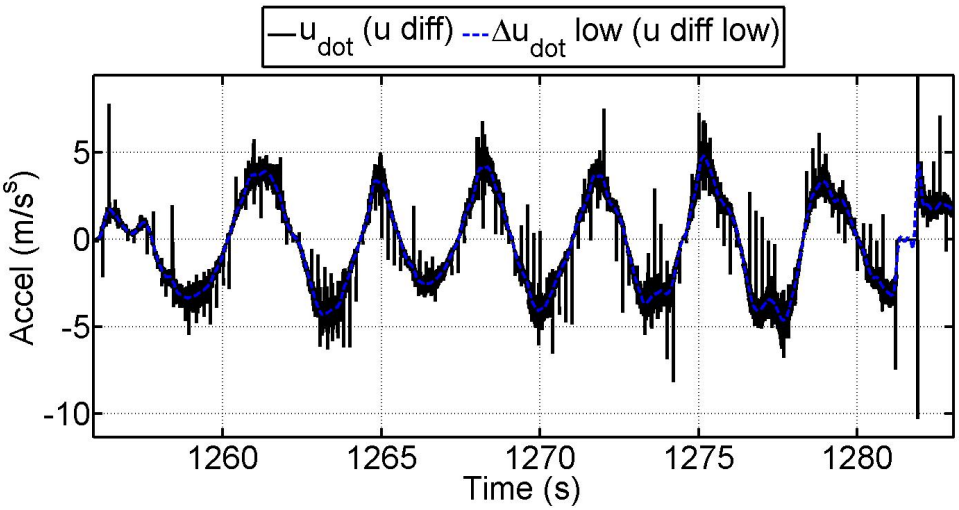

Fig. 7.6: Differentiated u velocity and low-passed differentiated u velocity. The differentiated u velocity is used in place of $\dot{u}$, which has uncompensated bias.

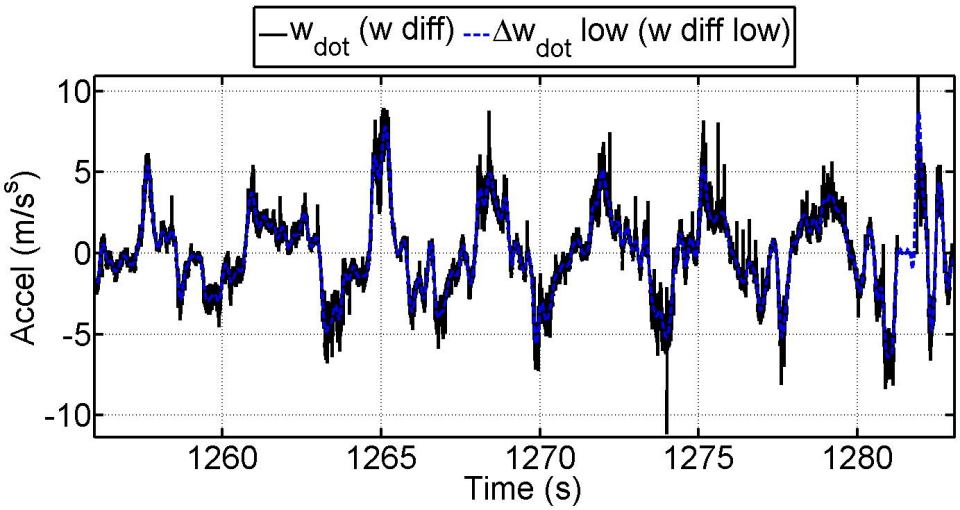

Fig. 7.7: Differentiated w velocity and low-passed differentiated w velocity. The differentiated w velocity is used in place of $\dot{w}$, which has uncompensated bias.

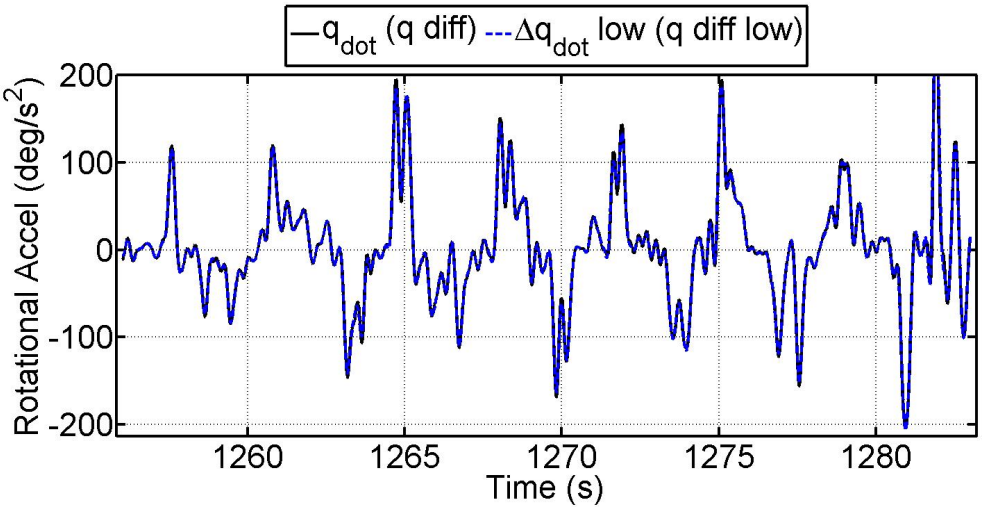

Fig. 7.8: Differentiated q rotational rate and low-passed differentiated q rotational rate.

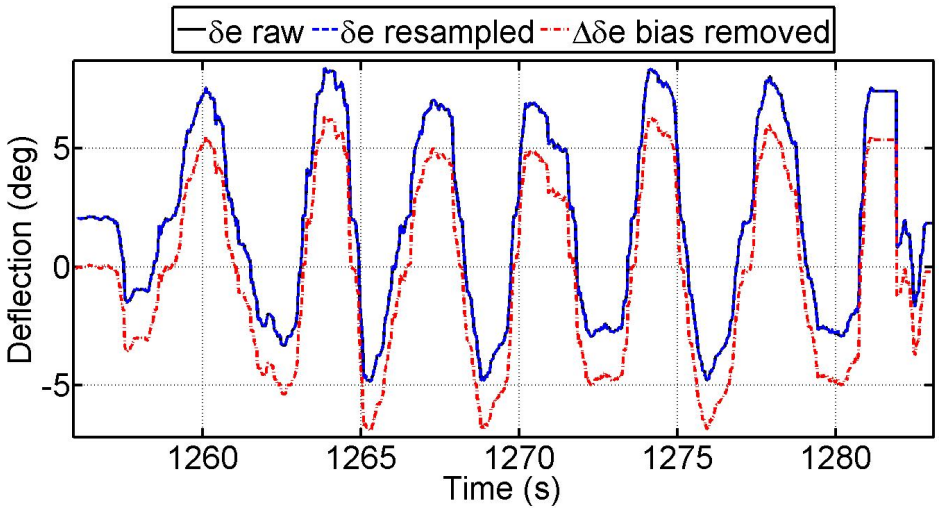

Fig. 7.9: The raw, resampled, and normalized $\Delta\delta e$ elevator deflection angle data.

7.7 Chapter Summary

System ID data processing is as follows:

- Linearly interpolate between data dropouts
- Low-pass data at 4 Hz
- Differentiate velocity and rotational velocity data
- Remove steady state values
- Separate system ID flight maneuvers

Table 7.1 summarizes how each variable is processed for system ID. A yes in the differentiate column indicates that the flight data was differentiated to determine that state.

Table 7.1: Summary of the data processing procedure of each data type

Sensor	***Data Variable***	***Interpolate***	***Filter***	***Differentiate***	***Remove Steady State***
VN-200	$\Delta\dot{u}$	Y	4Hz	Y	N
VN-200	$\Delta\dot{w}$	Y	4Hz	Y	N
VN-200	$\Delta\dot{q}$	Y	4Hz	Y	N
VN-200	$\Delta\dot{\theta}$	Y	4Hz	N	N
VN-200	Δu	Y	N	N	Y
VN-200	Δw	Y	N	N	N
VN-200	Δq	Y	4Hz	Y	N
VN-200	$\Delta\theta$	Y	N	N	Y
Auto Pilot	$\Delta\delta_e$	Y	N	N	Y

Chapter 8

Results and Comparison

The following chapter presents the results of the system ID of the small unmanned aerial vehicle (UAV) using batch least squares (BLS) and BLS with the Error Filtering Online Learning scheme (EFOL). The system ID uses a set of seven chirp maneuvers from two different flights to identify seven sets of model parameters. The mean value of the identified parameters are used to populate the nominal linear longitudinal model of the UAV. This step is called model training. Three other types of maneuvers: sine wave, doublet, and singlet, are used to evaluate how well the nominal model identifies the actual flight dynamics of the UAV. This step is called model validation. Statistical analysis is used to give metrics of how well the identified model fits the flight data. The process of model training and validation is summarized in Fig. 8.1. The system ID results from both BLS and BLS with EFOL are presents as follows:

- Mean and standard deviation of identified model parameters
- Mean and standard deviation of identified aerodynamic coefficients
- Identified nominal model
- Error and mean error of the identified nominal model's response vs. validation flight data
- Eigenvalues of the nominal model

Also, a model that uses all longitudinal flight data is compared to the BLS and BLS with EFOL models to determine if there is a significant advantage. The results of this comparison are given at the end of the chapter.

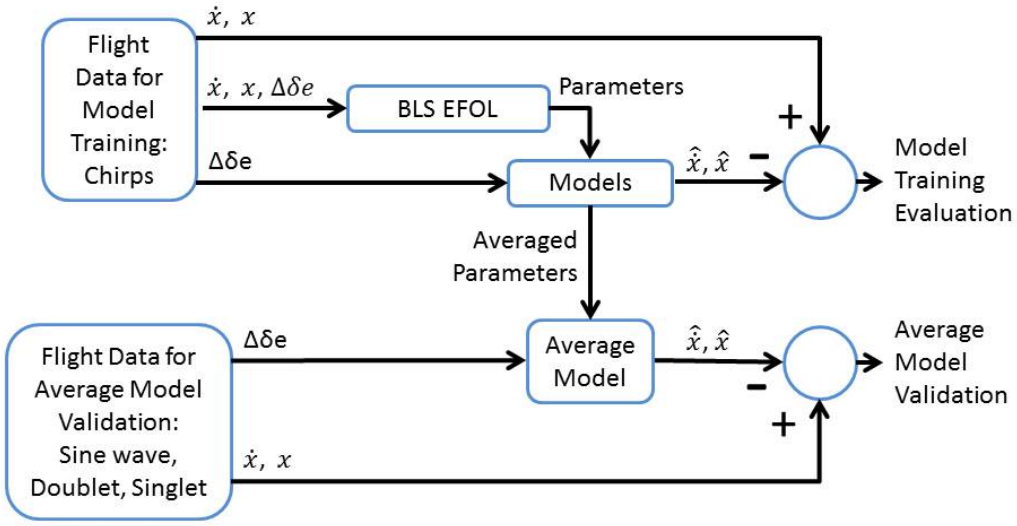

Fig. 8.1: Model training, evaluation, and average model validation process overview

8.1 Identified Model Parameters

Twelve parameters of the linear longitudinal equations of motion have been identified using BLS and BLS with EFOL. The mean value of the parameters with their associated standard deviations are presented in Tables 8.1 and 8.2 and in Figs. 8.2 and 8.3. In all cases the mean value of the parameters from BLS and BLS with EFOL lie within the standard deviation of each other. This is to be expected since the two methods are using the exact same set of data. The matching values confirm that using BLS with EFOL will not degrade the system identification.

Examining the standard deviation of the parameters in the A and B matrix, shows that some of the standard deviations are of the same magnitude as the parameters. This is especially evident in A_{12}, A_{13}, A_{33}, and B_1. These standard deviations all correspond to relatively small parameters. The larger parameters, A_{22}, A_{23}, and B_3, have significantly smaller standard deviations compared to the parameter value. The parameters with larger values are those that have been identified to dominate the dynamics. Since these parameters dominate the dynamics, they are more consistently resolved than parameters which have a smaller contribution to the dynamics. Thus parameters which have a larger influence on the motion of the aircraft are more consistently identified compared to the parameters which

have a smaller influence on the motion of the aircraft.

Table 8.1: The mean value of the identified parameters of the A matrix with standard deviations. BLS and BLS with EFOL consistently identify the same parameters and have the same standard deviations.

Parameter	***BLS mean***	***BLS std***	***EFOL mean***	***EFOL std***
A_{11}	-0.1811	0.05746	-0.1807	0.05725
A_{12}	0.1919	0.2412	0.1924	0.2421
A_{13}	0.1894	0.7662	0.1850	0.7743
A_{21}	-0.7612	0.2277	-0.7588	0.2276
A_{22}	-5.134	0.6511	-5.121	0.6531
A_{23}	14.05	2.465	13.98	2.483
A_{31}	-0.1130	0.09859	-0.1162	0.09948
A_{32}	-1.897	0.4998	-1.912	0.5097
A_{33}	-1.136	1.463	-1.084	1.488

Table 8.2: The mean value of the identified parameters of the B matrix with standard deviations. BLS and BLS with EFOL consistently identify the same parameters and have the same standard deviations.

Parameter	***BLS mean***	***BLS std***	***EFOL mean***	***EFOL std***
B_1	-0.4355	2.567	-0.4513	2.618
B_2	-18.12	9.025	-18.35	9.113
B_3	-37.53	5.654	-37.69	5.686

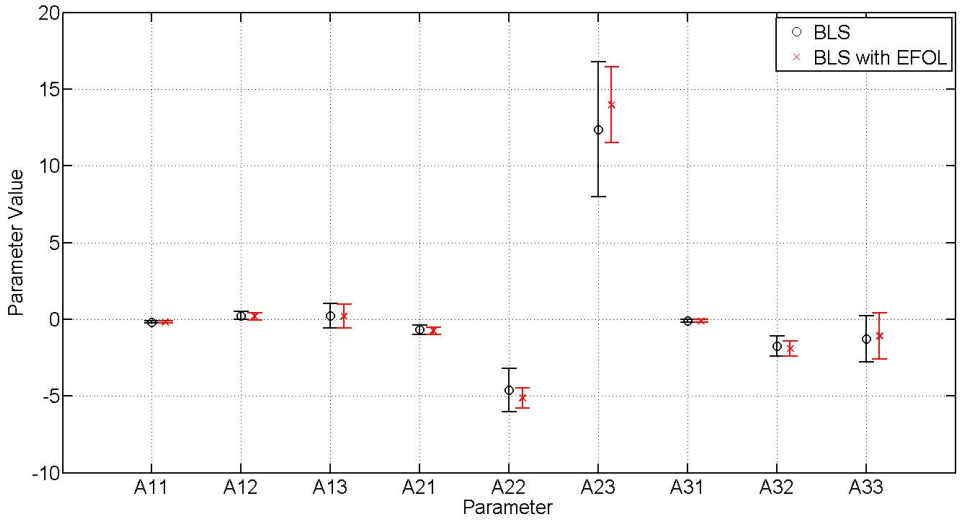

Fig. 8.2: The mean value of the identified parameters of the A matrix with standard deviation error bars. All BLS and BLS with EFOL parameters over lap within the error bounds.

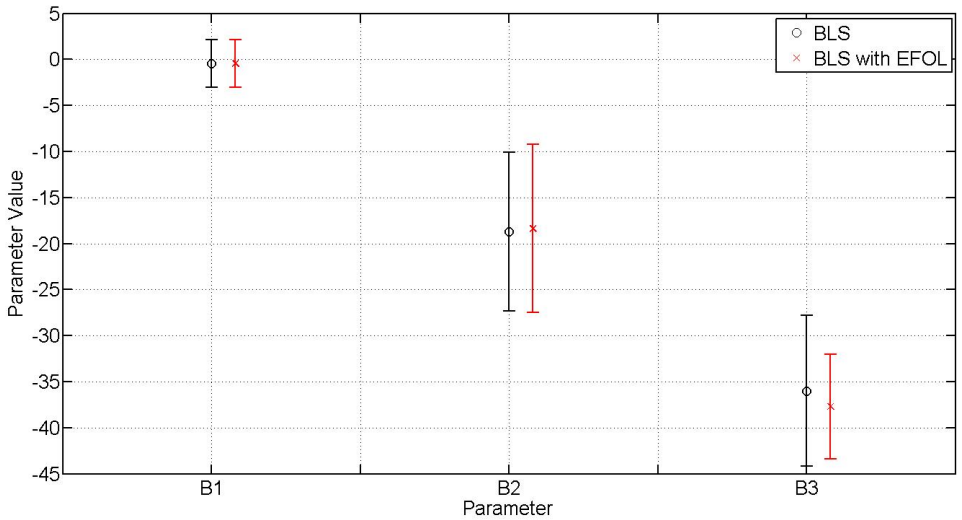

Fig. 8.3: The mean value of the identified parameters of the B matrix with standard deviation error bars. All BLS and BLS with EFOL parameters over lap within the error bounds.

8.2 Identified Aerodynamic Parameters

The 12 model parameters identified from each chirp maneuver are used to solve for the aerodynamic coefficients. The mean and standard deviation of the 12 aerodynamic coefficients from each chirp maneuver are presented in Table 8.3 and graphically in Figs. 8.4-8.6. The same correlation drawn between the model parameters values and their standard deviation cannot be applied here completely. However, the aerodynamic coefficients that correspond to the model parameters that dominate the dynamics do indeed have a relatively small standard deviations. The aerodynamic coefficients are calculated using the model parameters and Eqs. (4.107)-(4.109) derived in Chapter 4.

Table 8.3: Summary of the identified aerodynamic coefficients

Parameter	***BLS mean***	***BLS std***	***EFOL mean***	***EFOL std***
C_X	-0.0064	0.0020	-0.0064	0.0020
C_Z	-0.026	0.0080	-0.026	0.0080
C_m	-0.52	0.45	-0.53	0.46
$C_{X,\alpha}$	0.013	0.017	0.013	0.017
$C_{Z,\alpha}$	-0.36	0.046	-0.36	0.046
$C_{m,\alpha}$	-17.56	4.62	-17.70	4.71
$C_{X,q}$	0.00058	0.0023	0.00057	0.0023
$C_{Z,q}$	-0.027	0.0076	-0.027	0.0076
$C_{m,q}$	-0.45	0.58	-0.43	0.59
$C_{X,\delta e}$	-0.0013	0.0079	-0.0013	0.0080
$C_{Z,\delta e}$	-0.055	0.027	-0.056	0.028
$C_{m,\delta e}$	-15.10	2.27	-15.17	2.28

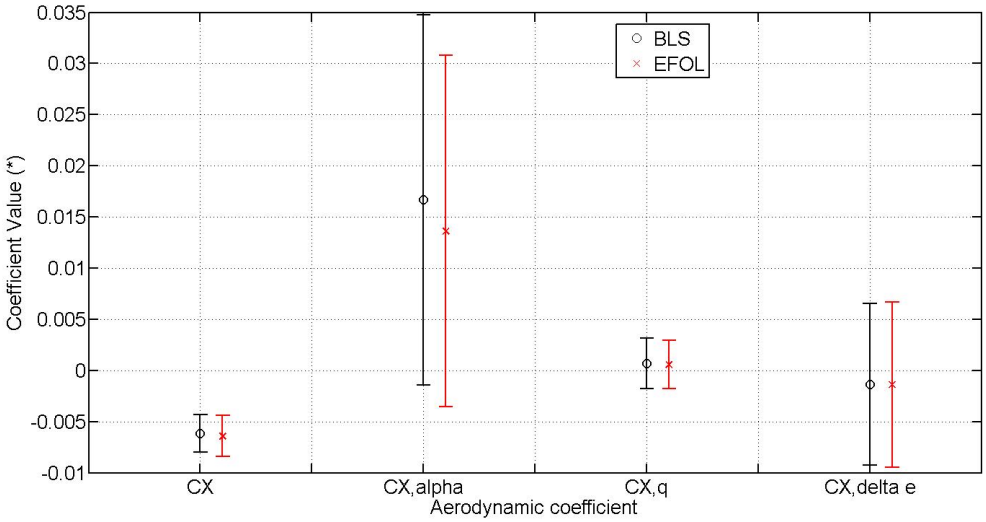

Fig. 8.4: The mean value of the identified aerodynamic coefficients with respect to x with standard deviation error bars. All BLS and BLS with EFOL coefficients over lap within the error bounds.

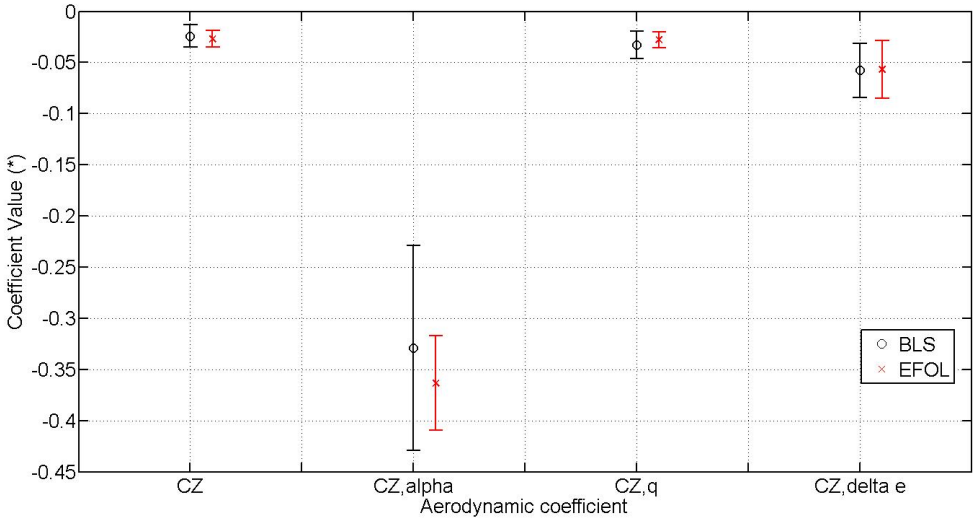

Fig. 8.5: The mean value of the identified aerodynamic coefficients with respect to z with standard deviation error bars. All BLS and BLS with EFOL coefficients over lap within the error bounds.

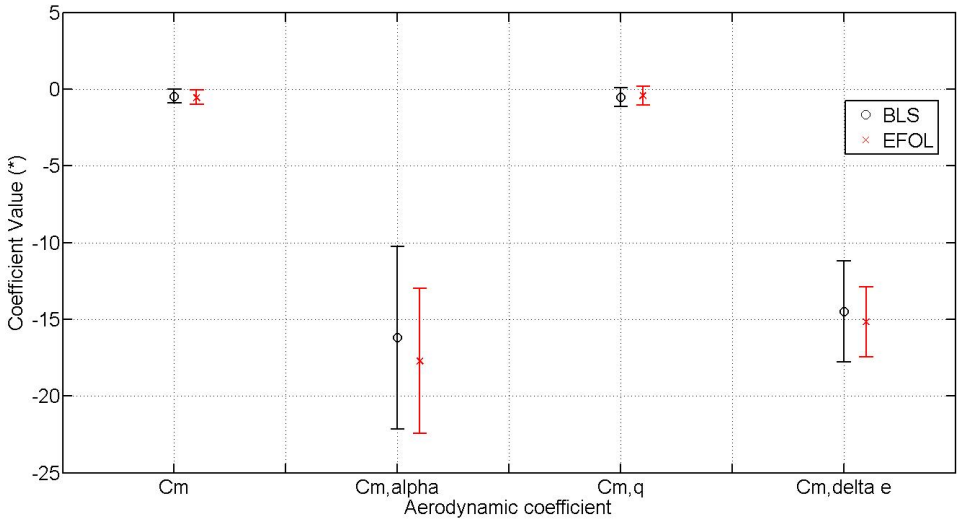

Fig. 8.6: The mean value of the identified aerodynamic coefficients with respect to m with standard deviation error bars. All BLS and BLS with EFOL coefficients over lap within the error bounds.

8.3 Identified Nominal Model vs. Flight Data

This section presents the nominal models identified using BLS and BLS with EFOL. The models are evaluated on how well they fit flight data. Three maneuvers are used to evaluate the nominal models: sine wave, doublet, singlet. It is important to note that the nominal models have been trained only with chirp maneuver flight data. The other maneuvers are only used to evaluate the identified nominal model's performance. This is standard procedure for evaluating identified models and determines if the nominal models have identified all dynamic modes. The BLS nominal model in Eq. 8.1 and the BLS with EFOL model in Eq. 8.2 are presented in context of the linear longitudinal equations of motion.

$$\begin{Bmatrix} \Delta\dot{u} \\ \Delta\dot{w} \\ \Delta\dot{q} \\ \Delta\dot{\theta} \end{Bmatrix} = \begin{bmatrix} -0.18 & 0.19 & 0.18 & -9.8 \\ -0.76 & -5.13 & 14.05 & 0 \\ -0.11 & -1.89 & -1.13 & 0 \\ 0 & 0 & 1 & 0 \end{bmatrix} \begin{Bmatrix} \Delta u \\ \Delta w \\ \Delta q \\ \Delta\theta \end{Bmatrix} + \begin{bmatrix} -0.43 \\ -18.12 \\ -37.53 \\ 0 \end{bmatrix} \Delta\delta e \tag{8.1}$$

$$\begin{Bmatrix} \Delta\dot{u} \\ \Delta\dot{w} \\ \Delta\dot{q} \\ \Delta\dot{\theta} \end{Bmatrix} = \begin{bmatrix} -0.18 & 0.19 & 0.18 & -9.8 \\ -0.75 & -5.12 & 13.98 & 0 \\ -0.11 & -1.91 & -1.08 & 0 \\ 0 & 0 & 1 & 0 \end{bmatrix} \begin{Bmatrix} \Delta u \\ \Delta w \\ \Delta q \\ \Delta\theta \end{Bmatrix} + \begin{bmatrix} -0.45 \\ -18.35 \\ -37.69 \\ 0 \end{bmatrix} \Delta\delta e \tag{8.2}$$

In evaluating the nominal models and comparing them to validation flight data, the nominal models are initialized with the validation flight data at time = 0. The models are then excited using the elevator deflection flight data. To be concise, only 3 model responses to flight data inputs will be presented. The results of the nominal models response display the characteristic results of the system ID. Figures 8.7-8.9 show the three types of inputs. Figures 8.10-8.15 show the comparison of validation flight data vs. the BLS and BLS with EFOL nominal model responses. Figures 8.16-8.21 show the error between the flight data and the nominal models. Table 8.4 shows the mean values of the error of the flight data and nominal models response.

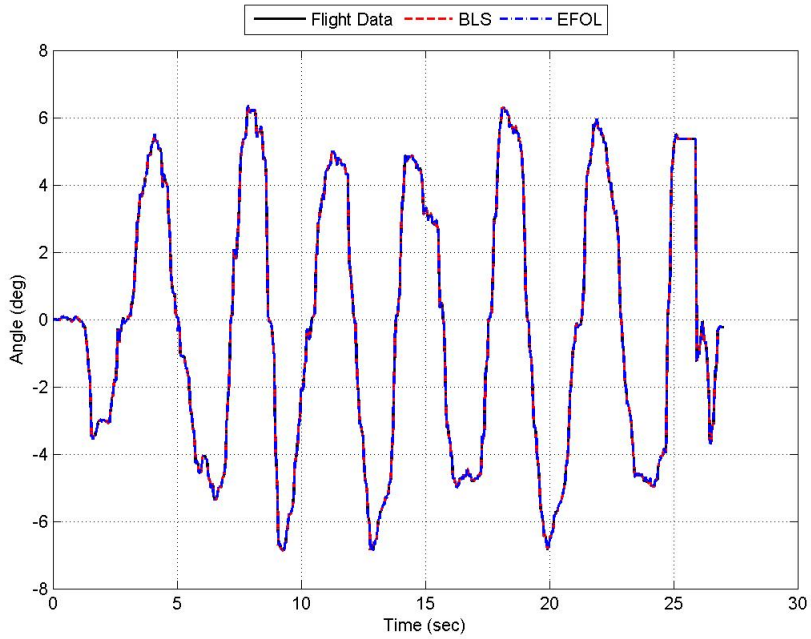

Fig. 8.7: The sine wave elevator command angle.

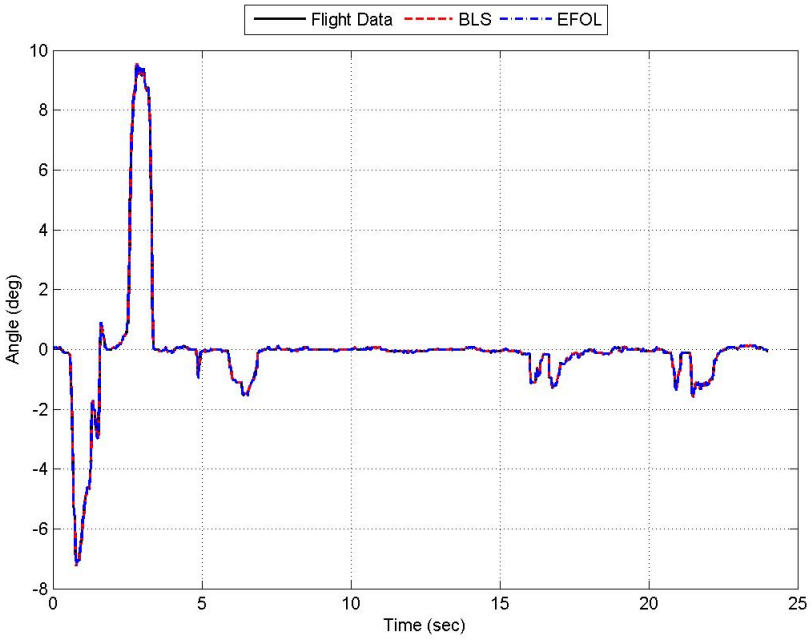

Fig. 8.8: The doublet elevator command angle.

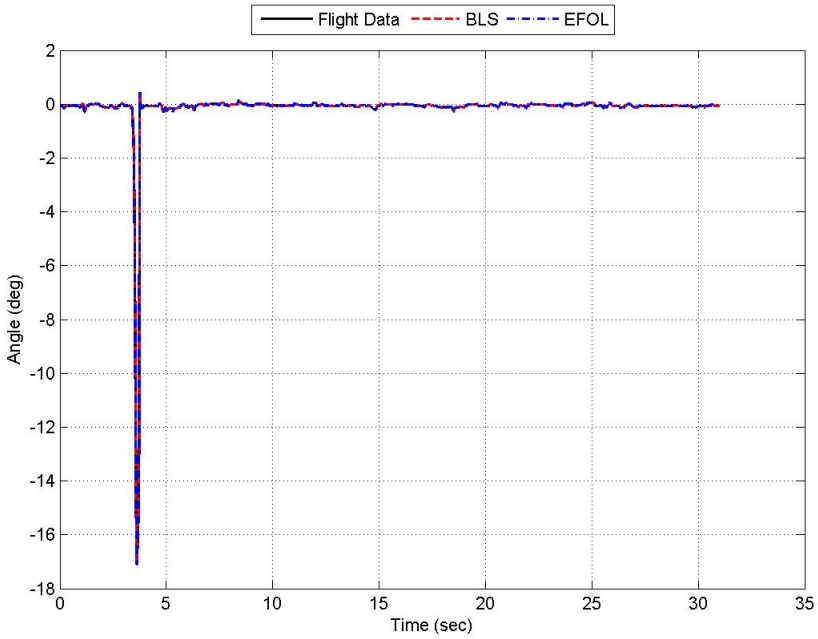

Fig. 8.9: The singlet elevator command angle.

The comparisons in Figs. 8.10-8.15 show the response of the nominal models with respect to the change in the state: x acceleration, z acceleration, pitch acceleration, and pitch rate and the state: x velocity, z velocity, pitch rate, and Euler angle.

In the comparison using the sine wave input in Figs. 8.10 and 8.11, the response of the nominal models compared to the change in the state show a good fit. A good fit is defined as following closely the overall shape of the flight data and having no offset. The comparison of the states show that the nominal models are able fit the pitch rate and Euler angle data well. The nominal models' pitch rate does differ only in its response at the peaks of the oscillations. The models do have trouble with the x and z velocity. The x velocity comparison shows that the models are able to capture the correct frequency response, but the amplitude is not consistent with the flight data. This is confirmed by the Fig. 8.17, which shows an error that is independent of the frequency but drifts in time.

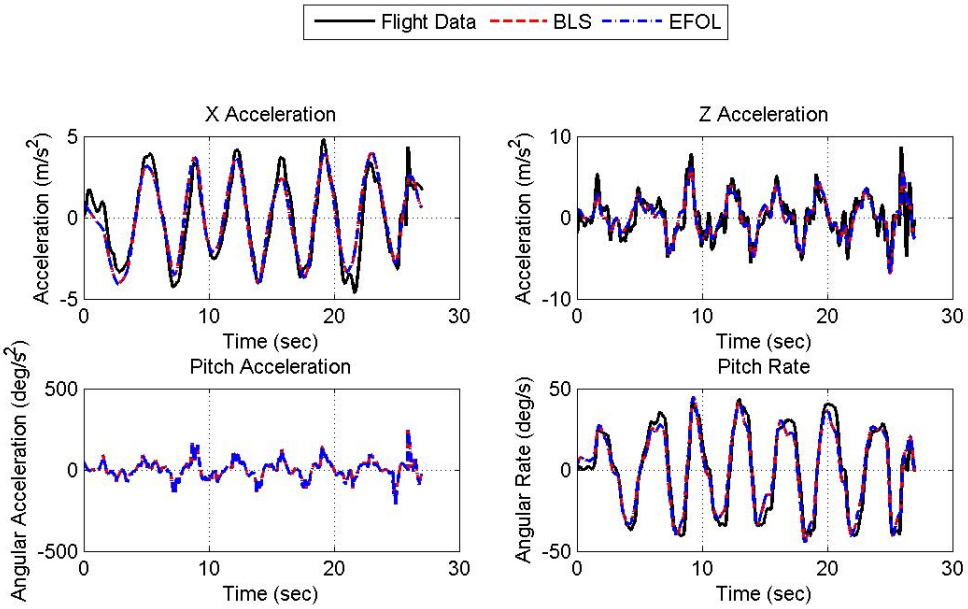

Fig. 8.10: The state derivative comparison of the flight data to the BLS and BLS with EFOL nominal models using a sine wave input.

The z velocity comparison also shows that the models are able to identify the correct frequency response but there is a bias in the mean value of the oscillations. This is confirmed in the Fig. 8.17, where the z velocity error plot shows a non-zero mean error. As with the pitch rate, the nominal models do not track well the motion at the peaks of the oscillation. This is most likely due to the fact that the models assumes a rigid body when in fact the UAV, especially the joints in the outboard wing panels are not rigidly attached. This results in the wings bending and flapping at the min and max of each oscillation.

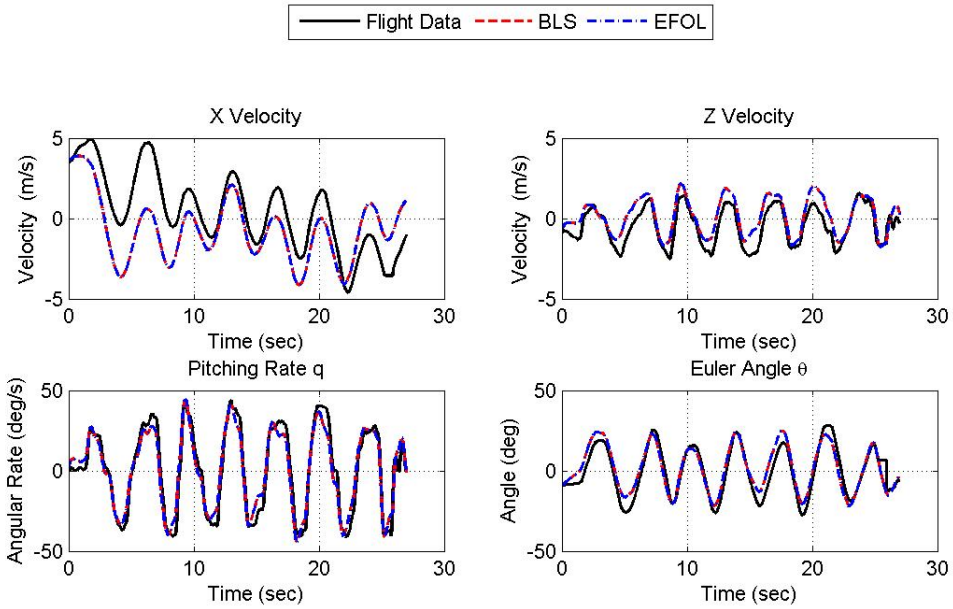

Fig. 8.11: The state comparison of the flight data to the BLS and BLS with EFOL nominal models using a sine wave input.

The doublet and singlet maneuvers are designed to excite both the short and long periods. These maneuvers differ from the sign wave and chirp maneuvers in that, after the control input is given, the aircraft is allowed to oscillate freely without additional control inputs. These maneuvers are especially important in evaluating how well the nominal models have identified the long period mode. The nominal models responds similarly to both maneuvers. In both the x acceleration and x velocity, the nominal models predicts an oscillatory motion that is at a higher frequency than the flight data. The oscillatory motion of the model is also more pronounce than the flight data. The x acceleration errors, shown in Figs. 8.18 and 8.20, indicate that nominal model predicts a frequency response different than the flight data. The x velocity errors, shown in Figs. 8.19 and 8.21, indicate that the models predict oscillations with a different amplitude seen as a none zero mean oscillation in the error. The 1-2 Hz osculations in all the state derivatives and the states is not resolved by the nominal models. This oscillation could be something structural and further analysis should be performed.

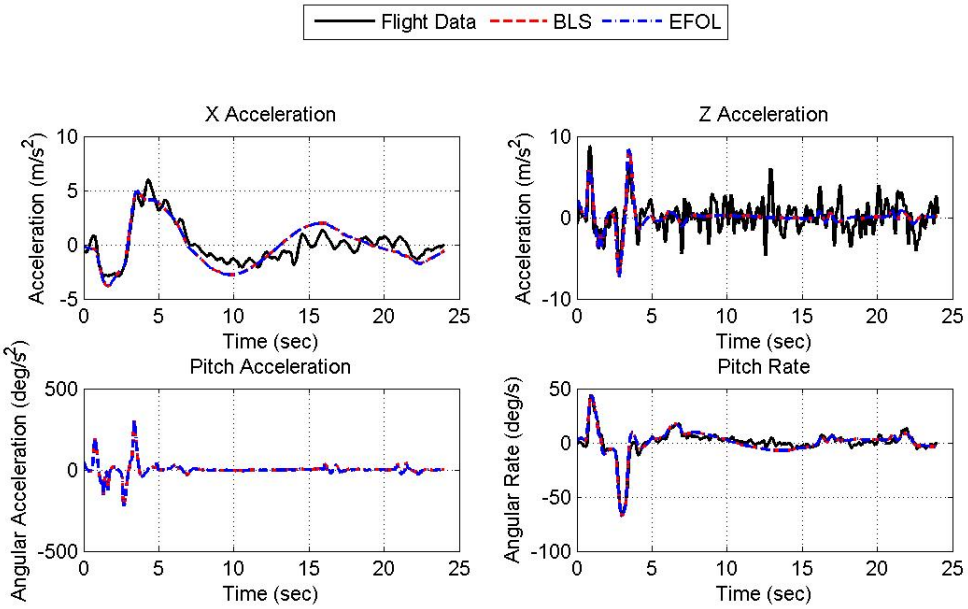

Fig. 8.12: The state derivative comparison of the flight data to the BLS and BLS with EFOL nominal models using a doublet input.

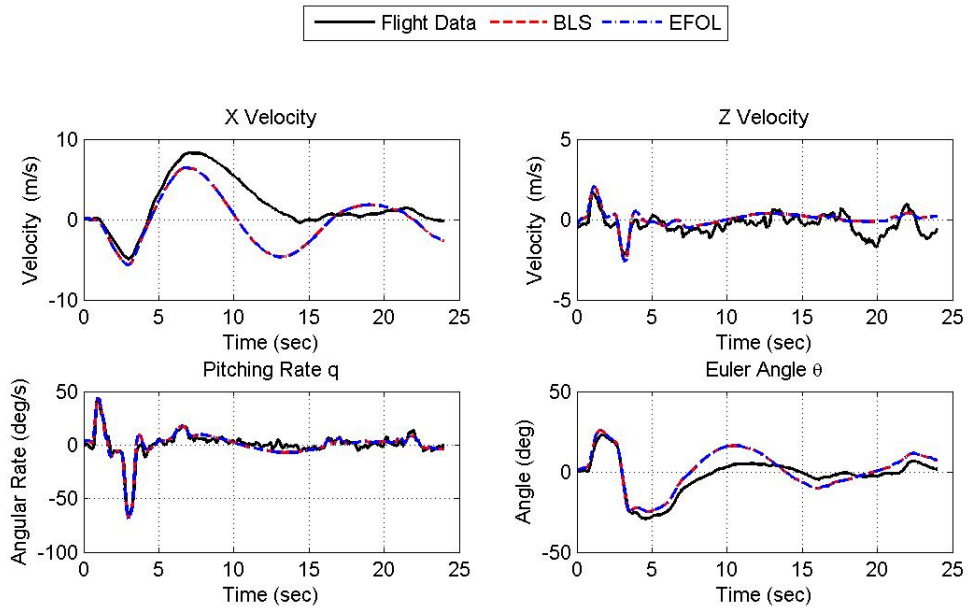

Fig. 8.13: The state comparison of the flight data to the BLS and BLS with EFOL nominal models using a doublet input.

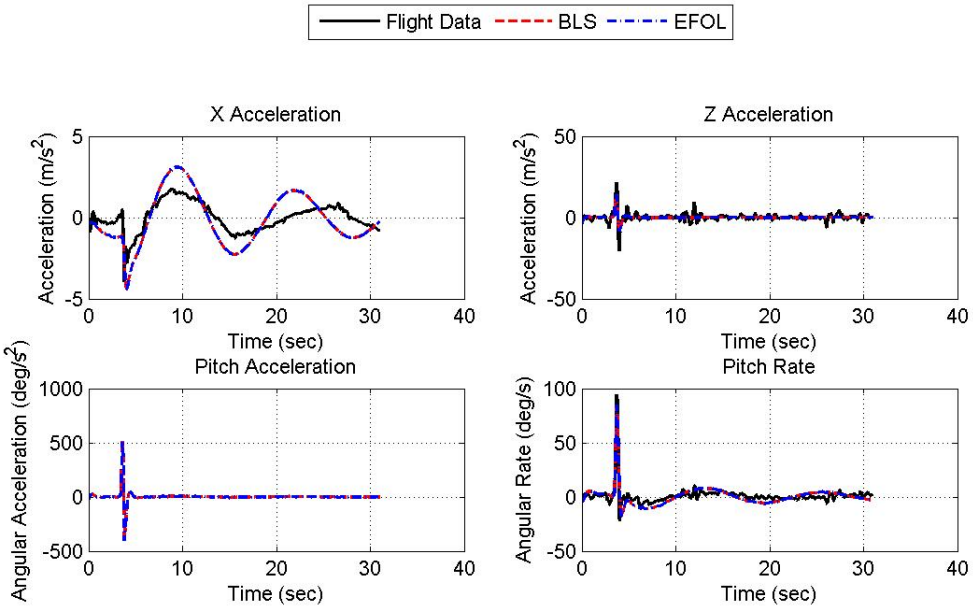

Fig. 8.14: The state derivative comparison of the flight data to the BLS and BLS with EFOL nominal models using a singlet input.

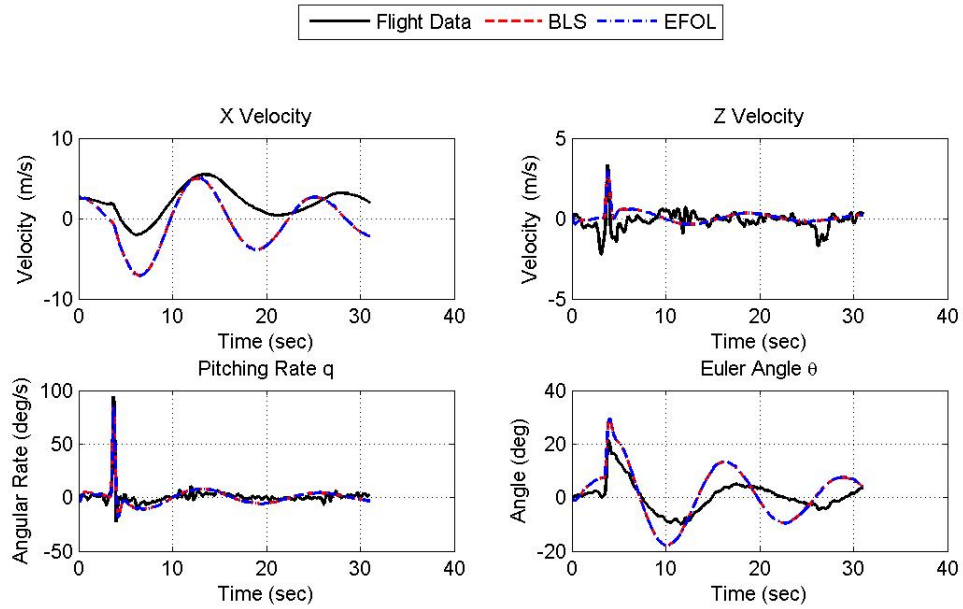

Fig. 8.15: The state comparison of the flight data to the BLS and BLS with EFOL nominal models using a singlet input.

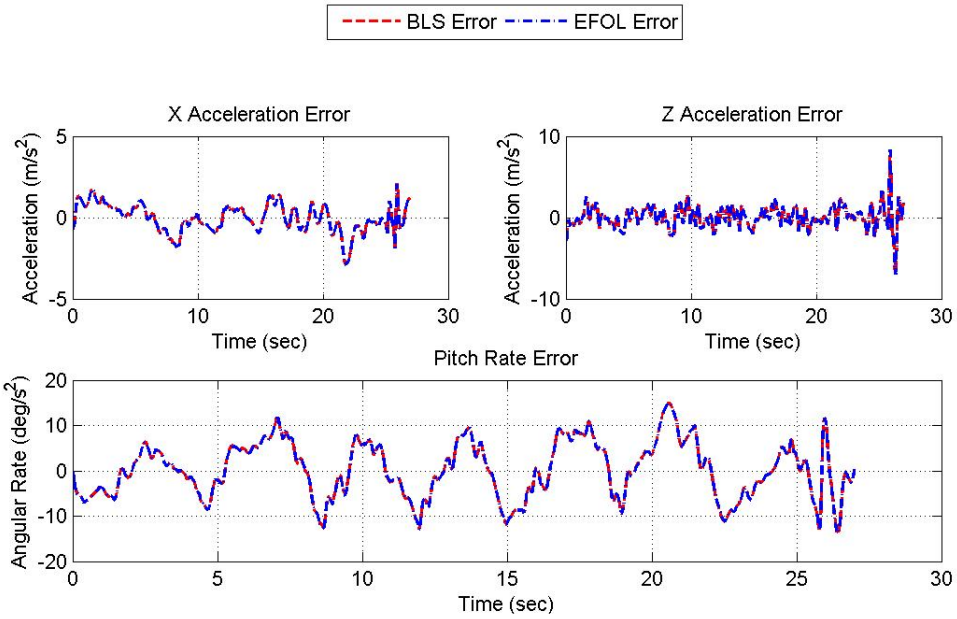

Fig. 8.16: The error from the state derivative comparison of the flight data to the BLS and BLS with EFOL nominal models using a sine wave input.

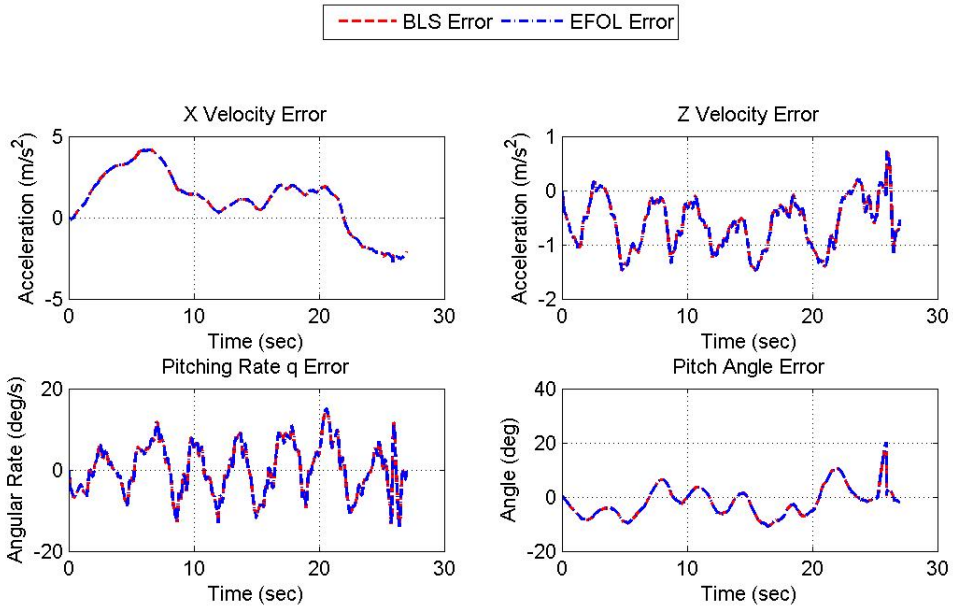

Fig. 8.17: The error from the state comparison of the flight data to the BLS and BLS with EFOL nominal models using a sine wave input.

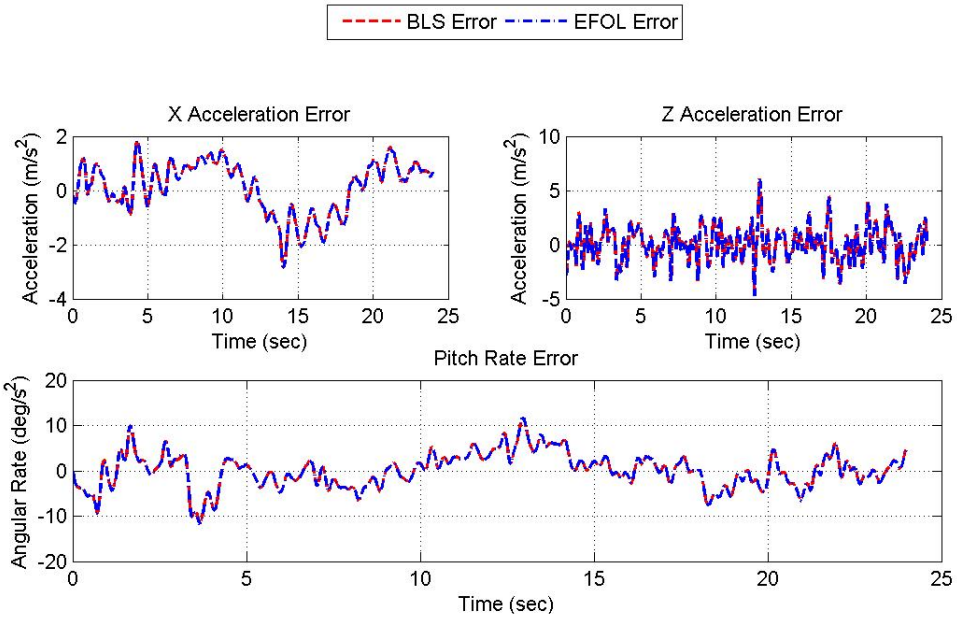

Fig. 8.18: The error from the state derivative comparison of the flight data to the BLS and BLS with EFOL nominal models using a doublet input.

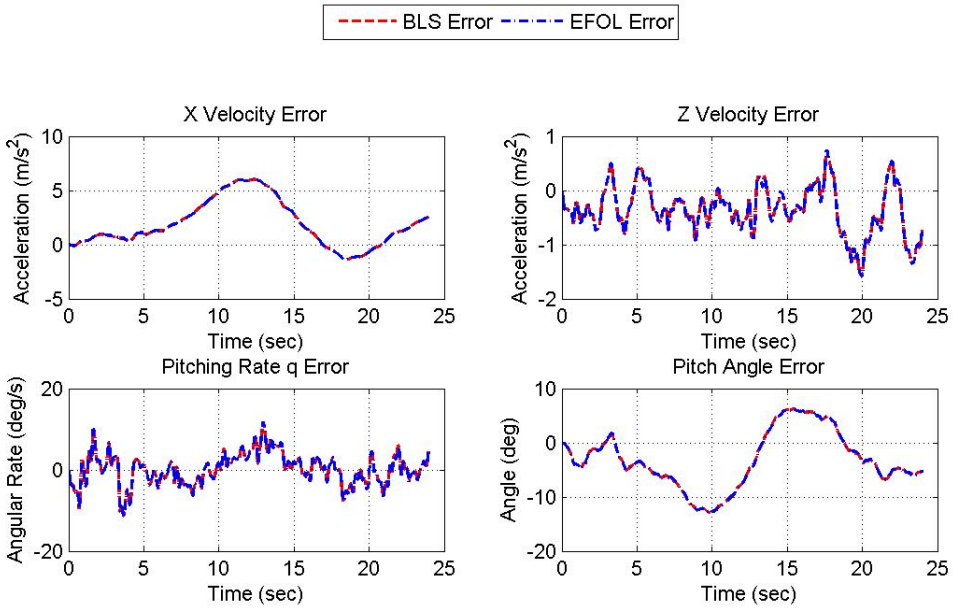

Fig. 8.19: The error from the state comparison of the flight data to the BLS and BLS with EFOL nominal models using a doublet input.

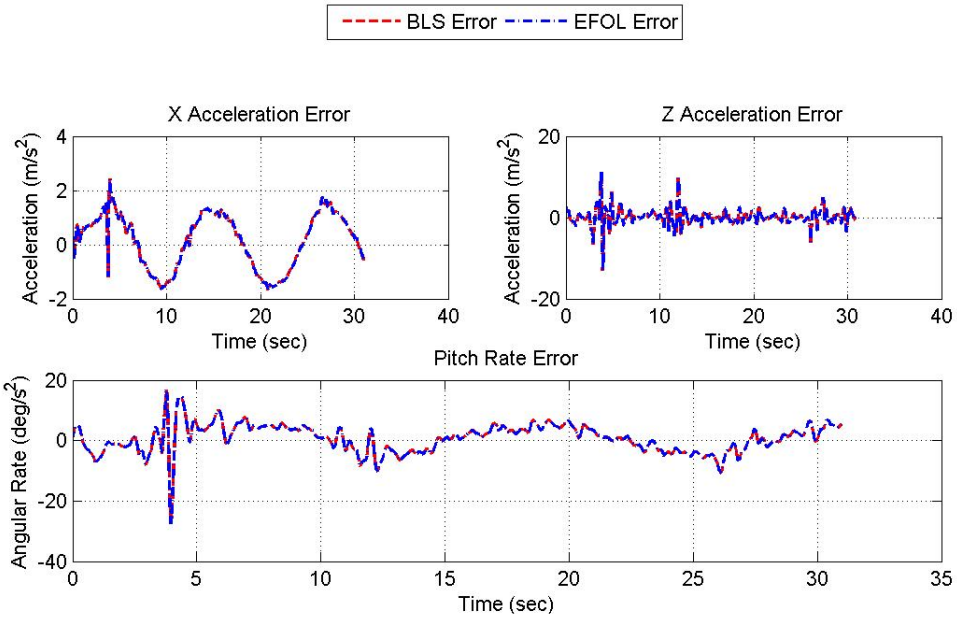

Fig. 8.20: The error from the state derivative comparison of the flight data to the BLS and BLS with EFOL nominal models using a singlet input.

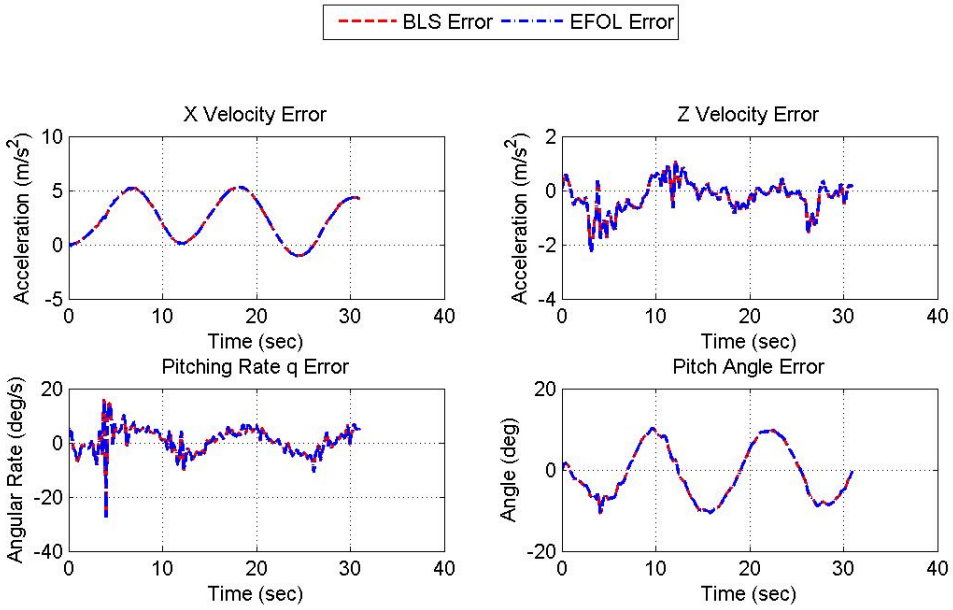

Fig. 8.21: The error from the state comparison of the flight data to the BLS and BLS with EFOL nominal models using a singlet input.

Table 8.4: The mean values of the error from the comparison of flight data to the nominal models

Parameter	***Sine wave***		***Doublet***		***Singlet***	
	BLS	***EFOL***	***BLS***	***EFOL***	***BLS***	***EFOL***
$\dot{u}$ $[m/s^2]$	0.6899	0.6902	0.8134	0.8151	0.8905	0.8969
$\dot{w}$ $[m/s^2]$	0.9170	0.9178	1.220	1.222	1.255	1.255
$\dot{\theta}$ $[deg/s]$	5.184	5.202	2.951	2.979	3.661	3.672
u $[m/s]$	1.806	1.811	2.118	2.119	2.519	2.521
w $[m/s]$	0.6400	0.6411	0.4682	0.4686	0.4487	0.4497
q $[deg/s]$	5.184	5.202	2.951	2.979	3.661	3.672
θ $[deg]$	4.721	4.738	5.236	5.242	5.821	5.861

Overall the nominal models are able to identify the oscillatory motion of the UAV when the oscillation is being driven by an input. The models are not, however, able to identify the oscillations that accompany a doublet or singlet. One of these maneuvers could be added to the model to increase the amount of training data the model has.

8.4 Identified Nominal Model Eigenvalues

The Eigenvalues of equations of motion are used to determine the stability an response of a system. In flight mechanics there are two modes associated with the linearized longitudinal equations of motion: short period and long period (phugoid). For a general aviation aircraft these two modes are convergent and oscillatory meaning that the eigenvalues are pairs having a negative real part and an imaginary part. The short period is always associated with the largest real Eigenvalue pair of the longitudinal motion and is generally characterized by a short period and large damping. The long period is then associated with the smaller Eigenvalue pair. For a general aviation aircraft the long period is characterized by a long period oscillation that is slightly damped. The Eigenvalues for the Minion class UAV are presented in Table 8.5 and Fig. 8.22.

Table 8.5: Summary of the Eigenvalues

Parameter	***BLS mean***	***BLS std***	***EFOL mean***	***EFOL std***
Short Period	-3.17 $\pm$4.70i	0.54 0.65i	-3.14 $\pm$4.70i	0.55 0.66i
Long Period	-0.05 $\pm$0.48i	0.035 0.12i	-0.05 $\pm$0.4876i	0.035 0.12i

The Eigenvalues shown in Fig. 8.22 indicate that the Minion class UAV has a convergent short period as is expected. The long period mean Eigenvalue indicates that the mode is convergent. Taking in to consideration the standard deviation of the real part indicates that the long period for this UAV could be slightly divergent. Since the long period stability is related to aircraft drag, it is possible that the Minion UAV, which is very stream lined, could indeed have a slightly divergent long period. In practice it is difficult to fully capture the long period mode. In order to identify the long period the UAV must be allowed to oscillate with no pilot input for at least one full period. This becomes difficult for a pilot when the aircraft must stay within visual line of sight. Consistently identifying the long period would require several full oscillations to be recorded. This is however impractical for a human pilot, which is the case here.

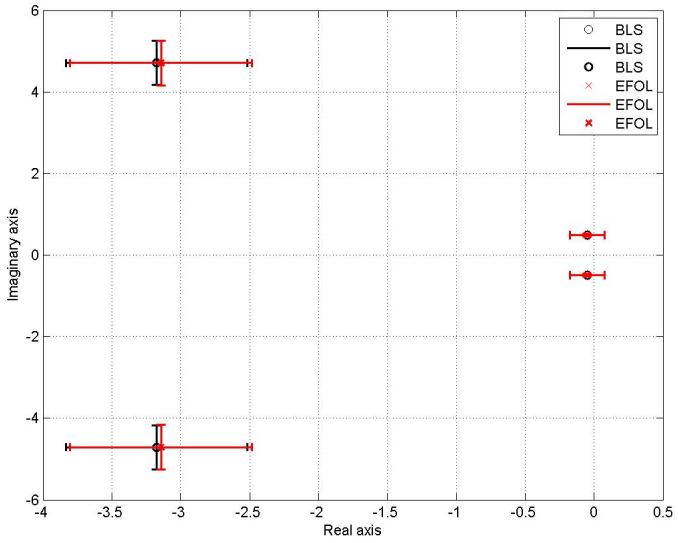

Fig. 8.22: The mean value of the eigenvalues of the identified models with standard deviation error bars. All BLS and BLS with EFOL coefficients over lap within the error bounds.

8.5 Identified All-Data Model vs. Flight Data

In an attempt to improve the performance of the identified model, all flight data (both training and evaluation data) is used to train the model. The data is from both flights and includes all maneuvers. This section presents the results of the all data model compared to the flight data.

The model identified from all longitudinal maneuvers tracks well the sine maneuvers as shown in Figs. 8.23 and 8.24. The all-data model has a same performance as the nominal models from BLS and BLS with EFOL with respect to tracking sine wave maneuvers.

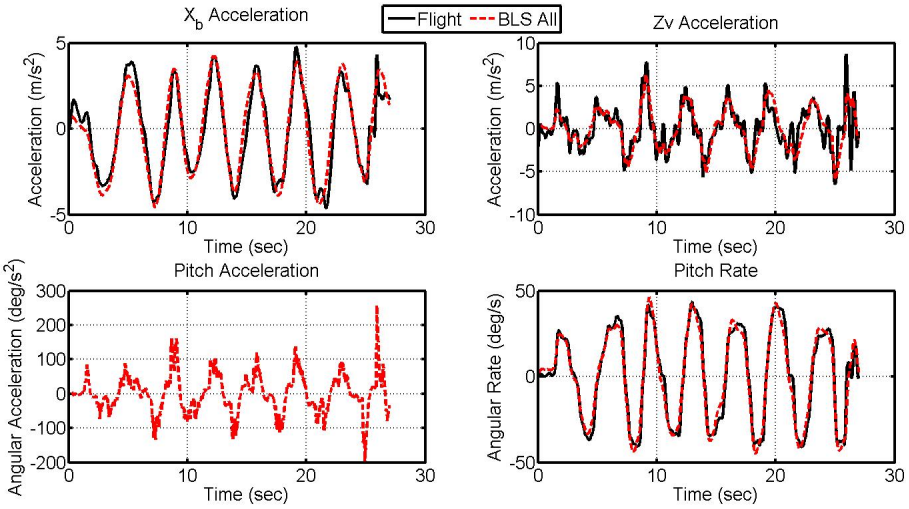

Fig. 8.23: The state derivative comparison of the flight data to the BLS all-data model using a sine input.

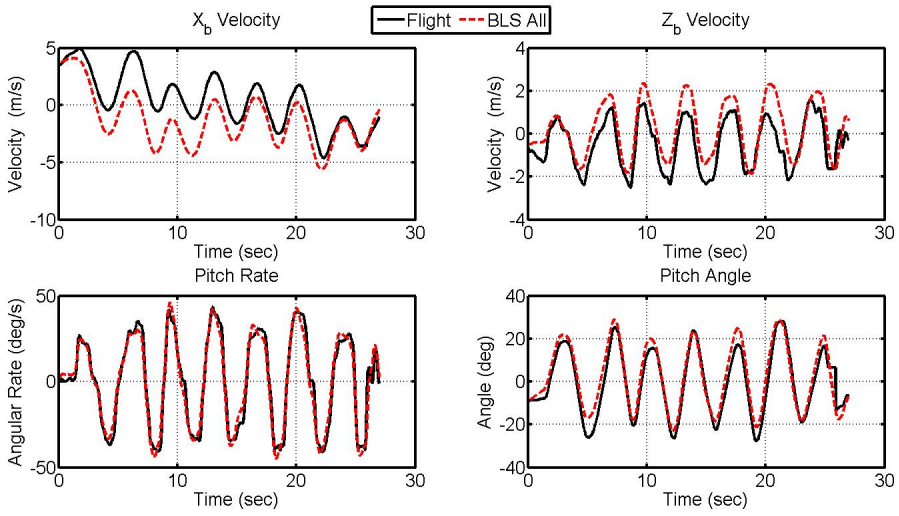

Fig. 8.24: The state comparison of the flight data to the BLS all-data model using a sine input.

Figures 8.25 and 8.26 show the all-data model's response to a doublet input. The all-data model follows well the frequency of the flight data but has difficulty at the end of the maneuver following the response. The all-data model predictive capabilities are similar to that of the nominal BLS and BLS with EFOL models.

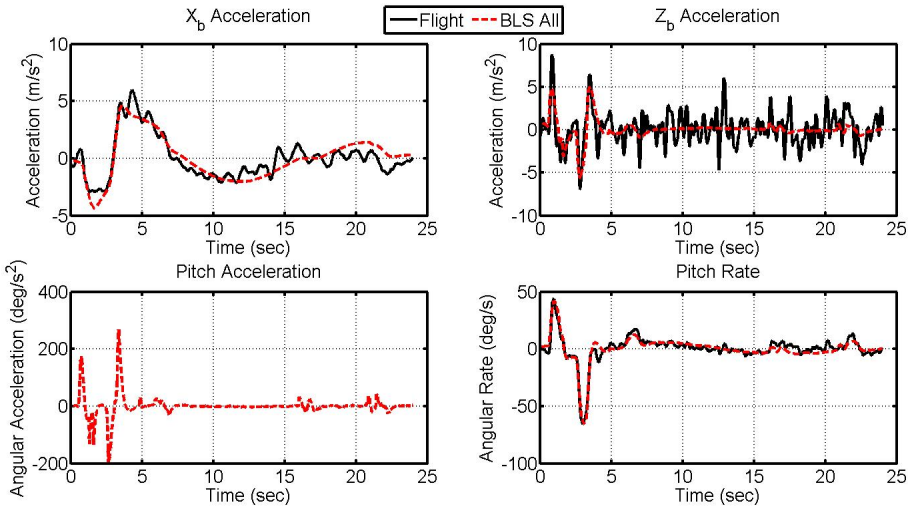

Fig. 8.25: The state derivative comparison of the flight data to the BLS all-data model using a doublet input.

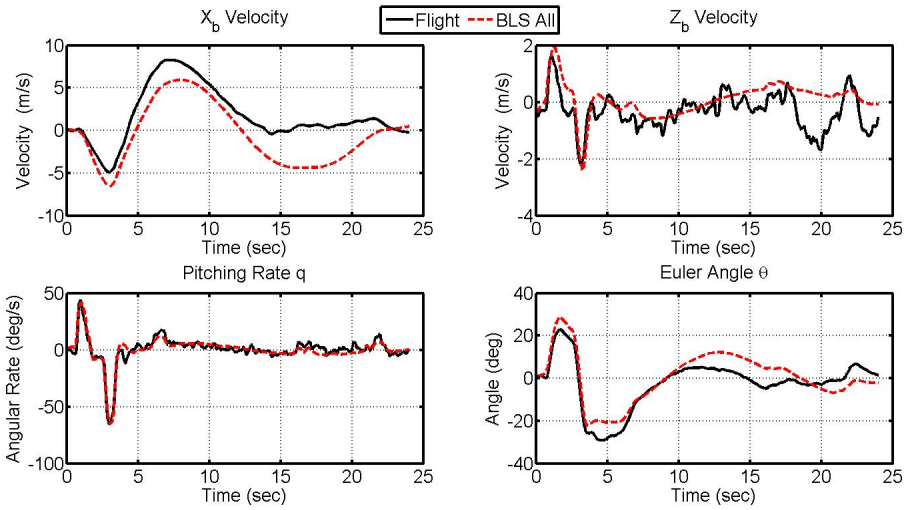

Fig. 8.26: The state comparison of the flight data to the BLS all-data model using a doublet input.

The singlet maneuver comparison of flight data and the all-data model is shown in Figs. 8.27 and 8.28. The all-data models does not match the frequency of the oscillations in the flight data. This response is similar to that of the nominal models.

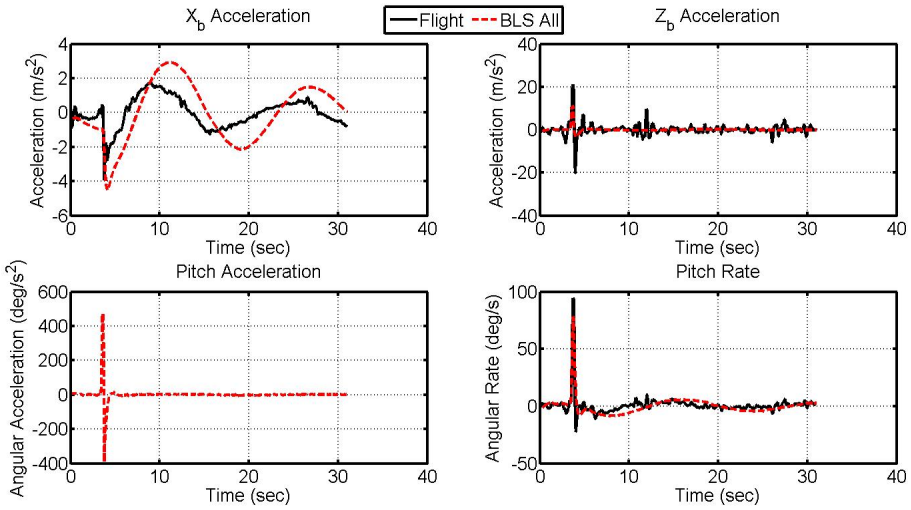

Fig. 8.27: The mean value of the eigenvalues of the identified models with standard deviation error bars. All BLS and BLS with EFOL coefficients over lap within the error bounds.

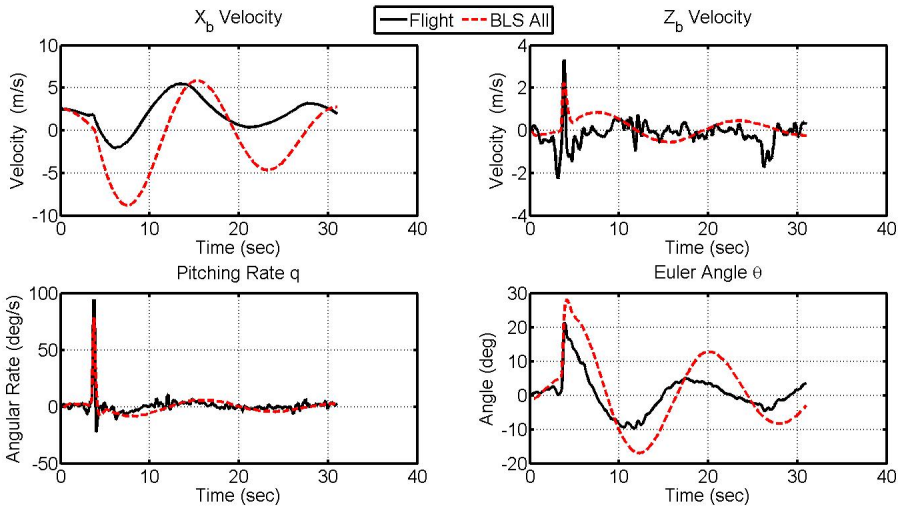

Fig. 8.28: The mean value of the eigenvalues of the identified models with standard deviation error bars. All BLS and BLS with EFOL coefficients over lap within the error bounds.

Overall using all longitudinal flight data to train the model does not seem to have a clear advantage over the nominal BLS and BLS with EFOL models. This is most likely due to the singlet and doublet maneuvers and not sufficiently long to identify properly the dynamics of the long period. If the aircraft was allowed to fly without input for 3 full cycles then the model may be more accurate at identifying the dynamics.

8.6 Chapter Summary

The identified linear longitudinal nominal model and its parameters have been shown. It has been shown that BLS with EFOL give the same response as BLS. The UAV has been simulated using the identified model and elevator inputs from flight data. The simulated data has been compared to the flight data. The error between the two sets of data has been discussed. The nominal model fits the chirp and sine wave data well, but does not correctly resolve the long period mode in the doublet and singlet maneuvers. The all-data models shows no significant advantage over the nominal models.

Chapter 9

Conclusion and Future Research

System identification has been and will continue to be an invaluable tool for determining mathematical models that accurately simulate dynamic systems. It is particularly useful for manned and unmanned aircraft where analytical solutions may fall short, wind tunnel testing is not available, or CFD methods maybe too time intensive. There are many advantages of system identification of UAVs but there are also several difficulties that must also be properly dealt with.

9.1 Summary

This thesis has presented the current state of system identification of small low-cost unmanned aerial vehicles. Research objectives have been described. The linear longitudinal equations of motion of the UAV have been rigorously derived. The least squares system identification method with an Error Filtering Online Learning Scheme has been developed. The batch least squares and batch least squares with EFOL has been applied to the Minion class UAV linear longitudinal dynamics. The flight test procedure and maneuvers have been described along with the data processing procedure. Finally the results of the system identification have been examined and a comparison of the identified UAV linear longitudinal flight dynamics to flight data have been given.

9.2 Lessons Learned

There are several important lessons to be learned about system identification of small unmanned aerial vehicles, especially when low-cost is the highest priority. The lessons learned are a direct result of struggling obtaining kinematically consistent flight data and identifying the linear longitudinal equation of motion parameters using Batch Least Squares.

The lessons learned are summarized:

- Flight data must be kinematically consistent or the system ID will be unsuccessfully.
- MEMS accelerometers have bias which is extremely difficult to remove, even for systems with Kalman/Extended Kalman filters.
- GPS is not susceptible to the same errors as MEMS accelerometers but have low update rates (4 Hz).
- For system ID using Least Squares, the sensor requirement is a GPS-Aided Inertial Navigation System with Kalman filtering.
- Do not use accelerometer data for Least Squares system ID. Instead use differentiated body velocity from a GPS-Aided Inertial Navigation System with Kalman filtering.

9.3 Conclusion

The BLS and BLS with EFOL system ID using flight data from VectorNav VN-200 GPS/INS is successful in identifying the linearized longitudinal equation of motion parameters for chirp maneuvers. The mean value of these parameters are used to form nominal models of the UAV. The nominal models fit flight data of sine wave maneuvers but have a poorer fit for the doublet and singlet maneuvers. This poor fit corresponds to incorrectly identifying the long period mode. A better fit can be obtained by using a doublet or singlet maneuver as part of the model training data. Also the nominal models do not predict the 1-2 Hz oscillations seen in the doublet and singlet maneuvers. The cause of these oscillations should be investigated to see if they are a result of aerodynamics or the structure of the aircraft.

9.4 Future Research

Future system identification efforts should focus on:

- Applying and evaluating continuous least squares with EFOL to the flight data that has been collected

- Expanding the system ID method to include lateral dynamics
- Expanding system ID method to include nonlinear dynamics
- Applying full state Extended Kalman Filter using the aerodynamic parameters as states
- Determining how well this system ID method is able to identify changes in the control surface aerodynamic coefficients for fault detection
- Determining how well suited this method is for online identification with limited computing resources
- Developing an online system identification process for real time parameter estimation
- Using the online system ID for adaptive control

References

[1] Engel, A., and Teichert, B., "The Photogrammetric Potential of Low-cost UAVs in Forestry and Agriculture," *The International Archives of the Photogrammetry, Remote Sensing and Spatial Information Sciences*, Vol. 1, No. B1, 2008, pp. 1207–1214.

[2] Rango, A., Berte, A. L., Steele, C., Herrick, J. E., Bestelmeyer, B., Schmugge, T., Roanhorse, A., and Jenkins, V., "Using Unmanned Aerial Vehicles for Rangelands: Future Potentials," *Environmental Practice*, Vol. 68, 2006, pp. 159–168.

[3] Jensen, A., Hardy, T., Mckee, M., and Chen, Y. Q., "Using a Multispectral Autonomous Unmanned Aerial Remote Sensing Platform (AggieAir) for Riparian and Wetlands Applications," *Proceedings of the 2011 IEEE International Geoscience and Remote Sensing Symposium*, 2011, pp. 3413–3416.

[4] "Integration of Civil Unmanned Aircraft Systems (UAS) in the National Airspace System (NAS) Roadmap," Tech. Rep., FAA, 2013.

[5] Dalamagkidis, K., Valavanis, K., and Piegl, L., "On unmanned aircraft systems issues, challenges and operational restrictions preventing integration into the National Airspace System," *Progress in Aerospace Sciences*, Vol. 44, No. 7-8, Oct. 2008, pp. 503–519.

[6] Dalamagkidis, K., Valavanis, K. P., and Piegl, L. A., "Current Status and Future Perspectives for Unmanned Aircraft System Operations in the US," *Journal of Intelligent and Robotic Systems*, Vol. 52, No. 2, Feb. 2008, pp. 313–329.

[7] Phillips, W. F., *Mechanics of Flight*, John Wiley & Sons, Inc, Hoboken, NJ, 2nd ed., 2009.

[8] Morris, S., and Holden, M., "Design of Micro Air Vehicles and Flight Test Validation," *Proceedings of the Fixed, Flapping and Rotary Wing Vehicles at Very Low Reynolds Numbers Conference*, 2000, pp. 153–176.

[9] Tischler, M. B., and Remple, R. K., *Aircraft and Rotorcraft System Identification: Engineering Methods with Flight Test Examples*, AIAA, Inc, Virginia, 2006.

[10] Crassidis, J. L., and Junkins, J. L., *Optimal Estimation of Dynamic Systems*, CRC Press, Boca Raton, FL, 2nd ed., 2011.

[11] Farrell, J. A., and Polycarpou, M. M., *Adaptive Approximation Based Control: Unifying Neural, Fuzzy and Traditional Adaptive Approximation Approaches*, John Wiley & Sons, Inc, Hoboken, NJ, 1st ed., 2006.

[12] Dorobantu, A., Murch, A., Mettler, B., and Balas, G., "Frequency Domain System Identification for a Small, Low-cost, Fixed-wing UAV," *Proceedings of the 2011 AIAA Guidance, Navigation, and Control Conference*, 2011.

[13] Chen, Y., Wen, C., Dou, H., and Sun, M., "Iterative Learning Identification of Aerodynamic Drag Curve from Tracking Radar Measurements," *Control Engineering Practice*, Vol. 5, No. 11, Nov. 1997, pp. 1543–1553.

[14] Putro, I., Budiyono, A., Yoon, K., and Kim, D., "Modeling of Unmanned Small Scale Rotorcraft Based on Neural Network Identification," *Proceedings of the 2008 IEEE International Conference on Robotics and Biomimetics*, 2009, pp. 1938–1943.

[15] Cory, R., and Tedrake, R., "Experiments in Fixed-wing UAV Perching," *Proceedings of the AIAA Guidance, Navigation, and Control Conference*, 2008.

[16] Hoburg, W., and Tedrake, R., "System Identification of Post Stall Aerodynamics for UAV Perching," *In: Proceedings of the AIAA Infotech@ Aerospace Conference*, 2009, pp. 1–9.

[17] Keesman, K. J., *System Identification: An Introduction*, Springer-Verlag, London, 2011.

[18] Isermann, R., and Münchhof, M., *Identification of Dynamic Systems: An Introduction with Applications*, Springer, 2010.

[19] Ljung, L., *System Identification-Theory for User*, Prentice Hall, Upper Saddle River, NJ, 2nd ed., 1999.

[20] Salman, S., Puttige, V., and Anavatti, S., "Real-time Validation and Comparison of Fuzzy Identification and State-space Identification for a UAV Platform," *Proceedings of the 2006 IEEE International Conference on Control Applications*, 2006, pp. 2138–2143.

[21] Mettler, B., Tischler, M. B., and Kanade, T., "System Identification of Small-size Unmanned Helicopter Dynamics," *Annual Forum Proceedings of the American Helicopter Society*, Vol. 2, 1999, pp. 1706–1717.

[22] Ivler, C., and Tischler, M., "System Identification Modeling for Flight Control Design," *Proceedings of the RAeS Rotorcraft Handling-Qualities Conference*, Vol. 47, 2008, p. 50.

[23] Mettler, B., Kanade, T., and Tischler, M., "System Identification Modeling of a Model-scale Helicopter," *Carnegie Mellon University, The Robotics Institute*, 2000, pp. 1–25.

[24] Adiprawita, W., Ahmad, A., and Sembiring, J., "Automated Flight Test and System Identification for Rotary Wing Small Aerial Platform Using Frequency Responses Analysis," *Journal of Bionic Engineering*, Vol. 4, No. 4, 2007, pp. 7.

[25] Yuan, W., and Katupitiya, J., "A Time-domain Grey-box System Identification Procedure for Scale Model Helicopters," *Proceedings of the 2011 Australasian Conference on Robotics and Automation*, 2011.

[26] Bottasso, C., Leonello, D., Maffezzoli, A., and Riccardi, F., "A Procedure for the Identification of the Inertial Properties of Small-size UAVs," *in XX AIDAA Congress*, 2009.

[27] Bhandari, S., Colgren, R., Lederbogen, P., and Kowalchuk, S., "Six-dof Dynamic Modeling and Flight Testing of a UAV Helicopter," *Proceeding of the AIAA Modeling and Simulation Technologies Conference and Exhibit*, 2005, pp. 992–1008.

[28] Morris, J., Van Nieuwstadt, M., and Bendotti, P., "Identification and Control of a Model Helicopter in Hover," *Proceedings of the American Control Conference*, 1994, pp. 1238–1242.

[29] Kim, H., and Shim, D., "A Fight Control System for Aerial Robots: Algorithms and Experiments," *Control Engineering Practice*, Vol. 11, No. 12, 2003, pp. 1389–1400.

[30] Kim, B., Chang, Y., and Lee, M., "System Identification and 6-dof Hovering Controller Design of Unmanned Model Helicopter," *JSME International Journal Series C*, Vol. 49, No. 4, 2006, pp. 1048–1057.

[31] Garratt, M., Ahmed, B., and Pota, H., "Platform Enhancements and System Identification for Control of an Unmanned Helicopter," *Proceedings of the 9th International Conference on Control Automation Robotics and Vision*, 2006.

[32] Cai, G., Chen, B., and Peng, K., "Modeling and Control of the Yaw Channel of a UAV Helicopter," *IEEE Transactions on Industrial Electronics*, Vol. 55, No. 9, 2008, pp. 3426–3434.

[33] Budiyono, A., Yoon, K., and Daniel, F., "Integrated Identification Modeling of Rotorcraft-based Unmanned Aerial Vehicle," *Proceedings of the 17th Mediterranean Conference on Control and Automation*, 2009, pp. 898–903.

[34] Schafroth, D., Bermes, C., Bouabdallah, S., and Seigwart, R., "Modeling and System Identification of the Mufly Micro Helicopter," *Journal of Intelligent and Robotic Systems*, Vol. 57, No. 1-4, Oct. 2010, pp. 27–47.

[35] Shim, D. H., Kim, H., and Sastry, S., "Control System Design for Rotorcraft-based Unmanned Aerial Vehicles Using Time-domain System Identification," *Proceedings of the 2000 IEEE International Conference on Control Applications Conference Proceedings*, Vol. 2000, No. 2, 2000, pp. 808–813.

[36] Hashimoto, S., Ogawa, T., Adachi, S., Tan, A., and Miyamori, G., "System Identification Experiments on a Large-scale Unmanned Helicopter for Autonomous Flight," *Proceedings of the 2000 IEEE International Conference on Control Applications Conference*, 2000, pp. 850–855.

[37] Ng, A., Coates, A., Diel, M., Ganapathi, V., Schulte, J., Tse, B., Berger, E., and Liang, E., "Autonomous Inverted Helicopter Flight Via Reinforcement Learning," *Experimental Robotics*, Vol. IX, 2006, pp. 363–372.

[38] Abbeel, P., Coates, A., Quingley, M., and Ng, A. Y., "An Application of Reinforcement Learning to Aerobatic Helicopter Flight," *Advances in Neural Information Processing Systems*, Vol. 19, 2007.

[39] Schafroth, D., Bermes, C., Bouabdallah, S., and Siegwart, R., "Modeling, System Identification and Robust Control of a Coaxial Micro Helicopter," *Control Engineering Practice*, Vol. 18, No. 7, July 2010, pp. 700–711.

[40] Rimal, B., Putro, I., Budiyono, A., Min, D., and Choi, E., "System Identification of NN-based Model Reference Control of RUAV During Hover," *Artificial Neural Networks - Industrial and Control Engineering Applications, InTech*, 2011, pp. 395–420.

[41] Kallapur, A., Samal, M., Vishwas, P., Sreenatha, A., Garratt, and Mathew, "A UKF-NN Framework for System Identification of Small Unmanned Aerial Vehicles," *Proceedings of the 2008 11th International IEEE Conference on Intelligent Transportation Systems*, 2008, pp. 1021–1026.

[42] Samal, M., Anavatti, S., and Garratt, M., "Real-time Neural Network Based Identification of a Rotary-wing UAV Dynamics for Autonomous Flight," *Proceedings of the 2009 IEEE International Conference on Industrial Technology*, IEEE, 2009.

[43] Samal, M., Anavatti, S., and Garratt, M., "Neural Network Based System Identification for Autonomous Flight of an Eagle Helicopter," *In: Proceedings of the 17th World Congress of the International Federation of Automatic Control*, 2008, pp. 7421–7426.

[44] Chowdhary, G., and Lorenz, S., "Control of a VTOL UAV via Online Parameter Estimation," *Proceeding of the AIAA Guidance, Navigation, and Control Conference and Exhibit*, Aug. 2005, pp. 1–15.

[45] Heredia, G., and Ollero, A., "Sensor Fault Detection in Small Autonomous Helicopters Using Observer/Kalman Filter Identification," *In: Proceedings of the 2009 IEEE International Conference on Mechatronics*, Vol. 00, No. April, 2009, pp. 1–6.

[46] Abbeel, P., Ganapathi, V., and Ng, A., "Learning Vehicular Dynamics, with Application to Modeling Helicopters," *Advances in Neural Information Processing Systems*, Vol. 18, 2006.

[47] Chowdhary, G., and Jategaonkar, R., "Aerodynamic Parameter Estimation From Flight data applying extended and unscented kalman filter," *In: Proceedings of the 2006 AIAA Atmospheric Flight Mechanics Conference*, 2006.

[48] Lei, X., and Du, Y., "A Linear Domain System Identification for Small Unmanned Aerial Rotorcraft Based on Adaptive Genetic Algorithm," *Journal of Bionic Engineering*, Vol. 7, No. 2, June 2010, pp. 142–149.

[49] Muhammad, H., Thien, H. P., and Mulyanto, T., "Total Least Squares Estimation of Aerodynamic Parameter of Micro Coaxial Helicopter from Flight Data," *International Journal of Basic & Applied Sciences*, Vol. 12, No. 02, 2012, pp. 44–52.

[50] Vélez, C., Agudelo, A., and Alvarez, J., "Modeling, Simulation and Rapid Prototyping of an Unmanned Mini-elicopter," *In: Proceedings of the AIAA Modeling and Simulation Technologies Conference*, 2006.

[51] Cai, G., Chen, B. M., and Lee, T. H., "An Overview on Development of Miniature Unmanned Rotorcraft Systems," *Frontiers of Electrical and Electronic Engineering in China*, Vol. 5, No. 1, Sept. 2009, pp. 1–14.

[52] Ahmad, S., Shaheed, M., Chipperfield, A., and Tokhi, M., "Non-linear Modeling of a One-degree-of-freedom Twin-rotor Multi-input Multi-output System Using Radial Basis Function Networks," *Proceedings of the Institution of Mechanical Engineers*, Vol. 216, No. 4, 2002, pp. 197–208.

[53] Hu, C., Huang, X., Hu, J., and Zhu, J., "System Identification of a Small UAV's Speeding Up Process Before Take-off," *Proceedings of the 2004 5th Asian Cotnrol Conference*, O'Reilly, 2004.

[54] Li, Z., Hoffer, N., Stark, B., and Chen, Y., "Design, Modeling and Validation of a T-tail Unmanned Aerial Vehicle," *Journal of Intelligent & Robotic Systems*, Vol. 69, No. 1-4, Aug. 2012, pp. 91–107.

[55] Debusk, W. M., Chowdhary, G., and Johnson, E. N., "Real-time System Identification of a Small Multi-engine Aircraft," *In: Proceedings of the AIAA Atmospheric Flight Mechanics Conference*, 2009, pp. 1–15.

[56] Teo, R., Jang, J., and Tomlin, C., "Automated Multiple UAV flight-the Stanford Dragonfly UAV Program," *In: Proceedings of the 43rd IEEE Conference on Decision and Control*, Vol. 4, 2004, pp. 4268–4273.

[57] Wu, H., Sun, D., and Zhou, Z., "Model Identification of a Micro Air Vehicle in Loitering Flight Based on Attitude Performance Evaluation," *IEEE Transactions on Robotics*, Vol. 20, No. 4, 2004, pp. 702–712.

[58] Manai, M., Desbiens, A., and Gagnon, E., "Identification of a UAV and Design of a Hardware-in-the-loop System for Nonlinear Control Purposes," *AIAA Guidance, Navigation, and Control Conference*, Vol. 8, 2005, pp. 6441–6446.

[59] Paw, Y. C., and Balas, G. J., "Development and Application of an Integrated Framework for Small UAV Flight Control Development," *Mechatronics*, Vol. 21, No. 5, Aug. 2011, pp. 789–802.

[60] Cho, J., Principe, J., Erdogmus, D., and Motter, M., "Modeling and Inverse Controller Design for an Unmanned Aerial Vehicle Based on the Self-organizing Map," *IEEE Transactions on Neural Networks*, Vol. 17, No. 2, 2006, pp. 445–60.

[61] Puttige, V., and Anavatti, S., "Real-time Neural Network Based Online Identification Technique for a UAV Platform," *In: Proceedings of the International Conference on Computational Intelligence for Modelling Control and Automation, and International Conference on Intelligent Agents, Web Tehcnologies and Internet Commerce*, 2006.

[62] Salman, S., Sreenatha, A., and Choi, J., "Attitude Dynamics Identification of Unmanned Aircraft Vehicle," *International Journal of Control of Automation and Systems*, Vol. 4, No. 6, 2006, pp. 782–787.

[63] Dongwon, J., and Panagiotis, T., "Modeling and Hardware-in-the-loop Simulation for a Small Unmanned Aerial Vehicle," *Proceedings of the 2007 AIAA Conference*, 2007.

[64] Nino, J., Mitrache, F., Cosyn, P., and Dekeyser, R., "Model Identification of a Micro Air Vehicle," *Journal of Bionic Engineering*, Vol. 4, No. 4, 2007, pp. 227–236.

[65] Chao, H., Luo, Y., Di, L., and Chen, Y. Q., "Roll-channel Fractional Order Controller Design for a Small Fixed-wing Unmanned Aerial Vehicle," *Control Engineering Practice*, Vol. 18, No. 7, July 2010, pp. 761–772.

[66] Atkins, E., Miller, R., Plet, T., Shaw, K., Ribbens, W., and Washabugh, D., "Solus: An Autonomous Aircraft for Flight Control and Trajectory Planning Research," *Proceedings of the 1998 American Control Conference*, 1998.

[67] Brunke, S., and Campbell, M., "Estimation Architecture for Future Autonomous Vehicles," *In: Proceedings of the 2002 American Control Conference*, Vol. 2, 2002, pp. 1108–1114.

[68] Puttige, V., and Anavatti, S., "Comparison of Real-time Online and Offline Neural Network Models for a UAV," *Proceedings of the International Joint Conference on Neural Networks*, 2007, pp. 412–417.

[69] Puttige, V., and Anavatti, S., "Real-time Multi-network Based Identification with Dynamic Selection Implemented for a Low Cost UAV," *Proceedings of the 2007 IEEE International Conference on Systems Man and Cybernetics*, 2007, pp. 759–764.

[70] Puttige, V., and Anavatti, S., "Real-time System Identification of Unmanned Aerial Vehicles: A Multi-network Approach," *Journal of Computers*, Vol. 3, No. 7, 2008, pp. 31–38.

[71] Hansen, S., and Blanke, M., "Control Surface Fault Diagnosis with Specified Detection Probability - Real Event Experiences," *Proceedings of the 2013 Internatinal Conference on Unmanned Aircraft Systems*, 2013, pp. 526–531.

[72] Park, W.-j., Kim, E.-t., Song, Y.-k., and Ko, B.-j., "A Study on the Real-time Parameter Estimation of Durumi-II for Control Surface Fault Using Flight Test Data (Longitudinal Motion)," *International Journal of Control of Automation and Systems*, Vol. 5, No. 4, 2007, pp. 410–418.

[73] Evans, J., Elkaim, G., and Parkinson, B., "System Identification of an Autonomous Aircraft using GPS," *Proceedings of the ION Global Positioning System Conference*, 1997, pp. 1065–1071.

[74] Carnduff, S., *System Identification of Unmanned Aerial Vehicles*, Ph.D. thesis, Cranfield University, 2008.

[75] Rao, J. J., Gong, Z. B., and Jiang, Z., "GA-based Flight Motion Model Parameter Identification of a Subminiature Fixed-wing Unmanned Aerial Vehicle," *Proceedings of the 2007 IEEE International Conference on Mechatronics and Automation*, 2007, pp. 3549–3554.

[76] Kallapur, A., Ali, S., and Anavatti, S., "Application of Extended Kalman Filter Towards UAV Identification," *Autonomous Robots and Agents*, Vol. 207, 2007, pp. 199–207.

[77] Luo, Y., Chao, H., Di, L., and Chen, Y., "Lateral Directional Fractional Order (pi) Control of a Small Fixed-wing Unmanned Aerial Vehicles: Controller Designs and Flight Tests," *IET Control Theory & Applications*, Vol. 5, No. 18, 2011, pp. 2156.

[78] Nong, Y., Qi, Z., and Lin, D., "System Identification of a Small Unmanned Aerial Vehicle Based on Time and Frequency Domain Technologies," *Proceedings of the 2011 9th World Congress on Intelligent Control and Automation*, 2011, pp. 711–718.

[79] Jung, D., Levy, E., Zhou, D., Fink, R., Moshe, J., Earl, A., and Tsiotras, P., "Design and Development of a Low-cost Test-bed for Undergraduate Education in UAVs," *Proceedings of the 44th IEEE Conference on Decision and Control*, 2005, pp. 2739–2744.

[80] Liu, M., Egan, G., and Ge, Y., "Identification of Attitude Flight Dynamics for an Unconventional UAV," *Proceedings of the 2006 IEEE/RSJ International Conference on Intelligent Robots and Systems*, 2006, pp. 3243–3248.

[81] Elfes, A., Montgomery, J., Hall, J., Joshi, S., Payne, J., and Bergh, C., "Autonomous Flight Control for a Titan Exploration Aerobot," *Proceedings of the 8th International Symposium on Artificial Intelligence, Robotics and Automation in Space*, 2005.

[82] Pounds, P., Mahony, R., and Corke, P., "System Identification and Control of an Aerobot Drive System," *Proceedings of the 2007 Information, Decision and Control Conference*, 2007, pp. 154–159.

[83] Koos, S., Mouret, J., and Doncieux, S., "Automatic System Identification Based on Coevolution of Models and Tests," *Proceedings of the 2009 IEEE Congress on Evolutionary Computation*, 2009, pp. 560–567.

[84] Derafa, L., Madani, T., and Benallegue, A., "Dynamic Modeling and Experimental Identification of Four Rotors Helicopter Parameters," *Proceedings of the IEEE International Conference on Industrial Technology*, 2006, pp. 1834–1839.

[85] Phang, S., Cai, C., Chen, B., and Lee, T., "Design and Mathematical Modeling of a 4-standard-propeller (4SP) Quadrotor," *Prodeedings of the 10th World Congress on Intelligent Control and Automation*, 2012, pp. 3270–3275.

[86] Finio, B. M., Perez-Arancibia, N. O., and Wood, R. J., "System Identification and Linear Time-invariant Modeling of an Insect-sized Flapping-wing Micro Air Vehicle," *Proceedings of the 2011 IEEERSJ International Conference on Intelligent Robots and Systems*, 2011, pp. 1107–1114.

[87] Ko, J., Klein, D., Fox, D., and Haehnel, D., "Gaussian Processes and Reinforcement Learning for Identification and Control of an Autonomous Blimp," *Proceedings of the 2007 IEEE International Conference on Robotics and Automation*, 2007, pp. 10–14.

[88] Eke, F. O., "Dynamics of Variable Mass Systems," Tech. Rep., UC Davis, 1998.

[89] Plastino, A. R., and Muzzio, J. C., "On the Use and Abuse of Newton's Second Law for Variable Mass Problems," *Celestial Mechanics and Dynamical Astronomy*, Vol. 53, No. 3, 1992, pp. 227–232.

[90] Beard, R. W., and McLain, T. W., *Small Unmanned Aircraft: Theory and Practice*, Princeton University Press, Princeton, NJ, 2012.

[91] Greenwood, D. T., *Principles of Dynamics*, Prentice Hall, Upper Saddle River, NJ, 2nd ed., 1988.